

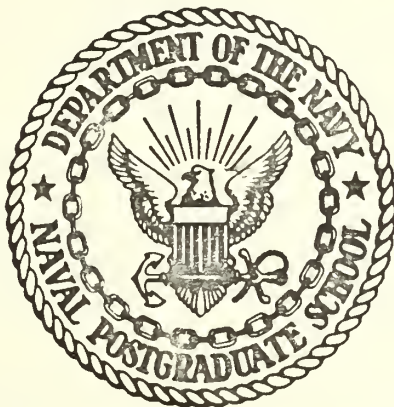
THE APPLICATION OF HOLOGRAPHIC INTERFEROMETRY
TO THE DETERMINATION OF ASYMMETRIC
THREE-DIMENSIONAL DENSITY FIELDS
IN FREE JET FLOW

by

Robert Dale Matulka



United States Naval Postgraduate School



THESIS

THE APPLICATION OF HOLOGRAPHIC INTERFEROMETRY
TO THE DETERMINATION OF ASYMMETRIC
THREE-DIMENSIONAL DENSITY FIELDS
IN FREE JET FLOW

by

Robert Dale Matulka

June 1970

*This document has been approved for public re-
lease and sale; its distribution is unlimited.*

T136456



The Application of Holographic Interferometry
to the Determination of Asymmetric
Three-Dimensional Density Fields
in Free Jet Flow

by

Robert Dale Matulka
Lieutenant Commander, United States Navy
B.S. , United States Naval Academy, 1960

Submitted in partial fulfillment of the
requirements of the degree of

DOCTOR OF PHILOSOPHY

from the

NAVAL POSTGRADUATE SCHOOL

June 1970

ABSTRACT

The successful application of holographic interferometry, and an associated mathematical reduction process, to the determination of an asymmetric three-dimensional density field of an aerodynamic phenomenon is reported.

An integral inversion method from the field of plasma physics has been computerized, extensively evaluated and applied to the determination of functions, both axisymmetric and asymmetric, which simulate aerodynamic density fields.

The application of holographic interferometry has been extended to provide multiple holograms about a test region, with sufficient coverage to provide interferometric data for the successful solution of the density field.

The analytical and experimental methods developed were applied to an experimental axisymmetric test field, the supersonic flow from a free jet, and shown to be comparable to a previous solution obtained by the Abel inversion method. Further, the free jet was tilted to provide a test field which was asymmetric in the plane of solution. Comparison of the resulting asymmetric solution was shown to be self-consistent with the previously obtained axisymmetric solution.

TABLE OF CONTENTS

ABSTRACT - - - - -	2
I. INTRODUCTION - - - - -	7
II. THEORETICAL ANALYSIS - - - - -	8
A. THE INTERFEROMETRY OF AERODYNAMIC FIELDS - - - - -	8
1. The Mach-Zehnder Interferometer - - - - -	10
2. Holography - - - - -	11
3. Holographic Interferometry - - - - -	13
a. Dark Field - - - - -	14
b. Light Field - - - - -	15
B. THEORETICAL APPROACH - THE INTEGRAL INVERSION - - -	16
1. The Basic Equation to Invert - - - - -	16
2. Maldonado's Inversion - - - - -	16
a. The Analytical Procedure - - - - -	17
b. The Numerical Procedure - - - - -	20
c. The Computer Program - HOLOFER - - - - -	22
(1) The Basic Program - - - - -	22
(2) Add-on Functions, Field Modification - - - - -	23
(3) Shock Waves - - - - -	24
d. Symmetry - - - - -	24
(1) Axisymmetric Fields - - - - -	25
(2) With Planes of Symmetry - - - - -	25

3. Theoretical Results - - - - -	26
a. Artificial Data Generation - - - - -	26
b. Test Inversions - - - - -	27
(1) Axisymmetric - - - - -	27
(2) Non-Axisymmetric - - - - -	28
III. EXPERIMENTAL APPROACH - - - - -	29
A. DESCRIPTION OF THE APPARATUS - - - - -	29
1. The Holographic Table - - - - -	29
2. The Test Section - - - - -	30
3. Laboratory Techniques - - - - -	31
B. HOLOGRAPHIC EXPERIMENTAL RESULTS - - - - -	32
1. Non-Flow Holographic Experiments - - - - -	32
2. Free Jet Experimentation - - - - -	33
3. Experimental Techniques and Considerations - - - - -	34
a. Photographic Technique - - - - -	36
b. Data Reduction - - - - -	37
IV. THE APPLICATION OF THE INTEGRAL INVERSION TECHNIQUE TO THE EXPERIMENTAL RESULTS - - - - -	39
A. Axisymmetric Solution - - - - -	39
B. Non-Axisymmetric Solution - - - - -	40
C. Discussion of the Errors - - - - -	41
1. Numerical Inversion Errors - - - - -	41
2. Errors in the Data - - - - -	43

V. SUMMARY - - - - -	45
A. CONCLUSIONS - - - - -	45
B. RECOMMENDATIONS - - - - -	46
C. ACKNOWLEDGEMENTS - - - - -	46
APPENDIX A - OTHER INVERSION METHODS - - - - -	79
APPENDIX B - MATHEMATICAL FOUNDATIONS - - - - -	81
APPENDIX C - HOLOFER - - - - -	86
1. The Description of Input Parameters - - - - -	87
2. A Sample Terminal Dialogue - - - - -	93
3. The Terminal Executive Files - - - - -	95
4. The Program - - - - -	98
5. The Input Data Files Used in the Experiment - - - - -	145
BIBLIOGRAPHY - - - - -	150
INITIAL DISTRIBUTION LIST - - - - -	154
FORM DD 1473 - - - - -	157

I. INTRODUCTION

Holography has enabled the aerodynamicist to "freeze" the interferometric view of a transient phenomenon and subsequently to view the field in three dimensions, as through a "window." This new capability has indicated the possibility of quantitatively determining the density in such a field, with no symmetric restrictions on its form.

To make quantitative determinations of asymmetric density fields, it was necessary to:

1) Invert the fringe number functions that describe the interferometric data,

$$g(\eta', \xi) = \int_{x_1'}^{x_2'} f(x, y) dx'$$

to obtain the asymmetric density function f from within the integral.

In the search for such an inversion process the possibility of using an asymmetric line integral inversion scheme which had been developed in the field of plasma emissivity [Maldonado, 1966], became evident. The method was evaluated by extensive computerized testing on density functions found in aerodynamics, including shock waves. The inversion method was found to be quite accurate, giving results which were generally within one percent of the test function.

2) Obtain holographic interferograms of sufficient angular coverage about a test region to provide the interferometric data required by the inversion process. To obtain the necessary experimental data, a holographic

work table was constructed and used to design the necessary optical arrangement. The capability of achieving multiple Q-switched holographic interferograms about a test region, with no opaque objects present, was demonstrated.

3) Apply real holographic interferometric data to an inversion process in order to demonstrate the practicality of the technique. A stepwise evaluation of the system included an axisymmetric evaluation of a free jet for comparison with the previously available solution of Winckler [1948]. Having attained a solution for the three-dimensional axisymmetric field, the asymmetric capability of the technique was tested by tilting the free jet, which destroyed the axisymmetry in the plane of inversion. The resulting data were inverted asymmetrically and compared with the axisymmetrically measured density. The result is shown to be a self-consistent comparison of the asymmetric inversion.

II. THEORETICAL ANALYSIS

A. THE INTERFEROMETRY OF AERODYNAMIC FIELDS

Holography has opened a new branch of interferometry for aerodynamic research. Ordinary Mach-Zehnder type interferograms have been restricted to the analysis of two-dimensional or axisymmetric flow fields. Such interferograms are able to examine only the light beam which has passed through the test region from a single direction. Holograms are able to reproduce a light wave in both amplitude and phase, and further to

simultaneously reproduce two such light waves which have occurred at different times. The resulting comparison of two reproduced light waves yields an interferogram which allows the analysis of the light which has passed through a test region from many different directions.

By interfering two coherent light waves with each other, interferometry compares their phases, and thus provides a measured comparison of their integrated index of refraction over their respective distances of travel from a common source to the film. This relative phase, expressed in multiples of wavelengths and commonly called fringe number, is described by the equation:

$$g = \frac{1}{\lambda} \int_{L_1}^{L_2} [n(x,y,z) - n_0(x,y,z)] dl \quad (1)$$

where: λ = the wavelength of the light at the film,

n = the index of refraction seen by the traveling light wave,

n_0 = the index of refraction seen by the wave of the comparison scene,

$L_2 - L_1$ = the total distance of travel for each of the waves.

The index of refraction of a gas is well represented as a function of the gas density [Liepmann and Roshko, 1957] by the first two terms of a Taylor expansion:

$$n = 1 + \beta \frac{\rho}{\rho_s} + \dots \quad (2)$$

where: ρ_s = the gas density at which β is measured,

β = the measured coefficient.

For air at 0°C. and 760 mm. Hg. , $\rho_s = .0012929$ gm/cc. , and for deep red light, $\theta = .000291$. Thus one can rewrite equation (1) :

$$g = \frac{\theta}{\rho_s \lambda} \int_{L_1}^{L_2} [\rho(x, y, z) - \rho_0(x, y, z)] dl \quad (3)$$

Equation (3) is a line integral equation for the unknown density. With sufficient evaluation of the function g (a function of three spatial variables which one obtains from the interferograms), one can invert the equation to obtain the density function.

1. The Mach-Zehnder Interferometer

Figure (1) is the schematic arrangement of a typical Mach-Zehnder interferometer [Ladenberg, ed. 1954]. The two light waves which are compared travel paths A and B respectively. Alignment of the instrument is critical to within the order of a wavelength of light, and the mirrors and lenses must be distortion free to one-tenth of that value. The chief practical disadvantage, however, is that one can evaluate the light beam from only one direction at a time through the test section.

By properly aligning the components with a uniform density field in the test section, one can exactly recombine the two light beams A and B at the film plane of the camera. Then with a flow in the test section, any phase differences recorded are those due to variations in the test section density. Such an interferogram is called "infinite fringe"

If one purposely misaligns one beam with the other (by rotating a mirror slightly) a deliberate fringe pattern is recorded. Variation in test section density is then recorded as a variation in the regularity of the

fringe pattern. This second variety of interferogram is called "finite fringe."

2. Holography

First reported by Denis Gabor [1948, 1949, 1951], holography is itself an interferometric process. By combining two coherent beams directly on a photographic film (Figures 2, 2a), one records a microscopically small interference pattern. Positions on the film where the two waves are in phase will record darkly. Positions where they are out of phase will remain light. When the developed photographic plate is reilluminated by the reference beam (Figures 3, 3a), the interference pattern acts as a very complex diffraction grating and diffracts three beams; these are the zero order, or transmitted illumination beam, and the positive and negative first orders, which are re-creations of the original object beam.

Mathematically, one can represent the phenomenon as the combination of any two general waves which obey the scalar wave equation [Brandt, 1968]. Let a wave be described as follows:

$$\tilde{E}(\vec{r}, t) = \tilde{A}(\vec{r}) e^{i\omega t} \text{ is the complex wave, where} \quad (4)$$

$$\tilde{A}(\vec{r}) = A(\vec{r}) e^{-i\Psi(\vec{r})} \text{ is the spatial portion,} \quad (5)$$

$$A(\vec{r}) = a f(\vec{r}) \text{ is the spatial amplitude,} \quad (6)$$

$\Psi(\vec{r})$ is the spatial phase function,

a is the reference amplitude,

$f(\vec{r})$ is the spatial variation of amplitude, and

\vec{r} is a position vector.

Since photographic film measures only the time averaged intensity over relatively many periods of the wave, one need not be concerned with the temporal portion $e^{i\omega t}$ of the wave. Denoting the object and reference light beams by the subscripts o and r, one can represent the combination of both beams at the photographic plate as:

$$\tilde{A} = \tilde{A}_r + \tilde{A}_o = A_r e^{-i\psi_r} + A_o e^{-i\psi_o} \quad (7)$$

The intensity recorded will be:

$$I = \tilde{A}\tilde{A}^* = (\tilde{A}_r + \tilde{A}_o)(\tilde{A}_r + \tilde{A}_o)^* = |A_r|^2 + |A_o|^2 + \tilde{A}_r^*\tilde{A}_o + \tilde{A}_r\tilde{A}_o^* \quad (8)$$

where * denotes complex conjugate. Assuming a linear ratio of intensity to transmittance of the developed hologram, the transmittance is:

$$T = 1 - T_1 I = 1 - T_1 (|A_r|^2 + |A_o|^2) - T_1 (\tilde{A}_r^* \tilde{A}_o) - T_1 (\tilde{A}_r \tilde{A}_o^*) \quad (9)$$

where T_1 is the transmittance corresponding to unit intensity. Upon reillumination by the reference beam, the transmitted wave is:

$$\tilde{A}_r T = \left[1 - T_1 (|A_r|^2 + |A_o|^2) \right] \tilde{A}_r - \left[T_1 |A_r|^2 \right] \tilde{A}_o - (T \tilde{A}_r \tilde{A}_o^*) \tilde{A}_o^* \quad (10)$$

where the quantities in square brackets represent attenuation. The first term represents the transmission of the reilluminating reference beam, the second term represents the production of an attenuated object beam, and the third term represents a modified reconstruction of the complex conjugate of the object beam (Figure 3). The modification of the conjugate object wave depends upon the nature and direction of the reference beam, but for simple reference waveforms there is usually only a magnification

and angular displacement to the opposite side of the reference wave. The negative sign on the reconstructed wave amplitude is immaterial, since a negative amplitude on a continuous wave simply represents a 180° phase change.

If the reillumination beam is different from the original reference beam, the reconstructed diffraction beams are distorted accordingly. For the most part, this distortion is due to different source location or different wavelength of light, which create magnification and angular displacement of the object waves.

For laboratory use, the reconstructed holographic image can be considered an almost exact duplication of the original.

3. Holographic Interferometry

The application of holography to interferometry [Heflinger, et. al., 1966] derives from the fact that the holographic film records the diffraction pattern almost linearly. When double exposed, the hologram records two diffraction patterns superimposed upon one another. Therefore, when a double exposed hologram is reilluminated, each recorded diffraction pattern will diffract its own first order beams. An observer will see both recorded scenes simultaneously. One may simply replace A_o by $A_{o1} + A_{o2}$ in equations (8-10). To produce a holographic interferogram of a test section as in Figure 2, one exposes the hologram for one-half the exposure time with no flow in the test section (the uniform field provides the

comparison beam); then completes the exposure with the subject flow field present. The two reconstructed waves will interfere with each other in much the same manner as do the two waves of the Mach-Zehnder in the infinite fringe configuration.

If, instead of making a second exposure of the hologram, one replaces it exactly in position and reilluminates both the hologram and the object, one can again compare the two waves, except that in this case one of the object scenes is real and the other is a reconstructed virtual image. Such real-time holographic interferometry is called the "live" fringe technique.

The chief advantage of either method is that, except for differences in the test section, both the test and the comparison beams have traveled through exactly the same optical regions. Optical components are then automatically matched. In practice rather crude optical components can be used with excellent results.

By a slight rotation of the hologram or of one of the mirrors between exposures, one can achieve the same finite fringe presentation as with the Mach-Zehnder.

a. Dark Field Interferograms

Dark field interferograms are produced when the test section does not contain any light scattering properties. The observer looking at the reconstructed image is unable to focus on anything other than the

source; objects in the test section, as well as regions of interference, can only be observed as shadows. Such interferograms correspond to those taken by ordinary methods with only one direction of light beam passage through the test field, corresponding to only one light source.

b. Light Field Interferograms

True three-dimensional interferograms are obtained when a diffuser plate is placed between the source and the test section. The object beam then becomes diffused through the test section and appears to the observer as a continuous background of source points against which the test section, and its interference pattern, become a silhouette. Because each point of the diffuse plate acts as an individual source for any line of sight passing through it, equation (3) may be evaluated for any line which passes through both the diffuser plate and the hologram. A continuous evaluation of the function g can thus be provided as a function of position and angle. This function g , the fringe pattern, changes as the observer changes viewing aspect, but generally the fringe patterns cannot be localized by their parallax.

By arranging several holographic plates about a test section, as in Figure 4, one can obtain the fringe number function for a rather continuous segment of angular variation about the z axis of the field. The resulting array of integral values can be applied to the inversion of equation (3) to provide a solution for the density field in the test section.

B. THE INTEGRAL INVERSION

1. The Basic Equation to Invert

Equation (3), rewritten for a plane of constant z is:

$$g(y', \xi, z_c) = Q \int_{x'_1}^{x'_2} f(x, y, z_c) dx' \quad (11)$$

where: $f(x, y, z_c) = \frac{\rho(x, y, z_c)}{\rho_\infty} - 1 \quad (12)$

and: $Q = \frac{\rho_\infty \beta}{\rho_s \lambda} \quad (13)$

x' and y' are measured in a coordinate system which is rotated by an angle ξ about the z axis (Figure 5).

2. Maldonado's Inversion

The integral inversion method utilized in this investigation was first reported by C. D. Maldonado et. al. in 1965 [1966; Olsen, 1968]. It was used for obtaining plasma emissivity within a particular region from the measured values of emission intensity measured from outside the region. The form of the equation resulting from such emissivity studies is identical to that of equation (11). The procedure involves the representation of the function f of equation (11) in a complete set of orthogonal functions, with the expansion coefficients evaluated by use of the orthogonality condition.

An earlier method involving series expansion of the function f had been reported in 1962 by S. I. Herlitz. The method applied to cases of asymmetric function of finite domain. Maldonado's method follows similar logic, but it is applicable to asymmetric functions of infinite domain.

The function f is assumed to be squared integrable over the infinite plane so that it may be expanded in a complete set of orthogonal functions. The selection of a suitable set of orthogonal functions is discussed in Appendix B.

a. The Analytical Procedure

The unknown function may be expanded in a special set of functions $U_{m+2k}^{\pm m}$ which are orthogonal with respect to the weighting function $e^{-(\alpha^2 x^2 + \alpha^2 y^2)}$:

$$f(x, y) = \sum_{m=0}^{\infty} \sum_{k=0}^{\infty} \epsilon_m \left[C_{m+2k}^m(\alpha) U_{m+2k}^m(\alpha x, \alpha y) + C_{m+2k}^{-m}(\alpha) U_{m+2k}^{-m}(\alpha x, \alpha y) \right] \cdot e^{-(\alpha^2 x^2 + \alpha^2 y^2)} \quad (14)$$

where $\epsilon_m = \frac{1}{2}$ for $m = 0$, $\epsilon_m = 1$ for $m = 1, 2, 3, \dots$ and $C_{m+2k}^{\pm m}$ are the unknown complex coefficients of expansion. α is an arbitrary scale factor which may be considered the reciprocal of a non-dimensionalizing coefficient.

The functions $U_{m+2k}^{\pm m}$ are defined:

$$U_{m+2k}^{\pm m}(\alpha x, \alpha y) = (-1)^k \alpha \left[\frac{k! (\alpha^2 x^2 + \alpha^2 y^2)^m}{m! (m+k)!} \right]^{\frac{1}{2}} e^{\pm i m \phi} L_k^m(\alpha^2 x^2 + \alpha^2 y^2) \quad (15)$$

where: $\phi = \tan^{-1}\left(\frac{y}{x}\right) - \frac{\pi}{2}$, and L_k^m is the associated

Laguerre polynomial:

$$L_k^m(\alpha^2 x^2 + \alpha^2 y^2) = \sum_{s=0}^k \left[\frac{(m+k)!}{(k-s)! (m+s)! s!} \right] \cdot \left[(-1)^s (\alpha^2 x^2 + \alpha^2 y^2)^s \right] \quad (16)$$

The function $U_{m+2k}^{\pm m}$ has a gauss transform:

$$I_{m+2k}^{\pm m}(\alpha y', \xi) = \int_{-\infty}^{\infty} U_{m+2k}^{\pm m}(\alpha x, \alpha y) e^{-\alpha^2 x'^2} dx' = \frac{e^{\pm i m \xi} H_{m+2k} \alpha y'}{[k! (m+k)!]^{\frac{1}{2}} 2^{m+2k}} \quad (16a)$$

where $H_{m+2k}(\alpha y')$ are Hermite polynomials of order $m+2k$.

The particular advantage of the set of functions $U_{m+2k}^{\pm m}$ is that they are "invariant in form" to a rotation of coordinate system [Maldonado, 1965]. That is, they remain an orthogonal set under a rotation of the coordinate system. Observe that in the equation for the polynomial (15), the angle ϕ occurs only in the complex exponential term.

In terms of the expanded function f , and utilizing the transform relation of equation (16), equation (11) becomes:

$$g(y', \xi) = \sum_{m=0}^{\infty} \sum_{k=0}^{\infty} \epsilon_m \left[k! (m+k)! 2^{m+2k} \right]^{-\frac{1}{2}} \left[C_{m+2k}^m(\alpha) e^{im\xi} + C_{m+2k}^{-m}(\alpha) e^{-im\xi} \right] H_{m+2k}(\alpha) e^{-\alpha^2 y'^2} \quad (17)$$

Equation (17) is subject to the following orthogonality condition:

$$\int_{-\pi}^{\pi} e^{\pm im\xi} e^{\mp in\xi} d\xi \int_{-\infty}^{\infty} H_{m+2k}(\alpha y') H_{n+2l}(\alpha y') e^{-\alpha^2 y'^2} dy' = \frac{2\pi^{\frac{3}{2}}}{\alpha} \left[(m+2k)! (n+2l)! 2^{m+2k} 2^{n+2l} \delta_{mn} \delta_{(m+2k)(n+2l)} \right] \quad (18)$$

Where δ is the kroneker delta function. The solution of equation (18)

applied to equation (17) leads to the expansion coefficients:

$$C_{m+2k}^{\pm m} \alpha = \frac{\alpha}{2\pi^{\frac{3}{2}}} \left[\frac{k! (m+k)!}{(m+2k)!} \right] \cdot \int_{-\pi}^{\pi} \int_{-\infty}^{\infty} g(y', \xi) e^{\mp im\xi} H_{m+2k}(\alpha y') dy' d\xi \quad (19)$$

Equation (17), with the coefficients of equation (19), represents the function g by a Gram-Charlier series in the radial direction, and by a Fourier series in the azimuthal direction.

Equation (14), with the coefficients of equation (19), becomes:

$$f(x, y) = \frac{\alpha}{\pi^{3/2}} \sum_{m=0}^{\infty} \sum_{k=0}^{\infty} \epsilon_m \frac{(k!(m+k)!)^{\frac{1}{2}}}{(m+2k)!} e^{-(\alpha^2 x^2 + \alpha^2 y^2)} \cdot \text{Real} \left[\int_{-\pi}^{\pi} \int_{-\infty}^{\infty} g(y', \xi) e^{-im\xi} H_{m+2k}(\alpha y') dy' d\xi \cdot U_{m+2k}^m(\alpha x, \alpha y) \right] \quad (20)$$

or, inserting equation (15):

$$f(x, y) = \left(\frac{\alpha}{\pi}\right)^2 \sum_{m=0}^{\infty} \sum_{k=0}^{\infty} \epsilon_m \frac{(-1)^k k!}{(m+2k)!} (\alpha^2 x^2 + \alpha^2 y^2)^{\frac{m}{2}} L_k^m(\alpha^2 x^2 + \alpha^2 y^2) \cdot \left[B_{m+2k}^m(\alpha) \cos(m\phi) + D_{m+2k}^m(\alpha) \sin(m\phi) \right] e^{-(\alpha^2 x^2 + \alpha^2 y^2)} \quad (21)$$

where:

$$B_{m+2k}^m(\alpha) = \int_{-\pi}^{\pi} \int_{-\infty}^{\infty} g(y', \xi) \cos(m\xi) H_{m+2k}(\alpha y') dy' d\xi \quad (22)$$

$$D_{m+2k}^m(\alpha) = \int_{-\pi}^{\pi} \int_{-\infty}^{\infty} g(y', \xi) \sin(m\xi) H_{m+2k}(\alpha y') dy' d\xi \quad (23)$$

Equations (21), (22) and (23) represent the fundamental inversion by Maldonado's method. Both analytical and numerical inversions were demonstrated in his series of three papers.

The method applies quite directly to density fields. The zero

value of the function $\Delta\varphi$ studied in interferometry is arbitrary and can always be chosen such that the function is zero outside of a given circular boundary. Singularities do not occur in real density fields except for the spaces occupied by opaque objects. Cases with simple solid objects appear amenable to this method, but will not be discussed here.

b. The Numerical Procedure

Since experimental data are not obtained in analytical form, the indicated operations must be performed numerically. The contractual report resulting from the investigation by Olsen, et. al. [1966], included a computer program. However, it appeared more prudent to reprogram the basic equations to fit the available computer, and to more closely meet the needs of the particular application.

The form of equation (24) is a truncated form of equation (21):

$$f(x,y) = \left(\frac{\alpha}{\pi}\right)^2 \sum_{m=0}^M \sum_{k=0}^K \epsilon_m \frac{(-1)^k k!}{(m+2k)!} (\alpha^2 x^2 + \alpha^2 y^2)^{\frac{m}{2}} L_k^m (\alpha^2 x^2 + \alpha^2 y^2) \quad (24)$$

$$\cdot \left[B_{m+2k}^m(\alpha) \cos(m\phi) + D_{m+2k}^m(\alpha) \sin(m\phi) \right] e^{-(\alpha^2 x^2 + \alpha^2 y^2)}$$

The numerical evaluations of the coefficients from equations (22) and (23) are accomplished approximately. Since the function is known to be zero outside of the circular domain of Figure (5), the integration over y' need only be made over finite limits, defined here as $-S/2$ to $+S/2$. The function g , which is always single-valued, is assumed to be constant within the discrete areas of the data plane represented

in Figures (6) and (7). This permits the integrals to be represented as a finite sum of integrals over the subregions:

$$B_{m+2k}^m(\alpha) = \sum_{i=1}^{IMAX} \sum_{j=1}^{JMAX} g(y'_j, \xi_i) \int_{\xi_{i-\frac{1}{2}}}^{\xi_{i+\frac{1}{2}}} \cos(m\xi) d\xi \int_{y'_{j-\frac{1}{2}}}^{y'_{j+\frac{1}{2}}} H_{m+2k}(\alpha y') dy' \quad (25)$$

$$D_{m+2k}^m(\alpha) = \sum_{i=1}^{IMAX} \sum_{j=1}^{JMAX} g(y'_j, \xi_i) \int_{\xi_{i-\frac{1}{2}}}^{\xi_{i+\frac{1}{2}}} \sin(m\xi) d\xi \int_{y'_{j-\frac{1}{2}}}^{y'_{j+\frac{1}{2}}} H_{m+2k}(\alpha y') dy' \quad (26)$$

The integrals are then evaluated over the sub-intervals with $\xi_{\frac{1}{2}} \equiv -\pi$,

$$\xi_{IMAX+\frac{1}{2}} \equiv +\pi, \quad y'_{\frac{1}{2}} \equiv -\frac{S}{2}, \quad \text{and} \quad y'_{JMAX+\frac{1}{2}} \equiv +\frac{S}{2}$$

The integrals over ξ are elementary, and the integrals over y' are evaluated by use of the derivative formula for Hermite polynomials [Erdelyi,

et. al., 1953]. The resulting general formulae for B and D are:

$$B_{m+2k}^m(\alpha) = \frac{1}{2\alpha(m+2k+1)} \sum_{i=1}^{IMAX} \sum_{j=1}^{JMAX} g(y'_j, \xi_i) \left[\frac{\sin(m\xi_{i+\frac{1}{2}}) - \sin(m\xi_{i-\frac{1}{2}})}{m} \right] \\ \cdot \left[H_{m+2k+1}(\alpha y'_{j+\frac{1}{2}}) - H_{m+2k+1}(\alpha y'_{j-\frac{1}{2}}) \right] \quad (27)$$

$$D_{m+2k}^m(\alpha) = \frac{-1}{2\alpha(m+2k+1)} \sum_{i=1}^{IMAX} \sum_{j=1}^{JMAX} g(y'_j, \xi_i) \left[\frac{\cos(m\xi_{i+\frac{1}{2}}) - \cos(m\xi_{i-\frac{1}{2}})}{m} \right] \\ \cdot \left[H_{m+2k+1}(\alpha y'_{j+\frac{1}{2}}) - H_{m+2k+1}(\alpha y'_{j-\frac{1}{2}}) \right] \quad (28)$$

which are valid for $m > 0$. The special case of $m = 0$ represents the axisymmetric solution. The terms within the brackets $\left[\right]$ are evaluated by l'Hospital's rule: $D_{0+2k}^0 = 0$, and

$$\lim_{m \rightarrow 0} \left\{ \frac{\sin(m\xi_{i+\frac{1}{2}}) - \sin(m\xi_{i-\frac{1}{2}})}{m} \right\} = \xi_{i+\frac{1}{2}} - \xi_{i-\frac{1}{2}} = \Delta\xi \quad (29)$$

c. The Computer Program - Holofer

In order to perform the inversions a FORTRAN IV computer program called HOLOFER, which includes a large number of variable parameters and optional modes of operation, was written. The complete program, with input parameter descriptions and the working data, is included in appendix C.

(1) The Basic Program. The data plane, called the G-array, consists of a discrete set of values of the function g of equation (11) taken over regular intervals of y' and ξ , of size IMAX by JMAX (Figure 7). The G-array is obtained in one of three modes. Mode one computes the G-array that corresponds to an optional test function by the numerical integration of equation (11) at regular intervals of y' and ξ . By generating its own data from a test function, mode one provides the basic program testing capability. In mode two operation, HOLOFER interpolates a regular G-array from an irregularly entered set of values such as those normally obtained in holographic interferometry. Mode three operation reads in a regular array of input values directly.

Next, equations (27) and (28) are evaluated for each set of coefficients B and D up to the series truncation values of $m = \text{MLIMIT}$

and $k = \text{KLIMIT}$. These B and D values are stored on external (DISK) storage.

Having computed the B and D coefficients, HOLOFER next evaluates equation (24) for each point in the test section individually. Either a cartesian or a cylindrically aligned array of spatial coordinates can be accommodated by choice of input parameters. In the evaluation of equation (24), truncation of each series is performed by first specifying an input parameter epsilon. If a certain number of terms in a row remain less than epsilon times the existing partial sum, the series is truncated. If the index values reach the limiting available set of B and D coefficients before the series has converged, the most recent few values of the partial sum are averaged.

(2) Add-On Functions. A second G-array may be computed and added to the original G-array prior to the inversion. The array is computed in the mode one operation from any given function. In addition, a gaussian random number of specified standard deviation may be added to the second G-array. The first feature provides the capability of adding a smoothing function to data with severe properties, such as from shock waves or opaque discontinuities in the interferograms. Peripheral information about the function may be used to determine a desirable function. The known add-on function is then automatically subtracted from the solution. The second feature allows one first to perform the inversion

of a set of data with a known error size and then to compare the result with a previous solution in order to estimate the possible error in the solution.

(3) Shock Waves. The polynomial series representation of discontinuous or high gradient regions such as those from shock waves requires a large number of terms. Accordingly, the inversion routine requires a large index of m and k to represent steep gradients. If sufficiently many data points are entered on input to provide adequate significance in the high order terms, one can utilize rather large values of MLIMIT and KLIMIT to obtain reasonably accurate inversions.

If one has prior knowledge of the function to be inverted, such as an isentropic solution of a flow field, an add-on function can be added which will smooth the net function at such discontinuities, i.e. the subtraction of a "plug" function shape in Figure (12). Such modification enhances the convergence of the resulting function, if it is well matched, and it therefore improves the accuracy of the result. An analogous method applicable to the Abel axisymmetric inversion has been described by Bennet, Carter, and Bergdolt [1952], called the method of "reduced functions," which operates on the fringe curve directly.

d. Symmetry

HOLOFER is designed to invert an asymmetric field. There

are, however, several simplifications to the process that result from symmetry in the field.

(1) Axisymmetric Fields. For axisymmetric fields, the angular variations disappear with the result that only one view or one line of the G-array need be considered. The coefficient evaluation integrals over the angular domain thus become zero, for all except the $m = 0$ case, and the summation process simplifies to a single series. Computation time in this mode is reasonably short, from 20 - 60 seconds on the IBM 360-67 digital computer for KLIMIT = 1000. The majority of program testing has been in this mode.

(2) With Planes of Symmetry. Planes of symmetry in the field reduces the angular requirements of the input data. In Figure (8), the data plane is shown divided into unique segments, only one of which need be supplied. Note that even in the asymmetric case, the data plane has two duplicate (though inverted) segments. The function looks the same from opposite sides of the domain, with reversed argument:

$$g(\gamma', \xi) = g(-\gamma', \xi + \pi) \quad .$$

Additionally, the domain of orthogonality is reduced for cases of planar symmetry greater than one. The regions which are not cross hatched, are subdomains of orthogonality. The region of integration for coefficient evaluation is reduced accordingly in the program. The index value m in the series representation corresponds to the Fourier mode of the expansion of the function f in the azimuthal

direction. Therefore, for cases of planar symmetry the coefficients are zero for certain values of m . To summarize:

Asymmetric:	uses all B and D coefficients:
One Plane:	uses B coefficients only, all
Two Planes:	uses B coefficients, $m = 0, 2, 4, 6,$
Three Planes:	uses B coefficients, $m = 0, 3, 6, 9 \dots$
Four Planes:	uses B coefficients, $m = 0, 4, 8, 12 \dots$
Five Planes:	uses B coefficients, $m = 0, 5, 10, 15 \dots$
etc.	

Axisymmetric corresponds to an infinite number of planes of symmetry: uses B coefficients $m = 0$ only.

While the higher numbers of symmetry planes have little practical value, they are included automatically in the generalization of the program symmetry tests.

3. Theoretical Results

a. Artificial Data Generation

Mode one of the program generates the G-array for a specified function. Several functions are included in subroutine FUNCT for use as program tests or as add-on functions. Provision is also made to enter an arbitrary function in subroutine SPFUN by simply entering the Fortran cards describing the function. In addition, a set of numerical values may be read in and used as a function with linearly

interpolated values between the given points. The G-array is evaluated at each value of y' and ξ as shown in Figure (7). Simple summation of the function value at 3.* (IMAX) points along the line $y' = \text{const.}$ is used to evaluate the integral. Once the data plane is filled, the inversion process makes no distinction between computed or experimental data in the G-array.

b. Test Inversions

(1) Axisymmetric. Figure (9) represents the function, computed fringe curve, and inverted solution of a gaussian function similar to Maldonado's test case:

$$f = e^{-\theta^2(x^2+y^2)} \quad (30)$$

The original analytical function is shown as a solid line, while the corresponding computed fringe curve is shown to a separate scale as a series of boxes. The greatest difference between the inverted solution and the original function was 0.001, or 0.1 percent of the maximum function value.

Figure (10) is a cosine-squared function:

$$f = \cos^2 \left(2\pi (x^2+y^2)/3 \right) \quad (31)$$

The greatest inversion error was 0.5 percent of the maximum functional value.

To determine the capability of the program to invert shock-wave type discontinuities, a circular square wave, or "plug" function, was inverted. Figure (11) shows a rounding off of the discontinuity that is

typical of a truncated series representation. The maximum error that occurs in the nearby region is 6.2 percent. At the center of the function, at radius zero, the series does not converge. The resulting 8.6 percent error is typical of the center point of inverted functions containing discontinuities.

Winckler, in an extensive application of the Abel inversion method to free jets [1948], used a hypothetical test function that is shown in Figure (12). Plots of the solutions he obtained are shown for comparison of the two methods. The characteristic "overshoot" of the Abel method near the discontinuity is shown, where the largest error by the Maldonado inversion was 3.8 percent.

Figures (13) and (14) are inversions of typical axisymmetric density functions from the Winckler analysis of a free jet. They demonstrate the capability of the inversion routine with realistic types of functions. Both inversions were accurate to within 2.6 percent.

(2) Non-Axisymmetric. Figure (15) represents three cross-sections of the same gaussian function as before, now centered at $x = .1, y = 0$. cm. This corresponds to the test example that Maldonado used in the verification of his inversion scheme. The solution is everywhere accurate to within 0.8 percent with a very low number of series terms. The function is planar symmetric and thus tests only the cosine terms of the expansion.

Figure (16) represents three-cross-sections of an asymmetric test case. The function is an elliptical cone of base diameters 0.7×0.5 cm., centered at $x = 0.707$, $y = 0.707$ cm. In the solution, the tip of the cone is rounded by the natural smoothing characteristics of the inversion method, but otherwise the maximum error is 1.5 percent. This test case represents a complete test of the inversion procedure, utilizing both B and D terms of both series expansions.

III. EXPERIMENTAL APPROACH

A. DESCRIPTION OF THE APPARATUS

1. The Holographic Table

A holographic work table was designed and constructed to provide optical bench facilities about a free jet, as shown in Figures (17) and (18). The table was designed to evaluate various arrangements of optical components to achieve a wide angle of holographic field of view, and to suppress the vibration caused by the free jet noise.

The table was made of pressed plywood laminate, two and one-half inches thick. The four by six foot table was mounted on a rotatable set of plywood boards, with a centerhole of eight inches diameter to accommodate the free jet. This arrangement provided the capability of rotating the entire table about the flow field. Below the rotating arrangement, the table rested on four small tire tubes to provide

structural vibration isolation from the building. For experiments conducted in C-W gas laser holography with up to thirty second exposure times (without the free jet) the arrangement was very successful. Beneath the inner-tube mounting, the table rested on four standard automobile type screw jacks. Recessed jack points allowed the table to be readily tilted to about 15° about the flow field.

A Korad K-1 pulsed ruby laser operating at a wavelength of 6941. Å. was employed with a Pockels cell Q switching device. The resultant effective hologram exposure time was about 20 ns., eliminating problems with vibration during the hologram exposure. There does remain the problem of vibratory misalignment of the optical components between the two exposures of the holographic interferogram. To help damp acoustically-caused vibration, the mirrors were all mounted on heavy metal blocks. The weakest link in the setup appeared to be the beam splitter holders. They were lightest of the table components, and as a result of their vibration, holographic interferograms obtained tended to have a finite fringe. Occasionally a hologram would be unusable because the fringe spacing became too fine to resolve.

2. The Test Section

The table was mounted around a standing free jet. The plenum chamber was about 45 cm. long by 30 cm. diameter. The jet extended 45 cm. above the plenum chamber with an inside diameter of 3.18 cm. and

a throat diameter of 2.0 cm. at the exit. The test section was defined by a square plexiglass enclosure, the four inside surfaces of which were inscribed with a one centimeter square grid. The grid box provided some vibration insulation for the jet, and also produced a self-contained coordinate system for the hologram and the corresponding photographs. The holograms were arranged about the grid box as shown in Figure (19), with the coordinate system established as shown. Commercial ground glass plate was used as the diffuser.

3. Laboratory Techniques

Alignment of the laser beam with the optical components was accomplished by aligning a continuous wave helium-neon gas laser through the rear mirror and along the ruby axis of the pulsed laser. A -20 cm. meniscus lens of inexpensive quality was used to diverge the beam. Care must be exercised in this arrangement to insure the convex side of the lens is towards the ruby laser. Concave surfaces in the near vicinity of a high power laser can themselves focus a high density of reflected energy, which might damage the laser itself or any near components.

Relative intensities of reference to object beams of about 4:1 were found to yield good holograms.

Since the arrangement of the several mirrors, beamsplitters, etc., so as to have the same optical path length from source to hologram for each beam is a tedious procedure, a cork pinboard was designed to

facilitate the table arrangements. Threads of the same length, each one representing a laser beam, were stretched from the laser source to their various holograms via different routes over a sketch of the table and held in position with pins. The table has a six inch grid painted on its surface to facilitate location of the components from the grid on the sketch. The pin board saved many hours of arrangement time.

Holograms were made on Agfa-Gaefert 8E75 holographic plates. Development was five minutes in Kodak D-19 developer, 30 seconds in acetic acid stop bath of standard dilution, five minutes in standard fixer, one minute water wash, followed by immersion in wetting agent (Kodak PhotoFlo) prior to drying. It was observed that good reconstructions of restricted field of view could be obtained immediately after developing, while the plate was still wet. Normal reconstructions were made with the continuous wave gas laser at 6328Å. The resulting image magnification from reconstruction at a different wavelength was not considered deleterious. The technique used in making photographs for data extraction will be discussed in the next section.

B. HOLOGRAPHIC EXPERIMENTAL RESULTS

1. Non-Flow Holographic Experiments

Holographic experience was gained with a Spectra-Physics model 124 gas laser. Both back-lighted scenes and diffuse objects were recorded.

Real time interferometry of a test area was demonstrated and surface deformation interferometry was obtained. Figure (20) shows the interference pattern on the surface of a small clamping device under strain. Figure (21) is one view of the interference pattern about a cigarette. Between exposures of the hologram, the cigarette had been radiantly heating the platform below it for about three minutes, and the platform shows the interference pattern caused by the resulting thermal expansion. The gas laser was used to confirm the optical arrangement of Figure (19) for multiple hologram viewing of the free jet test scene. Successful holographic interferograms were obtained of cigarettes at all hologram positions.

2. Free Jet Experimentation

The Korad giant pulse laser was installed on the table and holograms taken of the free jet exhausting to the atmosphere. Figure (22) shows a shadowgram taken at 35 psig plenum pressure. A shadowgram is produced directly on the hologram plate when the holographic image is recorded by a single exposure of the dark field technique (with the ground-glass diffuser absent).

Figures (23) and (24) show two views obtained from the same holographic interferogram of jet flow at 60 psig. The interferometric data from this hologram were inverted to provide an axisymmetric solution. The results of the solution follow in section D. Holographic

interferograms were also taken at 25, 40, 45, and 50 psig. , but were not reduced. Turbulent flow perturbations became more predominant as the pressure was reduced.

To provide a non-axisymmetric test of the method, the table was tilted 11° clockwise about the y axis of the table. As a result of the tilt, horizontal cross sections through the field became planar symmetric about the x-z plane. The solution of planar symmetric fields require a 90° field of view. Three simultaneous holographic interferograms were taken about the tilted jet at 60 psig. with the arrangement shown in Figure (19). Each of the three holograms provided a field of view of about 15° , one of which had several degrees obscured by the corner of the box. To provide more complete coverage, the table was rotated and additional holograms taken. Two rotations were required. Figures (25) and (26) show the interferograms taken at 5° and 85° which were used in the data reduction.

3. Experimental Techniques and Considerations

Previous work at this laboratory [Sullivan, 1968] had shown the intensity transmission of collimated laser light beyond commercial ground glass falls below 30 percent of the incident intensity beyond viewing angles of about $\pm 8^{\circ}$. Since the diffraction capability of a holographic plate exceeds $\pm 8^{\circ}$, the ground glass represents the limiting factor to the field of view. In fact, usable holographic interferograms were obtainable with from $\pm 5^{\circ}$ to $\pm 10^{\circ}$ field of view, centered about the object beam direction,

the field size being a function of the ratio of the intensities of object beam and reference beam.

The holographic interferogram appears as a completely three-dimensional set of fringes to the observer. Only special cases of the fringe pattern can be localized, those corresponding to Young's fringes (the finite fringe background pattern), or those corresponding to regions of spherical or cylindrical density variations. To obtain usable data from the fringe number function, one must sample discrete segments of the information. This is done by recording a series of photographic interferograms at regular angles about the test section. For a completely general field one requires 180° field of view, while the planar symmetric case studied required 90° .

There are two basic methods of obtaining sufficient angular coverage of the field. The first is to take several individual holograms, rotating the relative angle between the hologram setup and the test section for each hologram. Unsteadiness in the flow between the exposures will introduce errors. The second method involves arranging a series of holograms about the test section for simultaneous exposure. Intervals in the data from the second method are filled by interpolation. Interpolation over large angles requires that the function vary slowly in the angular direction. This experiment utilized a combination of both methods.

a. Photographic Technique

A normal photograph of the hologram records an image of the focus plane as shown in Figure (28). Each position on the photograph represents the line of sight from the image to the aperture (Figure 27). All of these lines of sight will represent a non-parallel set of lines. For reasonable camera focus distances, the deviation from parallelism is small and may be neglected. The spatial filtering technique shown in Figure (29) allows the selection of parallel sets of lines of sight for the recorded fringe pattern. The aperture stop at the focal plane of the lens filters out all but the lines parallel to the central angle. The resulting photographs are simpler to analyze since the angles are constant. In addition, fringe data from any z plane may be obtained from the single photograph. Mach-Zehnder interferograms, because of their single collimated source, provide the same type of interferogram.

The technique utilized for this investigation was an application of the lensless focusing capability of the hologram and is easier to achieve than the previous two methods. Figure (29a) shows a hologram being re-illuminated by a conjugate reference beam of small diameter. The real image of the test scene is formed in the same position as shown in Figure (3). Because the reconstruction beam is of small size, the illuminated portion of the hologram represents a small aperture. The resulting image has a large depth of field and a photographic film placed at the

image records the test scene. Additionally the rays may be focused in the most desirable plane by positioning the film plane, usually near the center of the disturbance. The lines of sight recorded represent the diverging bundle passing through the aperture position from the diffuser. The maximum angle of divergence at the edge of the test field encountered was $\pm 5^\circ$. For resolution greater than $\pm 5^\circ$, one must compensate for the variation. A subroutine of the computer program was written to accomplish this compensation, but the errors introduced by neglecting the bundle divergence have been acceptably small, and use of the routine has not been required.

The specular interference of coherent light from a diffuse surface causes a film graininess that is inversely proportional to recording aperture size [Tanner, 1967]. Although recording apertures of one millimeter were used, the speckle created no problems.

b. Data Reduction

To obtain the photographic interferograms, a camera back with viewing screen was placed in the position of the real image of the hologram as previously described (Figure 29a). The illumination of each position on the hologram corresponds to a particular effective aperture position. The hologram was positioned such that the desired set of front and rear grid lines lined up on the camera back viewing screen corresponding to the desired elevation and angle of view for the picture. Reference

to Figures (23) and (24) show grid alignments at $z = 3. \text{ cm.}$, $\xi = 0^\circ$ and $z = 1. \text{ cm.}$, $\xi = 0^\circ$ respectively. Polaroid P/N 55 film was used to record the image.

To obtain the graphical plot of the fringe number function, the negative was used in a photo enlarger to image directly upon graph paper. With the enlargement adjusted to match the scale of the paper, the positions of the maxima and minima of the fringes along the desired cross section were determined visually. The fringes were counted, and given a graphical elevation according to their number. Initial fringe numbering was arbitrary, commencing with a fringe well to one side of the field and proceeding across the field, the light regions representing integer values of the fringe number.

Figure (30) shows a typical working graph that was used for the $\xi = 5^\circ$ view of the tilted jet. The finite fringe reference line was drawn from the field edges and the curve was transcribed. Numerical values were then read from the curve at regular increments of radius (y') corresponding to the G-array size IMAX.

For the axisymmetric case the entire procedure was repeated for each level z plane to be solved. Since each aperture position on the hologram corresponds to a particular elevation and angle of view, a new picture was made for each horizontal z plane through the field.

For the asymmetric case, a new picture was taken for each angle ξ desired. When the angle desired was not available because of gaps in the holographic coverage, the curve was graphically interpolated from nearby curves on either side. Fringe curves were obtained in the standard manner for angles on each side. The two curves were then overlaid on a light table and an intermediate curve drawn at the proper relative distance.

IV. THE APPLICATION OF THE INTEGRAL INVERSION TECHNIQUE TO THE EXPERIMENTAL RESULTS

A. AXISYMMETRIC SOLUTION

The interferometric data from the hologram of the free jet at 60 psig. were reduced at eight positions out to $z = 2.0$ cm. in the manner described previously. Figure (31) shows the fringe curves obtained at $z = 0.5$ cm. and $z = 1.5$ cm. with their corresponding density solutions. The complete set of solutions are shown topologically in Figure (32). The solution compares quite well with the topological features of the free jet solutions obtained by Ladenberg, Van Voorhis, and Winckler [1949] in their very extensive interferometric analysis of free jets of one centimeter diameter. Figure (33) is an isodensity line plot of the obtained data. Qualitatively, the densities compare very well with the similar plot of the Winckler solution (Figure 34). Exhaust density in the central region

of the exit plane agrees within 0.2 mg/cc (5.3 percent of the maximum field density) and in the central region at $z/d=1$. (d = nozzle diameter) within about 0.1 mg/cc (2.8 %), rising to a maximum of 0.4 gm/cc (10.6%) between. At a relative radius of one-half, the difference in the two solutions runs from about 0.05 mg/cc (1.4%) at $z/d=0$. rising to about 0.2 mg/cc at $z/d=0.25$ and falling to 0.1 mg/cc at $z/d=1$. At the jet radius, the maximum differences fall to about 0.05 mg/cc.

B. NON-AXISYMMETRIC SOLUTION

Figure (35) shows the measured fringe curves obtained for the free jet at 60 psig. and eleven degrees of tilt, on a horizontal plane which intersects the jet axis at a point 0.5 cm from the nozzle. A total of nine angular positions were sampled, every other one being shown in the figure. The significant trend in these data is the shoulder increasing with decreasing angle on the left-hand side and with increasing angle on the right-hand side. A contour map of the data surface from $\xi = 0^\circ$ to $\xi = 90^\circ$ is shown in Figure (36). Since not all data could be obtained simultaneously, the run number from which the holograms used were obtained is shown. The non-regularities appear to be the effects of errors introduced in the correlation of angular views taken at different times. A data smoothing technique used by Maldonado, et. al. on this data plane was that of fitting smooth curves to the plotted points and adjusting the data to fit the

smoothed curves. For this experiment, however, the data were used without smoothing. Figure (37) shows a sketch of the tilted plane through the jet, with the five lines shown along which solutions were obtained. Figure (38) shows the solution at the five diametric cross sections from $\xi = 0^\circ$ to $\xi = 90^\circ$. The effects of the shoulder variation in the input data show up here as variations in the position and size of the density "valley" which one can see in the axisymmetric topological plot of Figure (32). The comparison of the solution from the tilted plane at $\xi = 0^\circ, 45^\circ$, and 90° is made with the solutions taken from the axisymmetric experiment in common plots of the two functions. The shoulder and valley features of the two solutions appear consistent. The central "hill," is consistent in the two solutions, to the point of showing a common inflection in the slope near radius ± 0.5 . The outer five points on either side of the 90° curve include convergence errors arising from failure of their series evaluations to converge. The maximum difference in the two solutions is about 8 percent, although the mean deviation is much less.

C. DISCUSSION OF THE ERRORS

1. Numerical Inversion Errors

Several function shapes were investigated with the axisymmetric inversion to determine the effect of inversion parameters upon the accuracy of the inversion. Errors resulted from two basic causes: one

was the failure of the series evaluation to converge within the maximum number of terms for which computed coefficients B and D were available; the other was the approximation caused by representation of the continuous function g by a discrete set of values.

Convergence of the series evaluation is fastest in regions where the functional shape matches a gaussian. As few as five terms of the K series were sufficient to evaluate the gaussian function to within one percent everywhere. The asymmetric test of Figure (15) of the displaced gaussian used only a maximum of 25 terms, corresponding to $MLIMIT=5$, $KLIMIT=5$ to achieve accuracy to within 0.8 percent. The opposite extreme occurs when functions with steep gradients or discontinuities are inverted. For example, in the test of Winckler's function (Figure 12), the region near the discontinuity required up to 1700 terms for convergence; at the discontinuity itself, convergence was not achieved with 2000 terms. For functions with such discontinuities, or for experimental data inversions where there are normal irregularities in the data, the center position (at radius zero) often fails to converge, resulting in error at that position of up to 10 percent. When convergence has failed, however, the index count of the output information clearly indicates the failure, and this point value may be simply neglected. Interpolation of the missing value from nearby convergent points normally reduces the error to within two percent.

Decreasing the number of points of the data plane reduces the significance of the higher order modes of the series expansion. This rounds normally smooth functions, and causes oscillations in functions with discontinuities. For example, the step function of Figure (11) had a maximum error of 6.2 percent with $IMAX = 200$, and maximum error of 12.7 percent with $IMAX = 100$. Additionally, the inversion at $IMAX = 100$ caused a severe oscillation over most of the step.

Since there is no mathematical requirement in the inversion for regular spacing of the data grid, modification of the numerical equations could be made to accommodate finer mesh sizes in the regions of special interest.

2. Errors in the Data

The errors in the final solution are mostly due to errors in the data. There are several independent sources of data errors, covered here individually.

Probably the greatest source of error in the data arises from the unsteadiness of the jet flow. The three apparent perturbations in the solution of Figure (33) correspond to 0.1 mg/cc and 0.2 mg/cc respectively. Based upon the maximum density in the field, these correspond to 2.8 and 5.6 percent errors. Variations in the flow between the runs are considered responsible for the major fluctuations evident on the data plane shown in Figure (36). The asymmetric solution tends to spread

errors over the whole field, reducing their effect by statistical averaging.

Graphical positioning of the interferogram and scale matching in the photo-enlarger to graph paper step is accurate to within two percent. However, a two percent position error might be magnified to a five percent density error in regions of normally high density gradient. The accuracy to which one can determine the fringe number position in reading the interferogram is within $\pm 1/8$ th. of a fringe, or within about 1.5 percent of the maximum fringe number of the flow interferograms studied. Winckler has provided an analysis of the relative merits in reading several different fringe arrangements to minimize the fringe number error. Figure (39) shows the inverted solution of the axisymmetric test case at $z = 0.75$ cm. with a second solution superimposed. The second solution has been made from data with added random error of 0.0625 standard deviation, corresponding to $\pm 1/8$ th. fringe number error in reading the data. The resulting error varies with a maximum of 2.1 percent.

The background finite fringe spacing is assumed to be constant through the field. Figure (40) illustrates the type of error that could exist by the failure of linearity. An error curve that starts at zero at the boundaries of the flow and rises to one-half fringe in the number

would yield a maximum solution error of 0.18 mg/cc at the center, or about 5.0 percent for the axisymmetric solution.

It is estimated in the solution presented herein that probable errors are less than 8 percent everywhere, corresponding to the maximum difference in comparison of the two solutions in Figure (38).

V. SUMMARY

A. CONCLUSIONS

A self-consistent method has been demonstrated for the acquisition of interferometric data about a three-dimensional density field of one plane of symmetry. The data set has been successfully inverted by the application of a recently developed mathematical inversion scheme and shown to be reliable to within eight percent of the density range. The mathematical model has been tested for realistic density patterns, representing supersonic wakes and jets. The pulsed laser method of holographic interferometry can be successfully applied in environments relatively hostile to normal interferometry. There are no inherent restrictions to the application of the method to generally asymmetric fields. The optical arrangement of the system is highly flexible and can be modified for interferometric studies of wakes, rockets, turbo-machinery flows and other hostile, or highly transient events.

B. RECOMMENDATIONS

Most of the errors introduced in the solution were the results of the data-reduction methods used. The use of an appropriately designed densitometer for determining fringe locations on the negatives might improve the accuracy of fringe location and merits investigation. Measurable features on some object in the test area should be incorporated for accurate scaling and positioning of the data coordinates.

Experimental improvements could be accomplished as follows.

An effort should be made to increase the field of view from the diffuser plate to provide increased angular coverage. The use of heavy, naturally damped mounts should be provided for the beam splitters for better control of the spacing of finite background fringes.

C. ACKNOWLEDGEMENTS

The writer wishes to gratefully acknowledge Dr. D. J. Collins for his sponsorship, guidance and assistance during the course of this investigation; Dr. A. E. Fuhs for his initial encouragement in the field; Drs. R. L. Kelly, T. H. Gawain, L. V. Schmidt, and G. D. Sackman for their time and support during the period; Dr. A. B. Witte, of TRW Systems, Inc., for his initial mention of Maldonado's work; the technical staff of the Department of Aeronautics under R. Besel and T. Dunton, particularly N. Leckenby and G. Gulbranson, for their able assistance; B. Taylor, of

the Department of Physics, for the loan of many little lenses and mirrors; Mrs. Kathryn Todd, for her considerable effort in the final preparation; and my wife and family for their noble patience and encouragement.

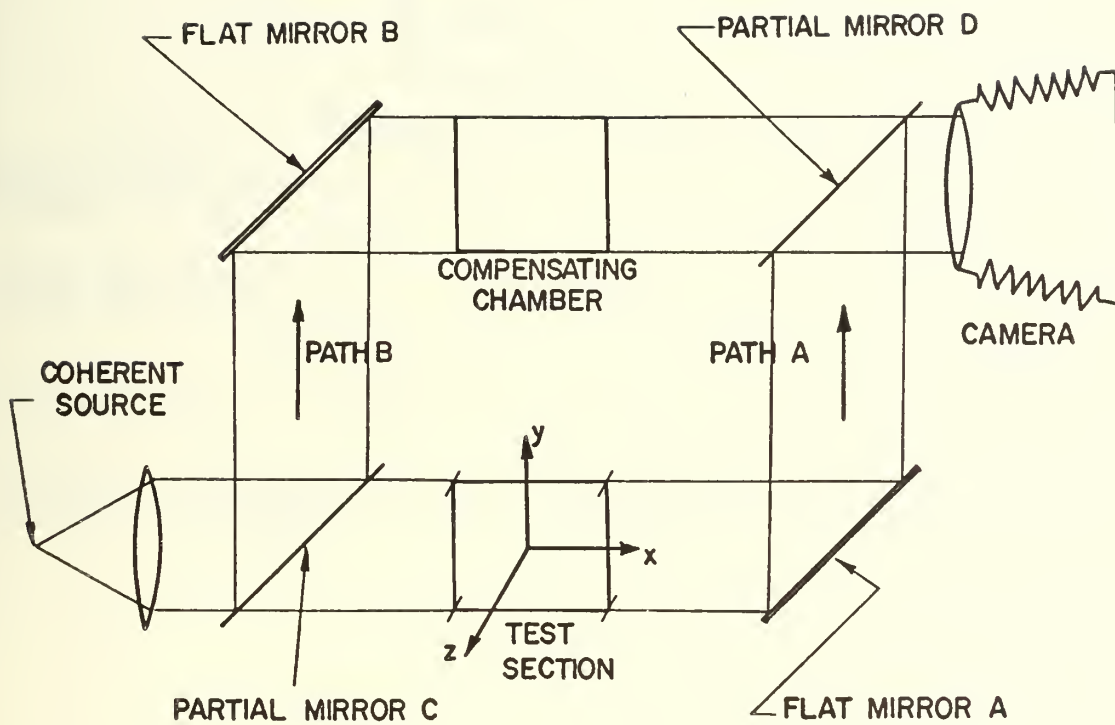


FIGURE 1: THE SCHEMATIC ARRANGEMENT OF A MACH ZEHNDER INTERFEROMETER.

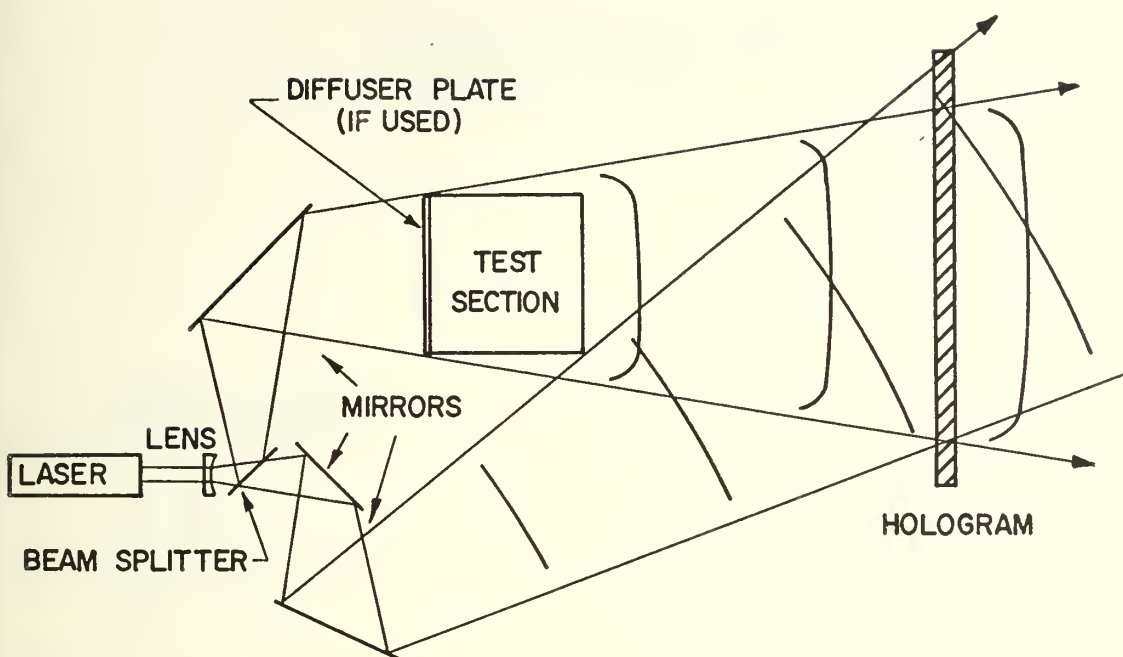


FIGURE 2: PRODUCTION OF A HOLOGRAM OF A TRANSILLUMINATED OBJECT.

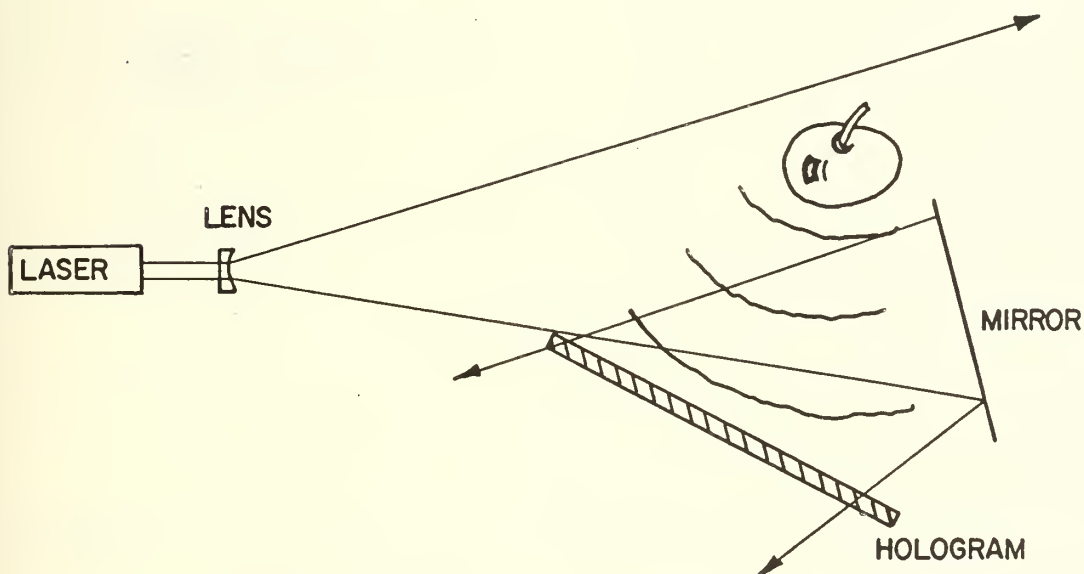


FIGURE 2a: PRODUCTION OF A HOLOGRAM OF A DIFFUSELY REFLECTING OBJECT.

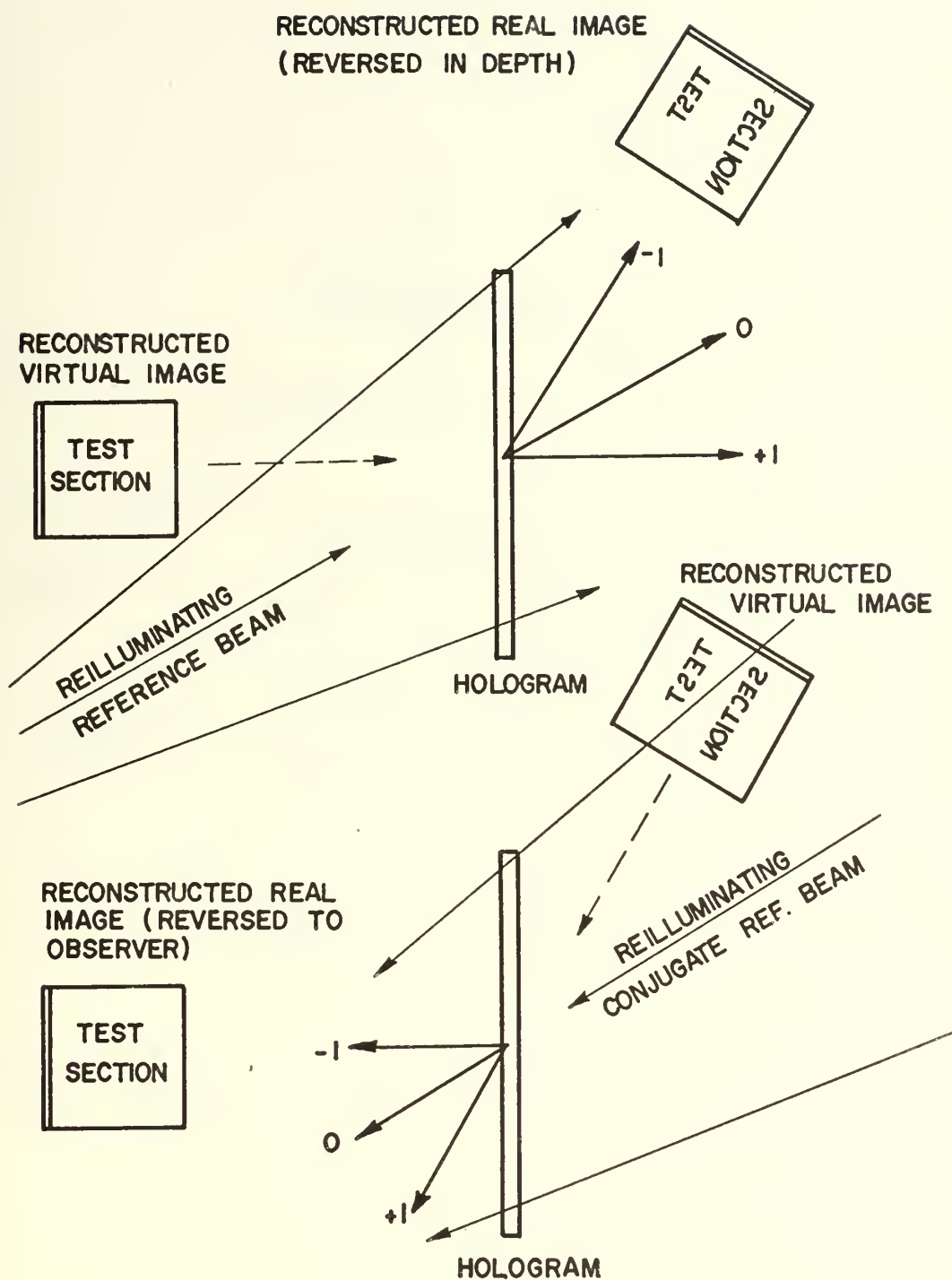


FIGURE 3: SHOWING IMAGES CREATED BY RECONSTRUCTION FROM EITHER SIDE.

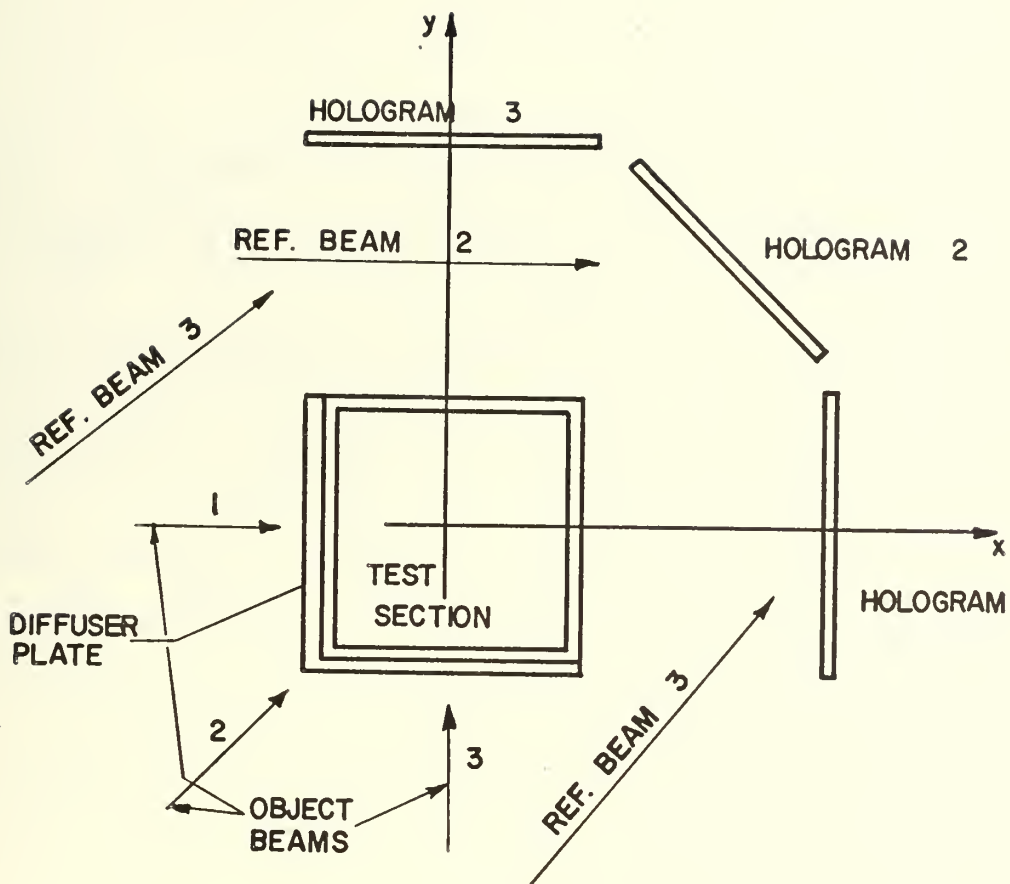


FIGURE 4: HOLOGRAM ARRANGEMENT FOR WIDE ANGULAR RANGE OF VIEWS.

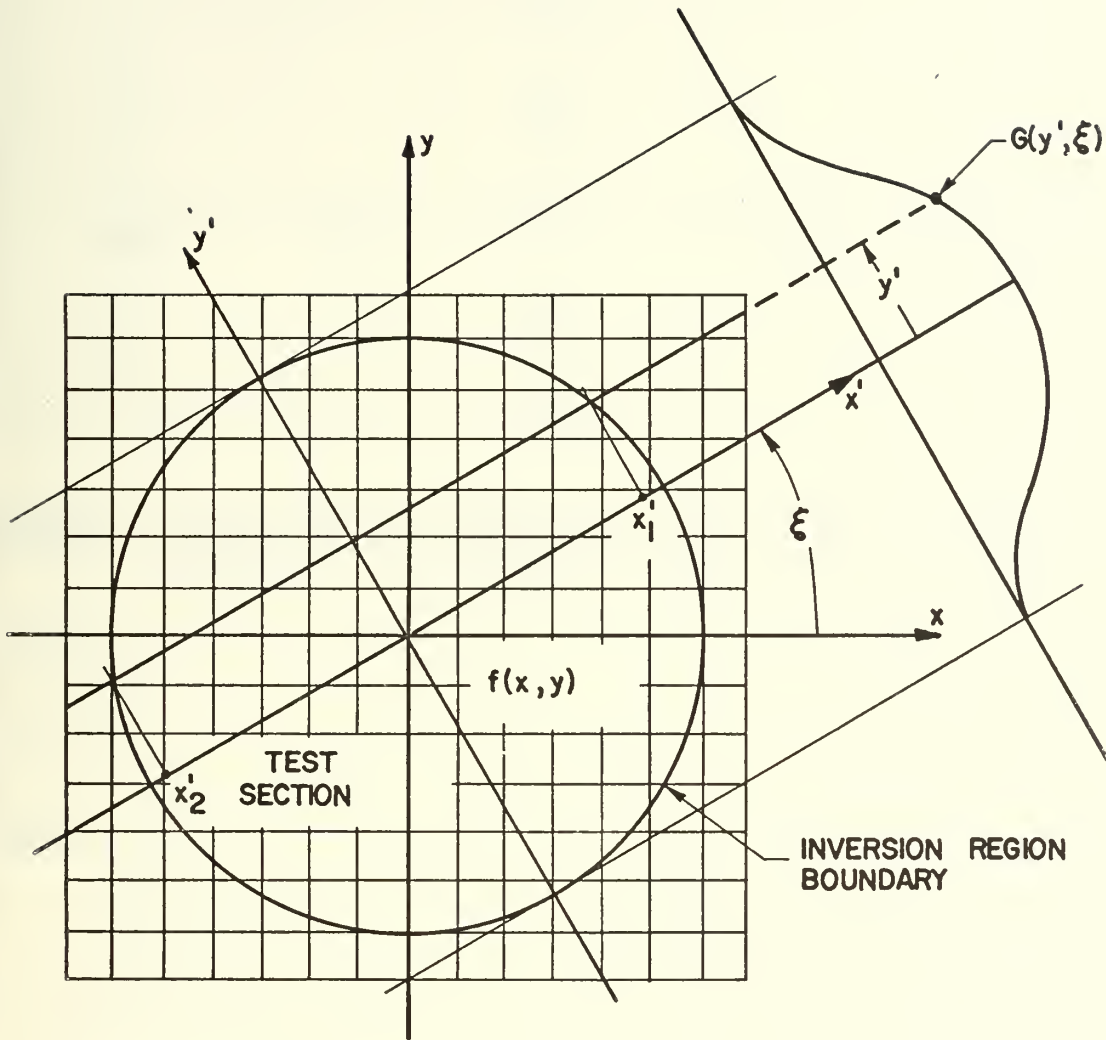


FIGURE 5: BASIC COORDINATE SYSTEM OF INVERSION PROCESS.

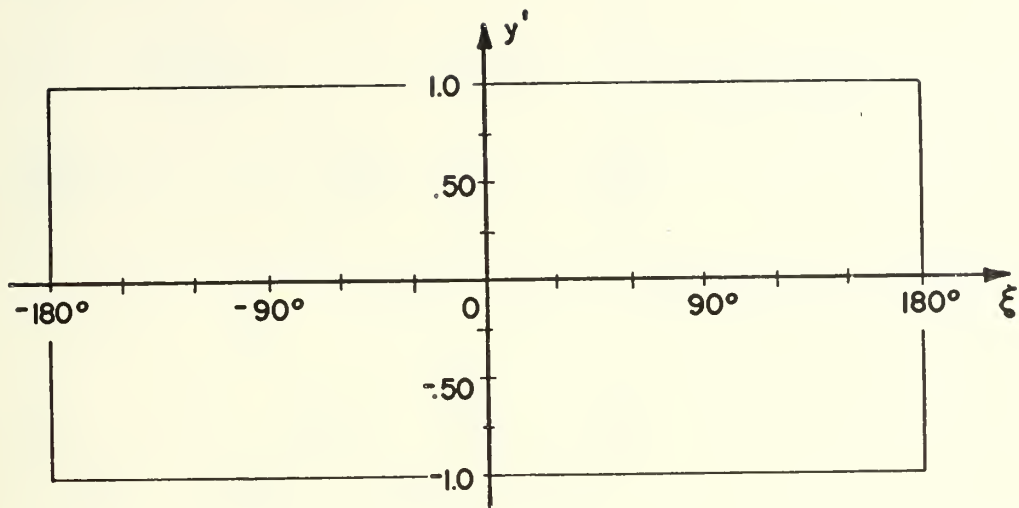


FIGURE 6 : DOMAIN OF THE FUNCTION G OVER WHICH ORTHOGONAL INVERSION IS PERFORMED IN THE GENERAL CASE :

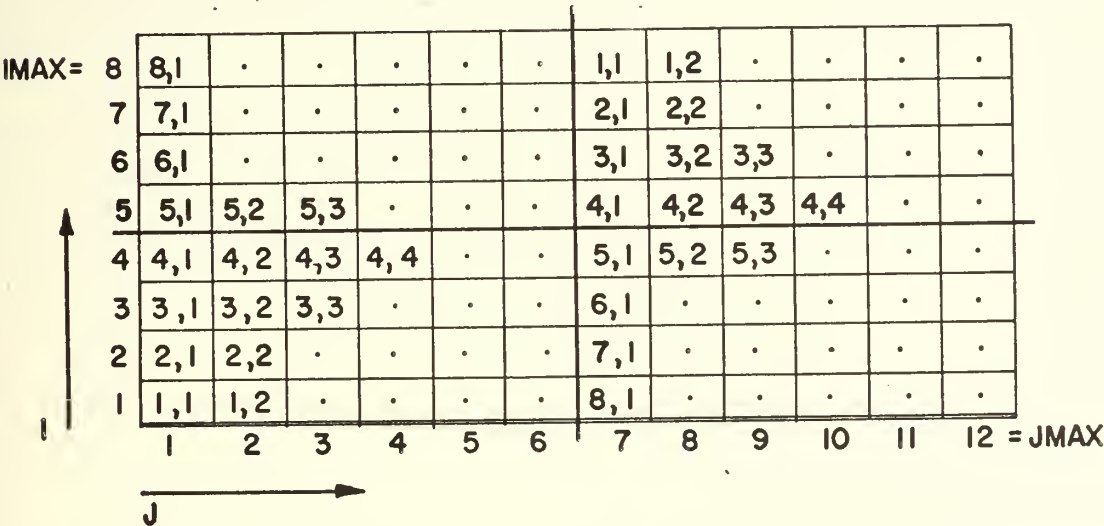


FIGURE 7 : DISCRETE ARRAY OF G VALUES CORRESPONDING TO DOMAIN OF FIGURE 6. SHOWING DUPLICATION OF THE FUNCTION.

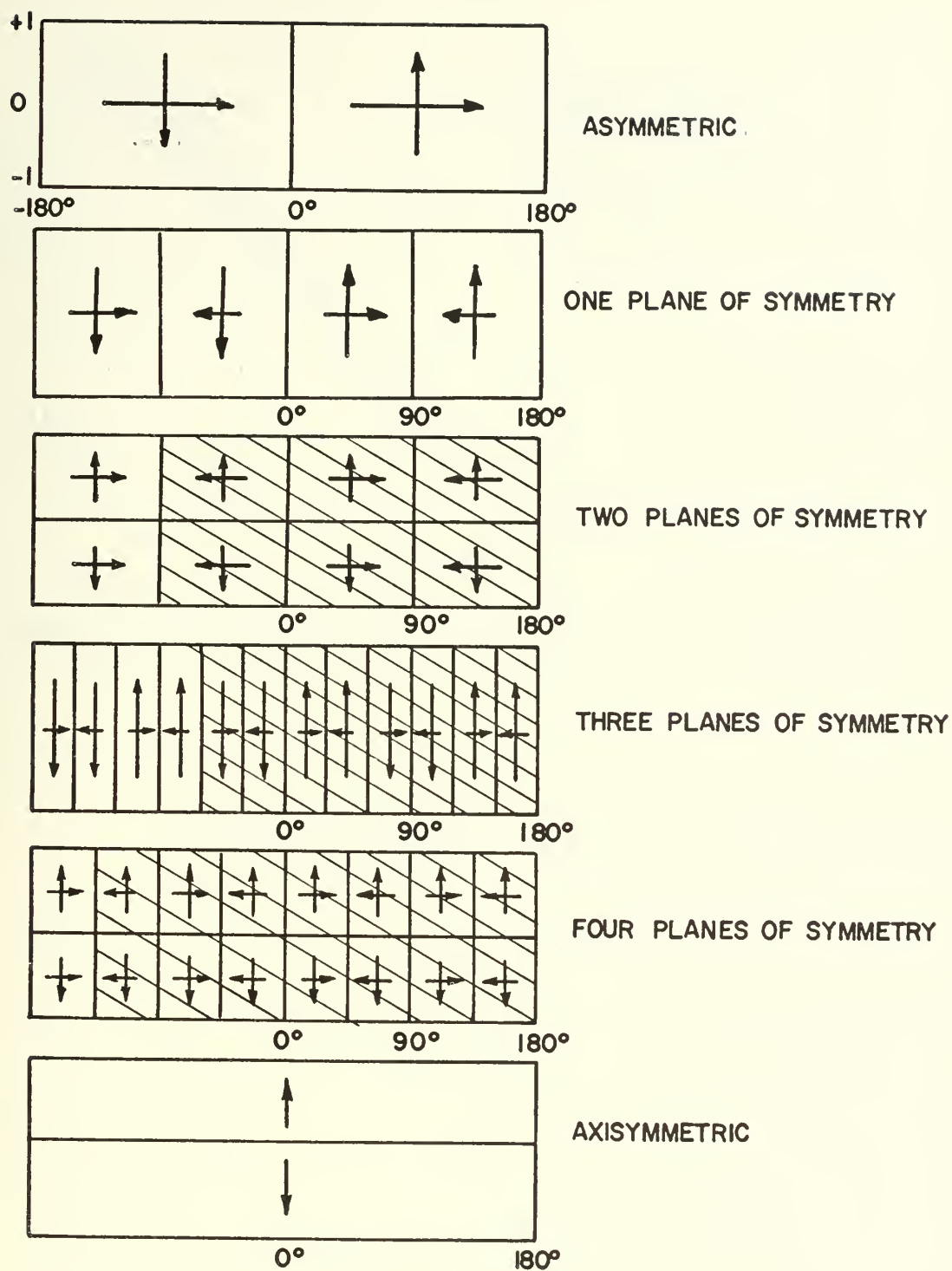


FIGURE 8. THE EFFECTS OF SYMMETRY OF THE FUNCTION F UPON THE REPEATABLE CHARACTER AND INTERVAL OF ORTHOGONALITY IN THE G FUNCTION.

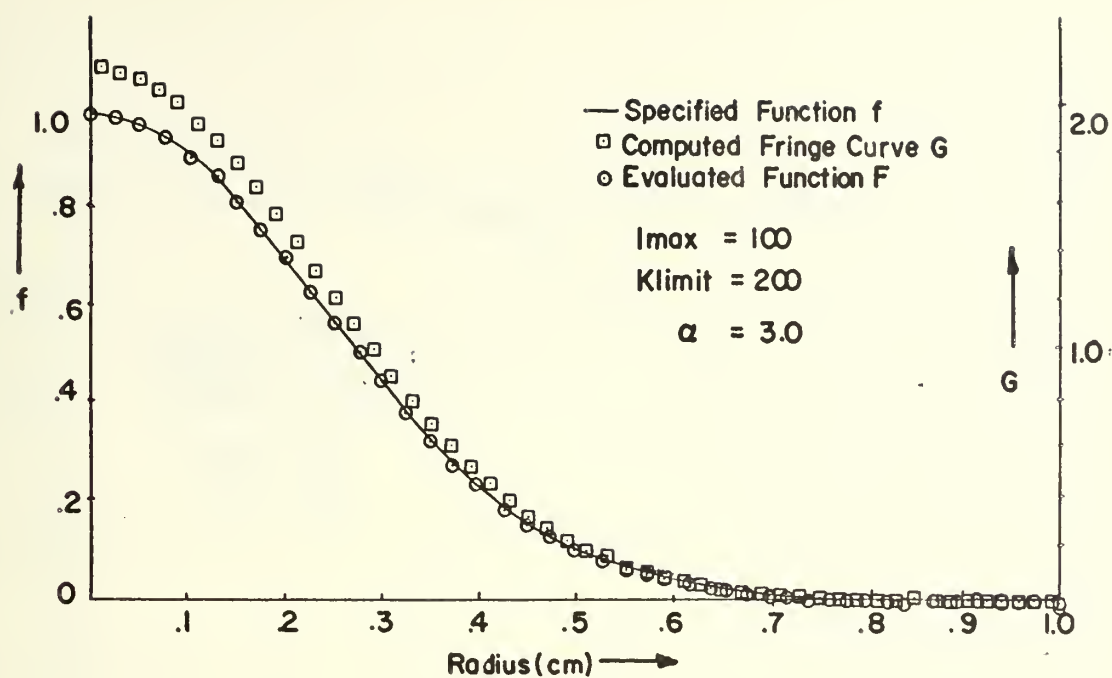


FIGURE 9. AXISYMMETRIC TEST CASE — GAUSSIAN FUNCTION

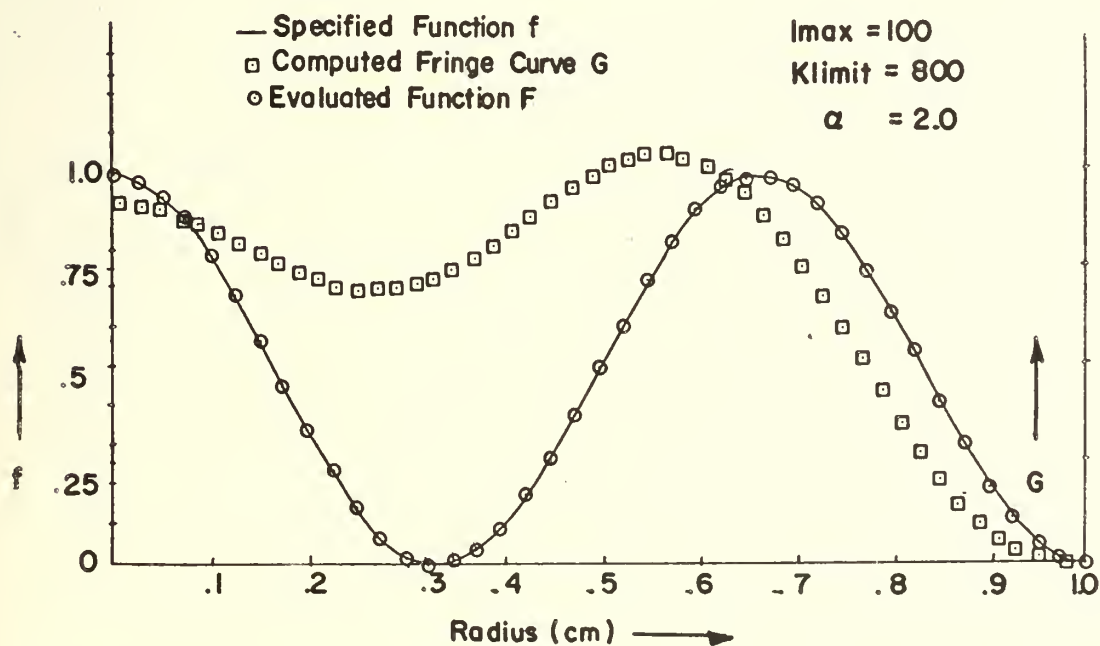


FIGURE 10. AXISYMMETRIC TEST CASE — $(\cosine)^2$ FUNCTION

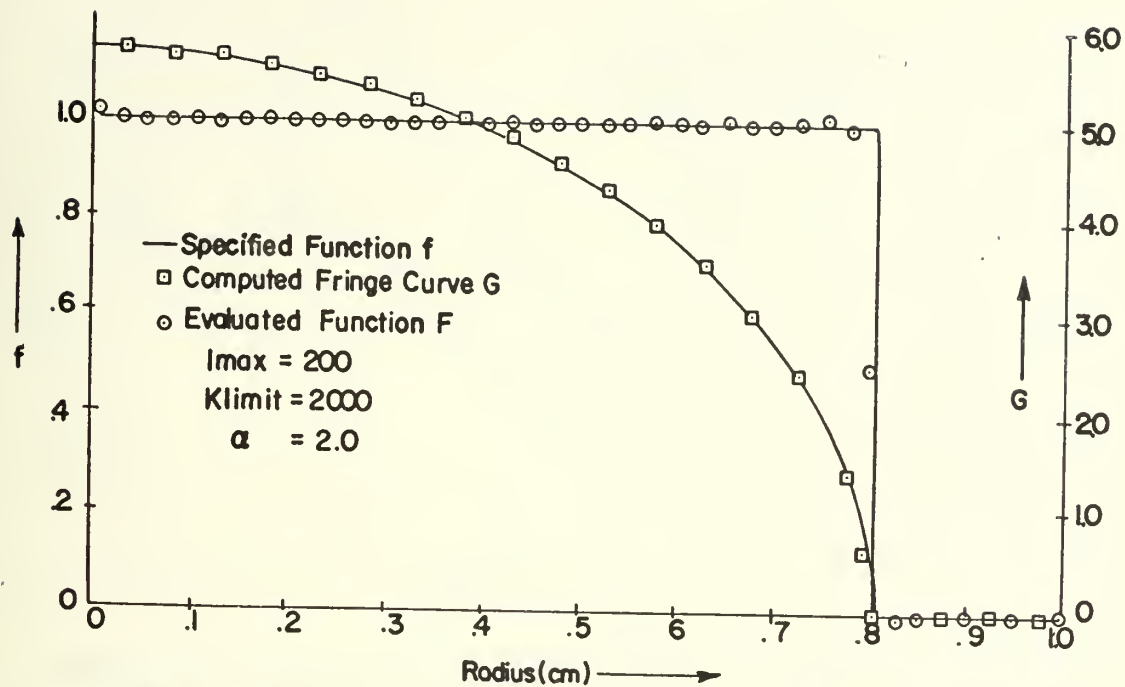


FIGURE 11. AXISYMMETRIC TEST CASE — STEP FUNCTION

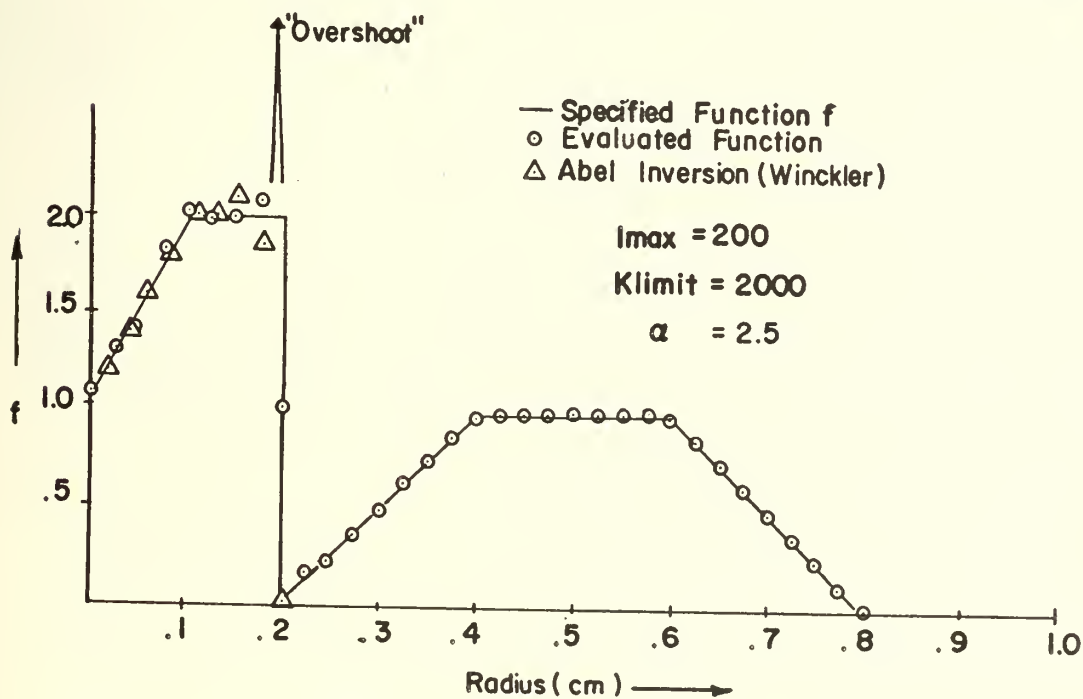


FIGURE 12. AXISYMMETRIC TEST CASE — WINCKLER'S TEST

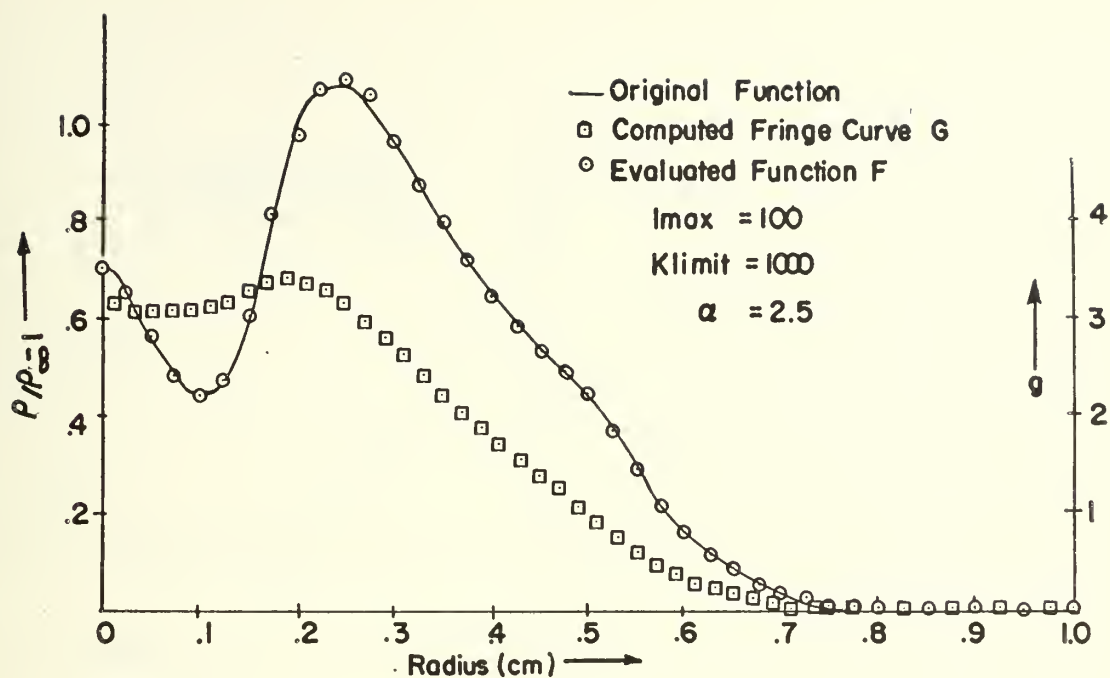


FIGURE 13. AXISYMMETRIC TEST CASE — FREE JET FLOW #1

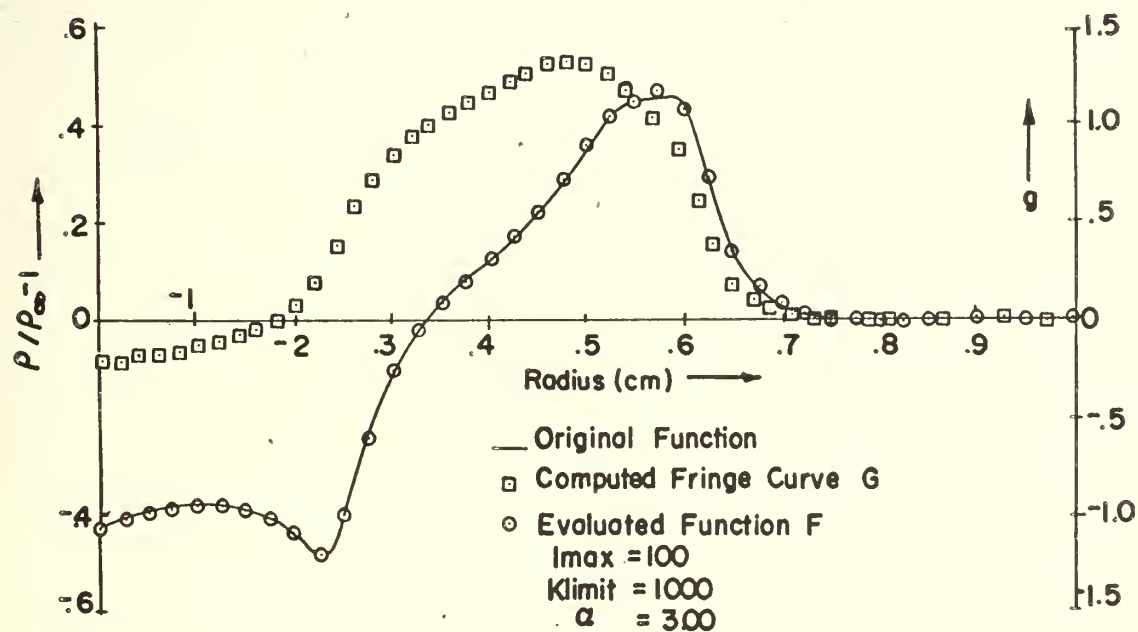


FIGURE 14. AXISYMMETRIC TEST CASE — FREE JET FLOW #2

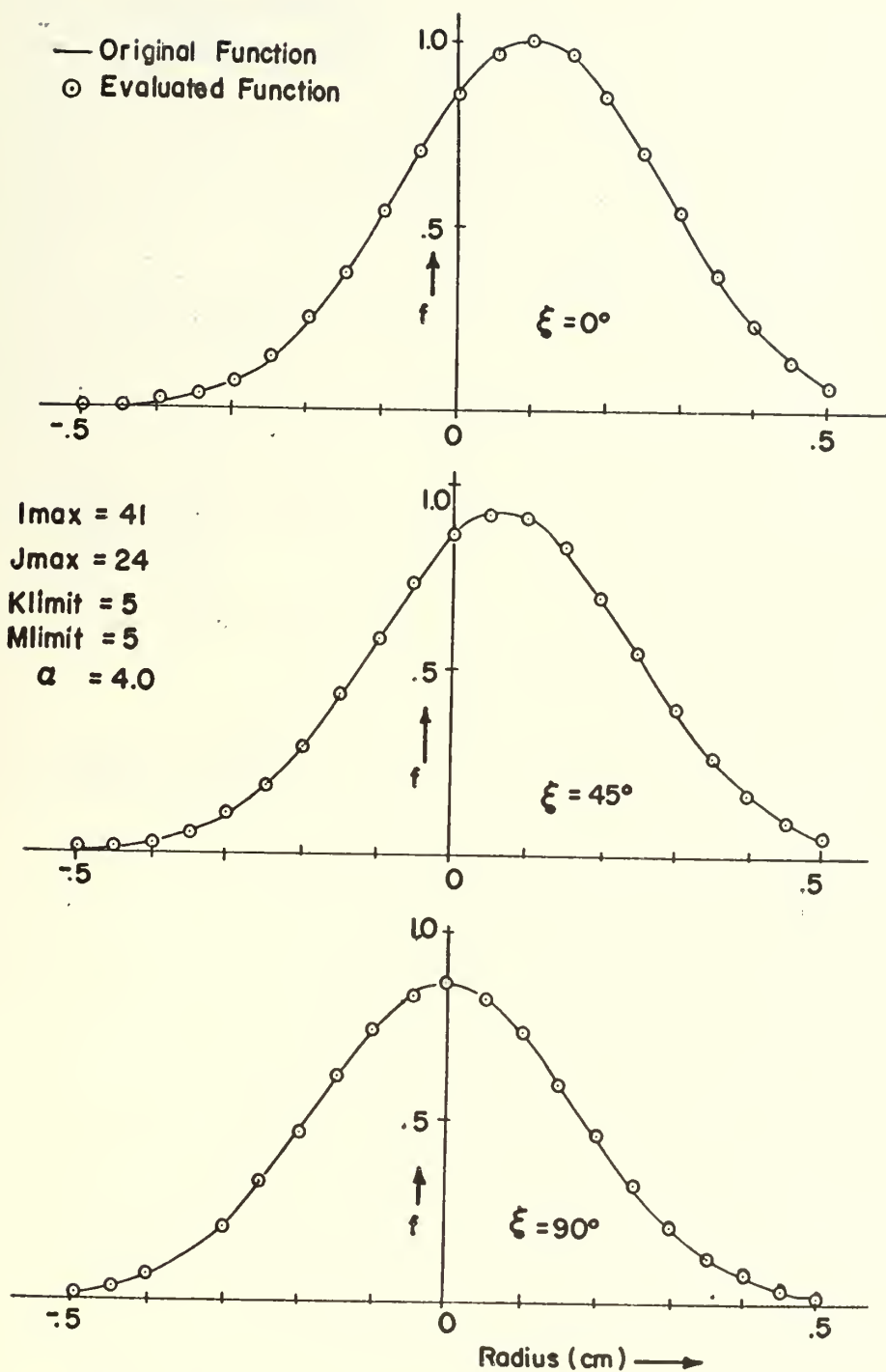


FIGURE 15. TEST INVERSION — DISPLACED GAUSSIAN

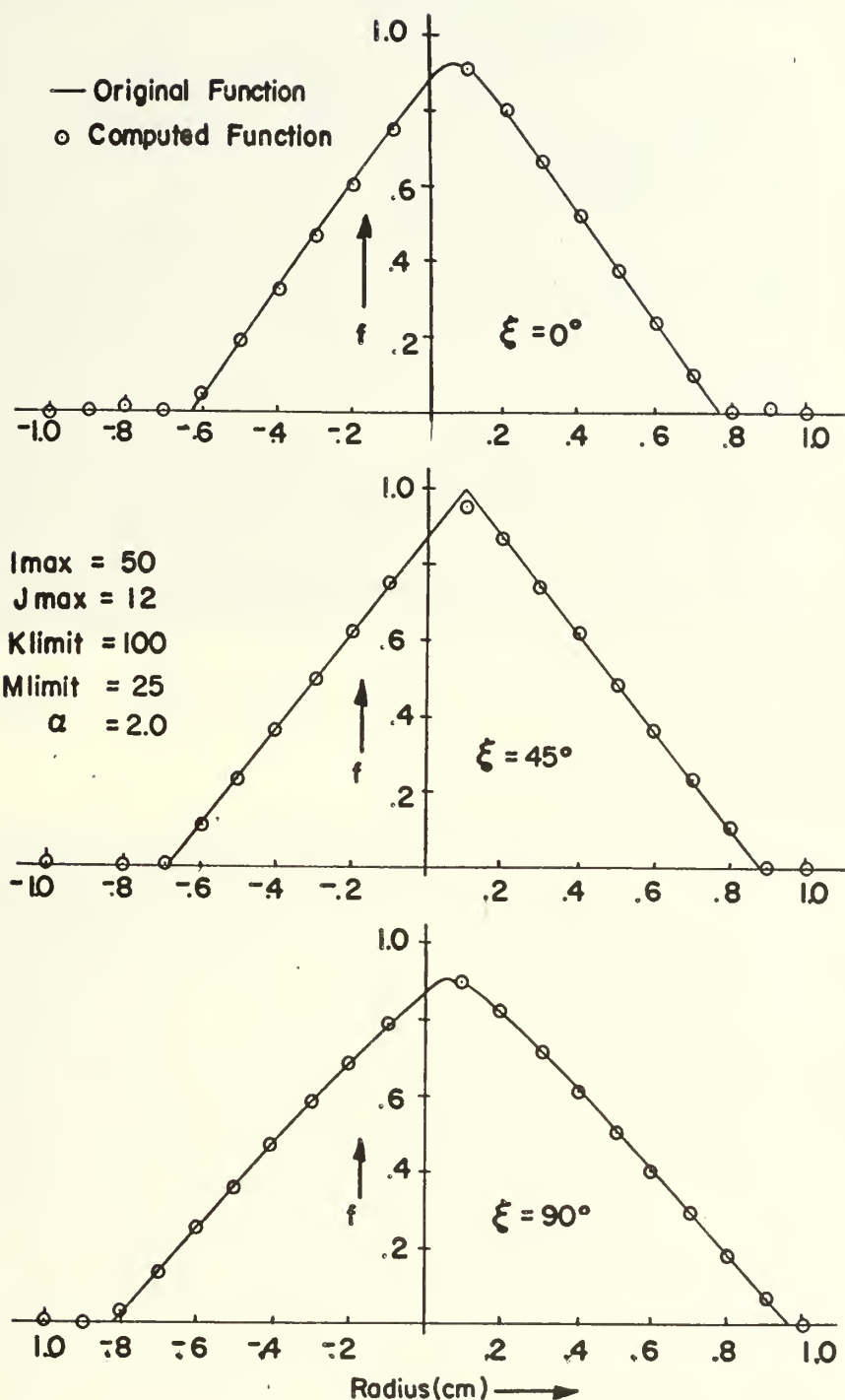


FIGURE 16 ASYMMETRIC TEST CASE—ELLIPTICAL CONE,

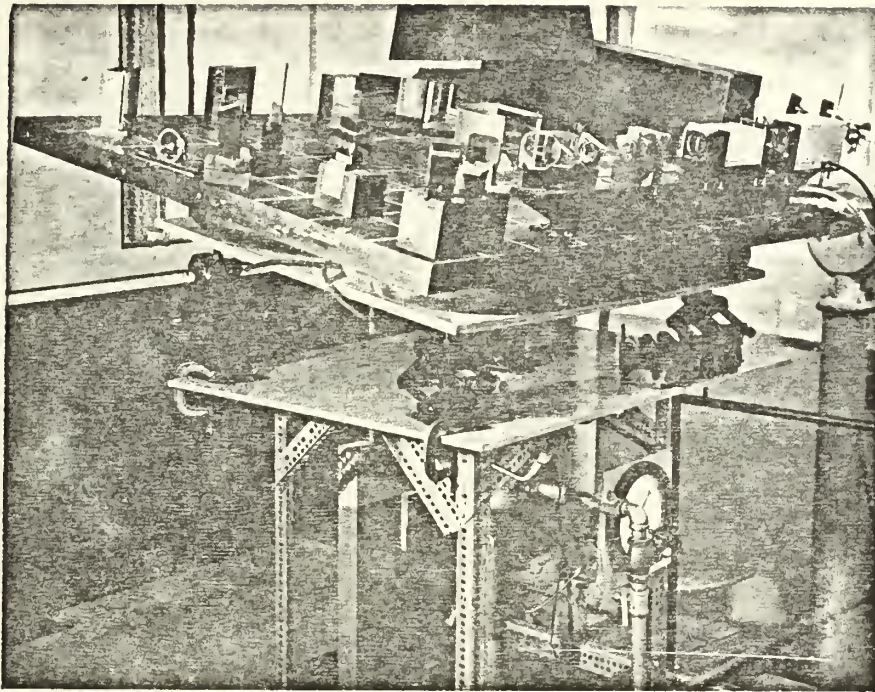


FIGURE 17. PHOTOGRAPH OF THE HOLOGRAPHIC TABLE

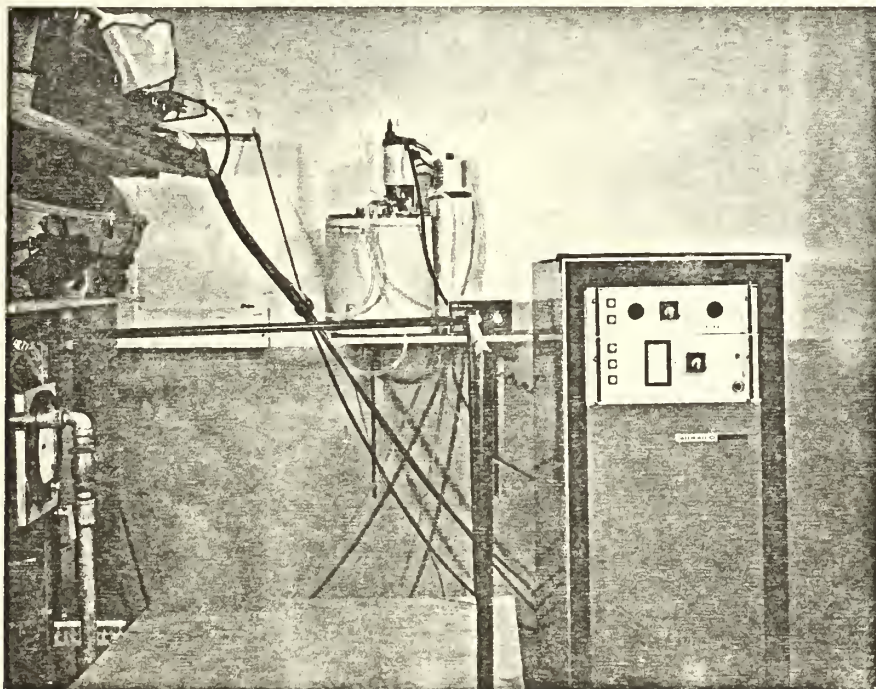


FIGURE 18. PHOTOGRAPH OF THE LASER POWER SUPPLY

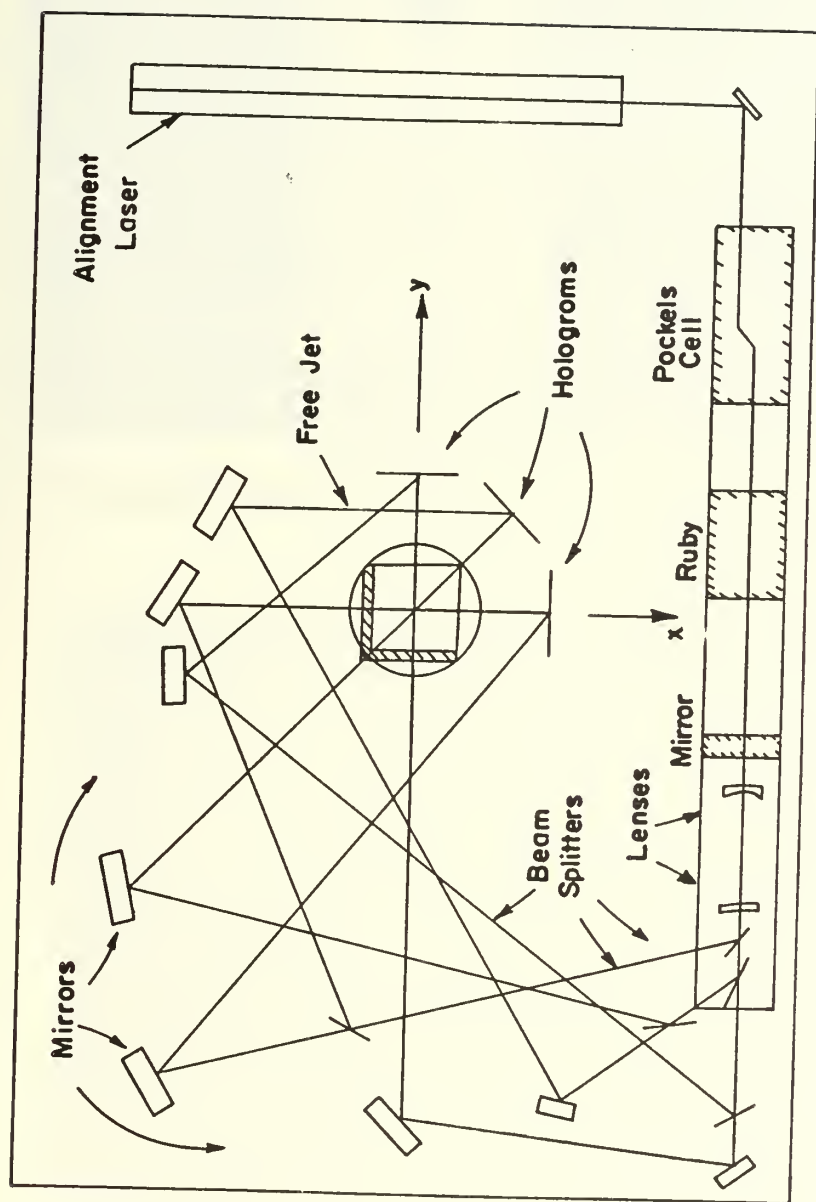


FIGURE 19. SCHEMATIC ARRANGEMENT OF HOLOGRAPHIC TABLE

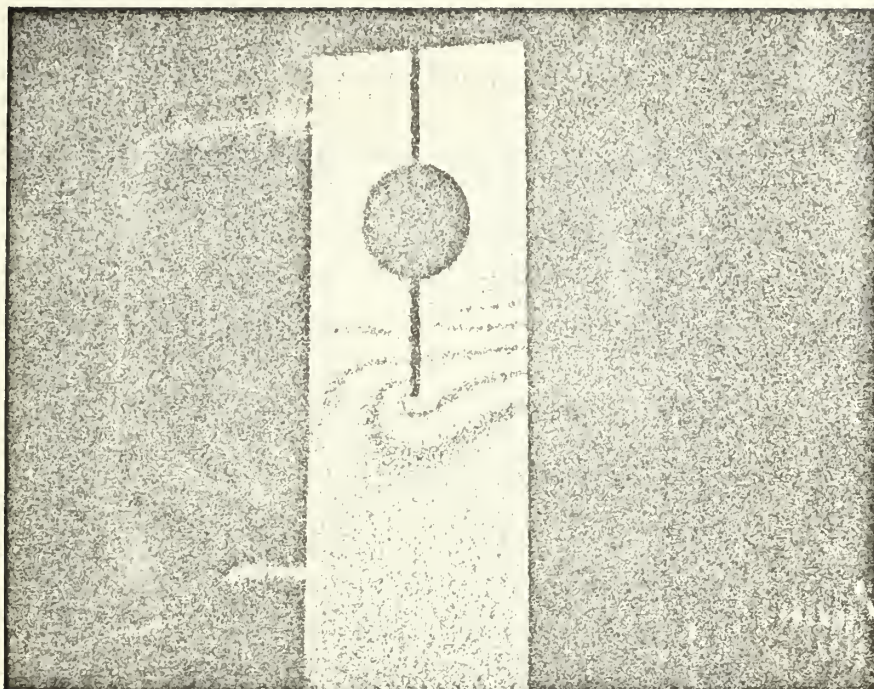


FIGURE 20. SURFACE INTERFEROGRAM OF A CLAMP UNDER STRAIN.

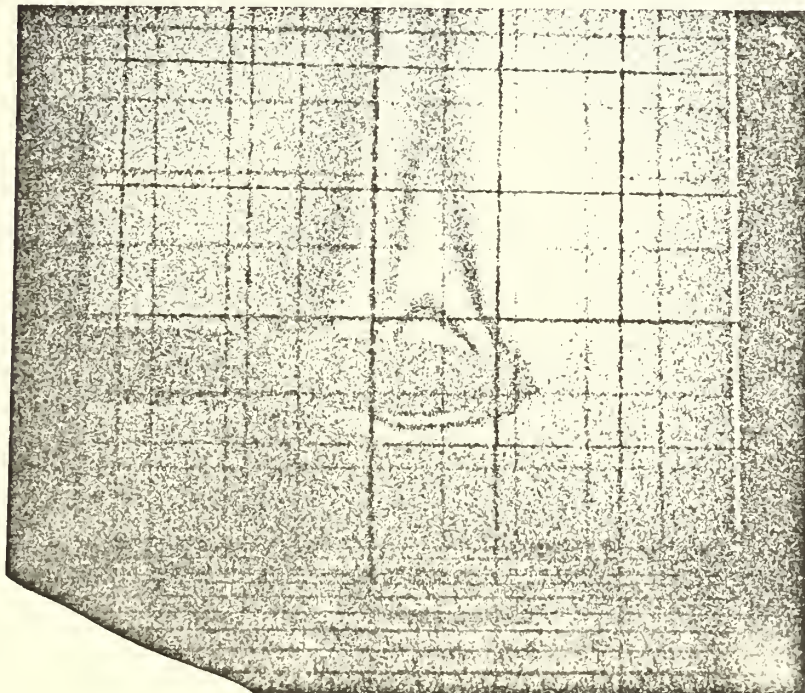


FIGURE 21. INTERFEROGRAM OF A CIGARETTE.

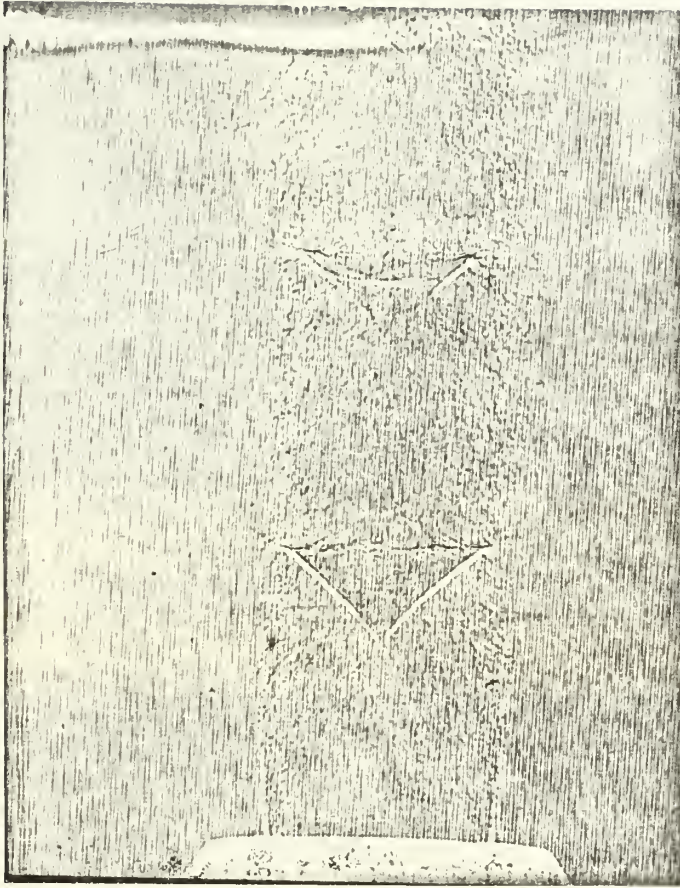


FIGURE 22. DIRECT PRINT OF A HOLOGRAM (DARK FIELD)
SHOWING SHADOWGRAPH OF A FREE JET AT
35 PSIG.



FIGURE 23. AXISYMMETRIC FREE JET, 60 PSIG. $Z=3.0$ CM

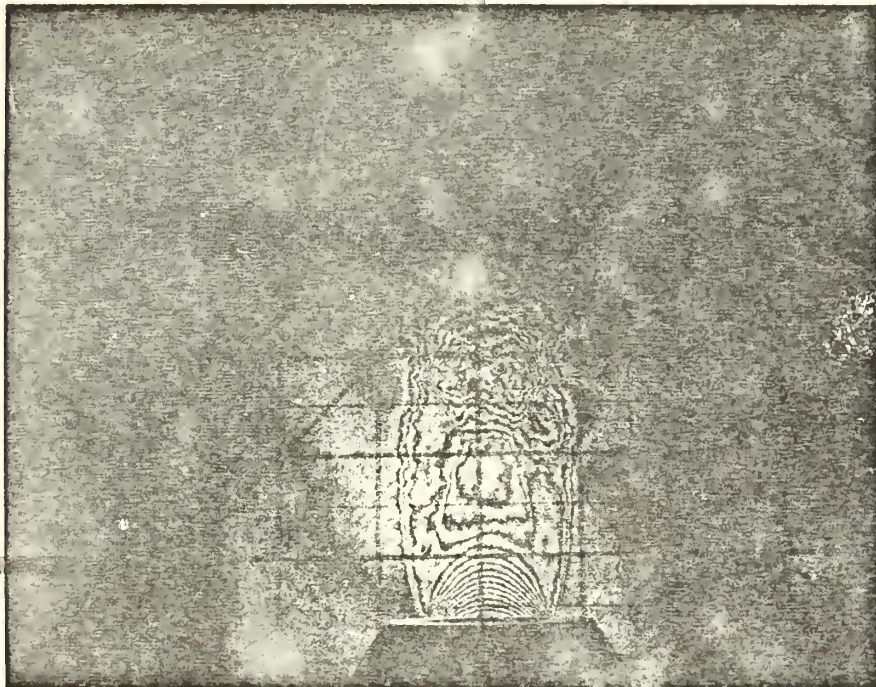


FIGURE 24. AXISYMMETRIC FREE JET, 60 PSIG. $Z=1.0$ CM.

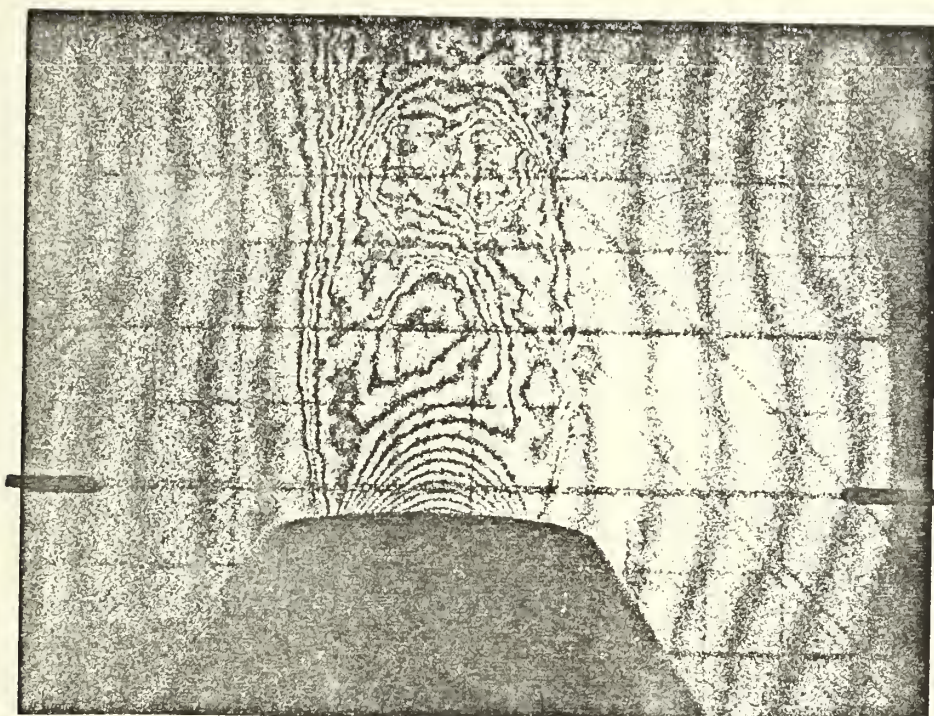


FIGURE 25. ASYMMETRIC SECTION OF A FREE JET, 60 PSIG.,
 $Z = .5 \text{ CM.}$, 11° TILT, $\xi = 5^\circ$



FIGURE 26. ASYMMETRIC SECTION OF A FREE JET, 60 PSIG.,
 $Z = .5 \text{ CM.}$, 11° TILT, $\xi = 85^\circ$

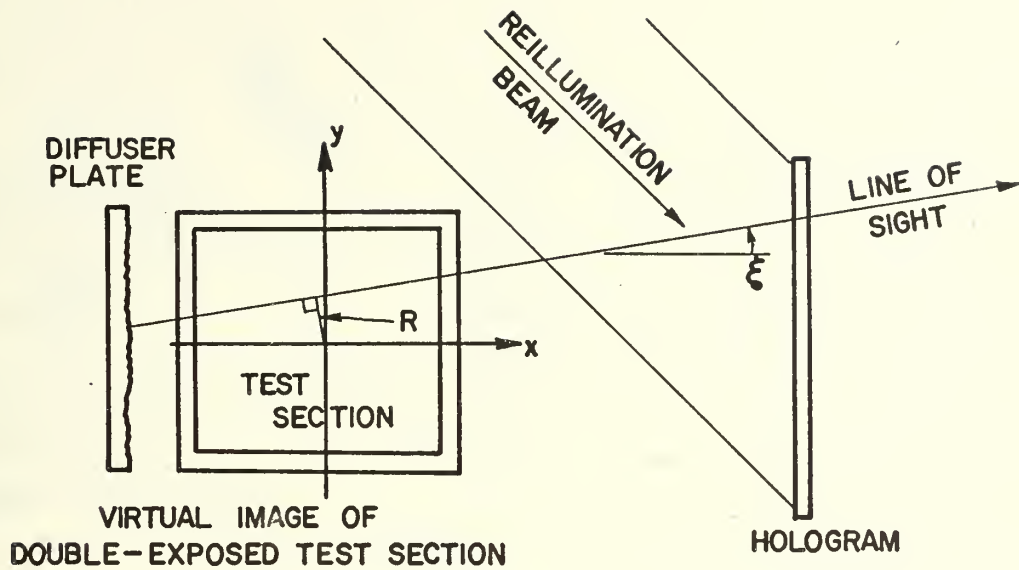


FIGURE 27: (R, ξ) COORDINATES FOR A LINE OF SIGHT THROUGH THE RECONSTRUCTED TEST SECTION

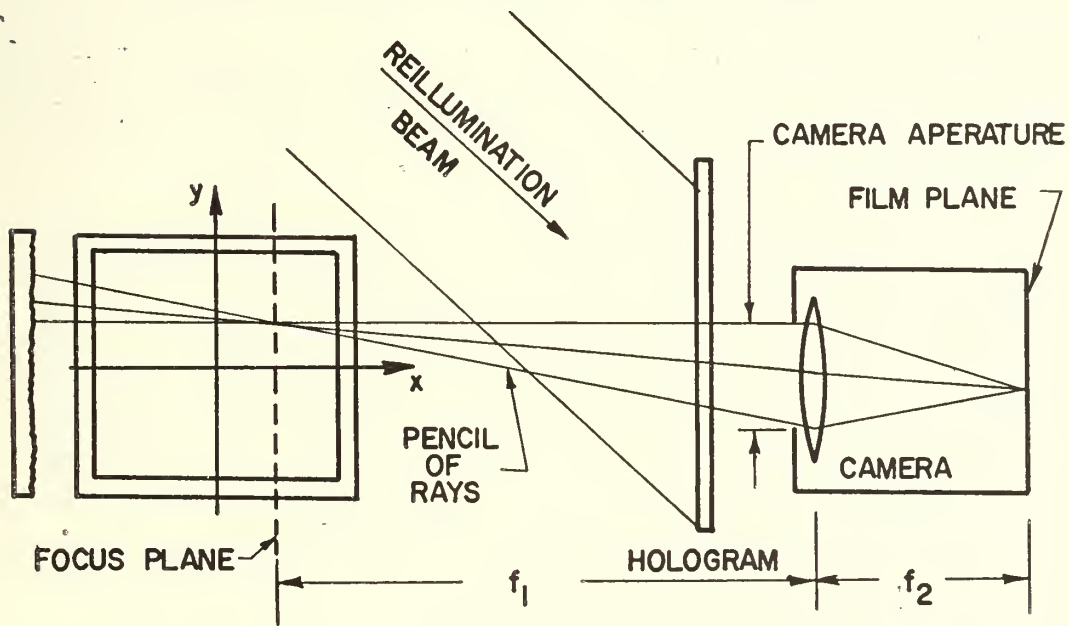


FIGURE 28: EFFECT OF APPERATURE SIZE AND FOCUS PLANE POSITION ON PENCIL SIZE OF RAYS ABOUT A LINE-OF-SIGHT RECORDED BY CAMERA.

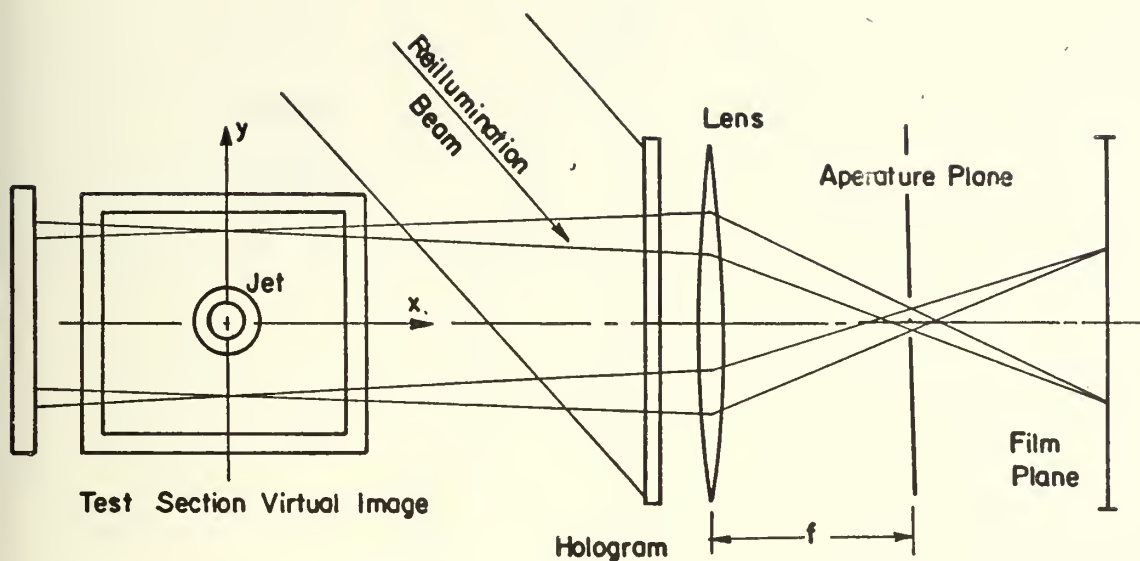


FIGURE 29 SPATIAL FILTERING TECHNIQUE FOR SELECTING PHOTOGRAPH OF CONSTANT ANGLE LINES OF SIGHT

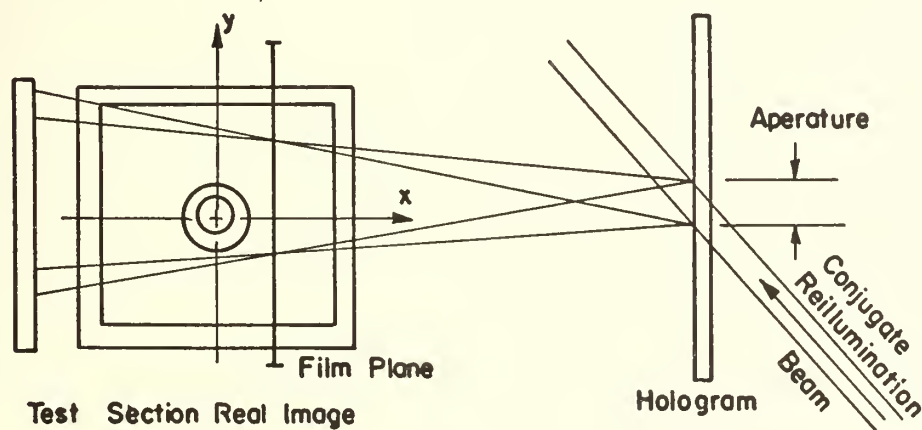


FIGURE 29a LENSELESS PHOTOGRAPHIC TECHNIQUE USING CONJUGATE REILLUMINATION BEAM OF SMALL DIAMETER

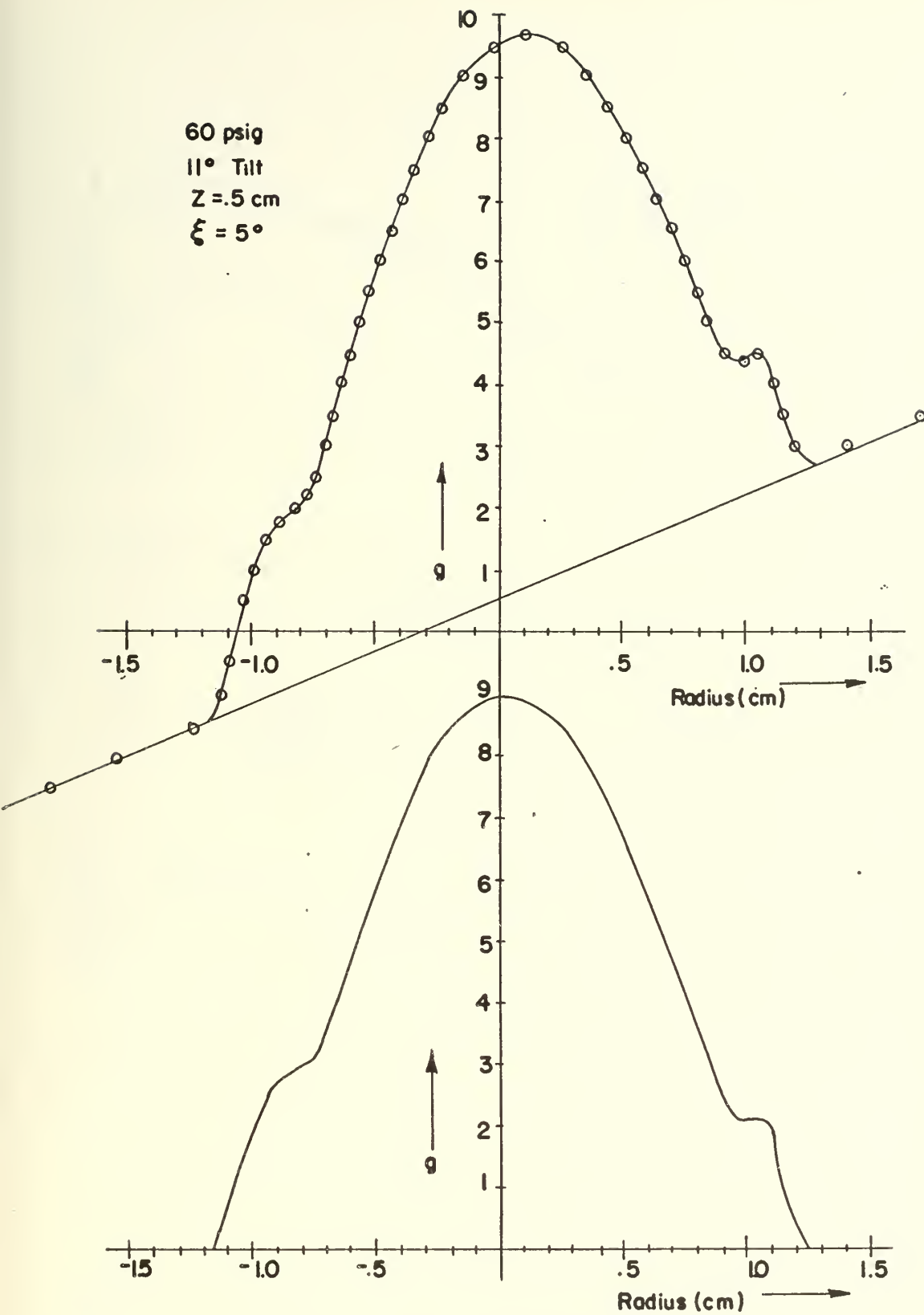


FIGURE 30 EXAMPLE GRAPHICAL WORK SHEET CURVES

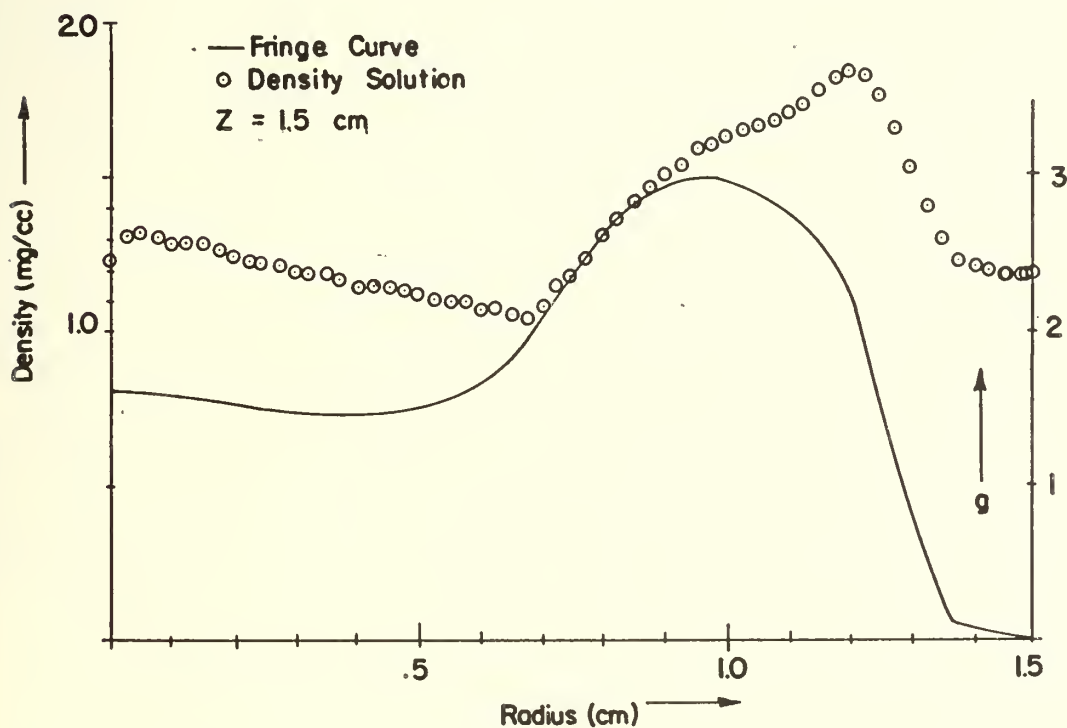
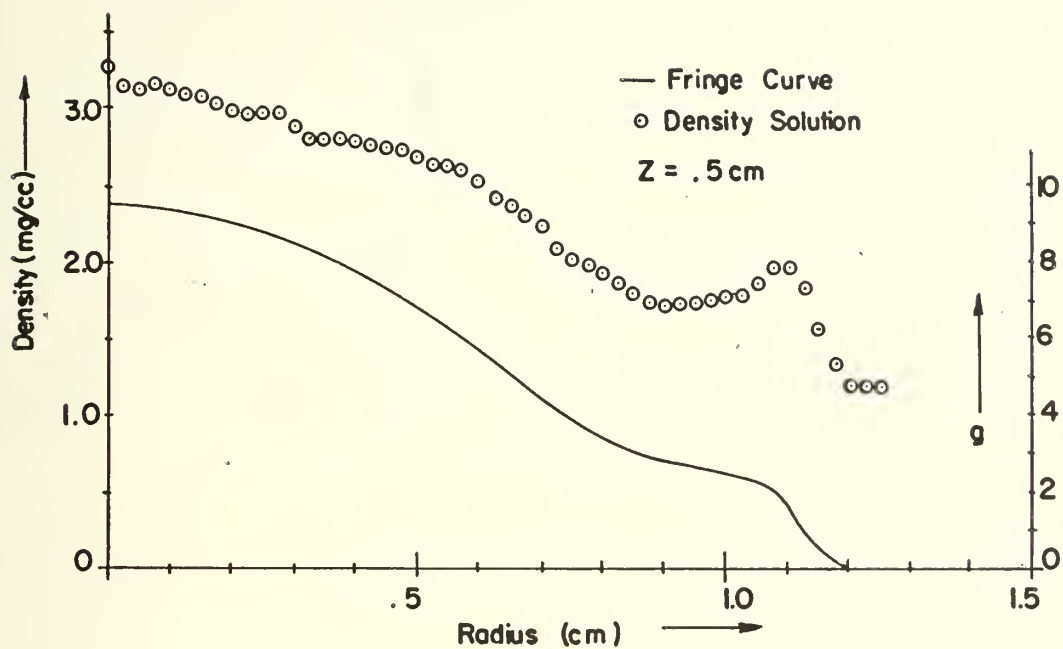


FIGURE 31 FRINGE CURVES AND CORRESPONDING SOLUTIONS FOR TWO STATIONS, AXISYMIC FREE JET, 60 PSIG

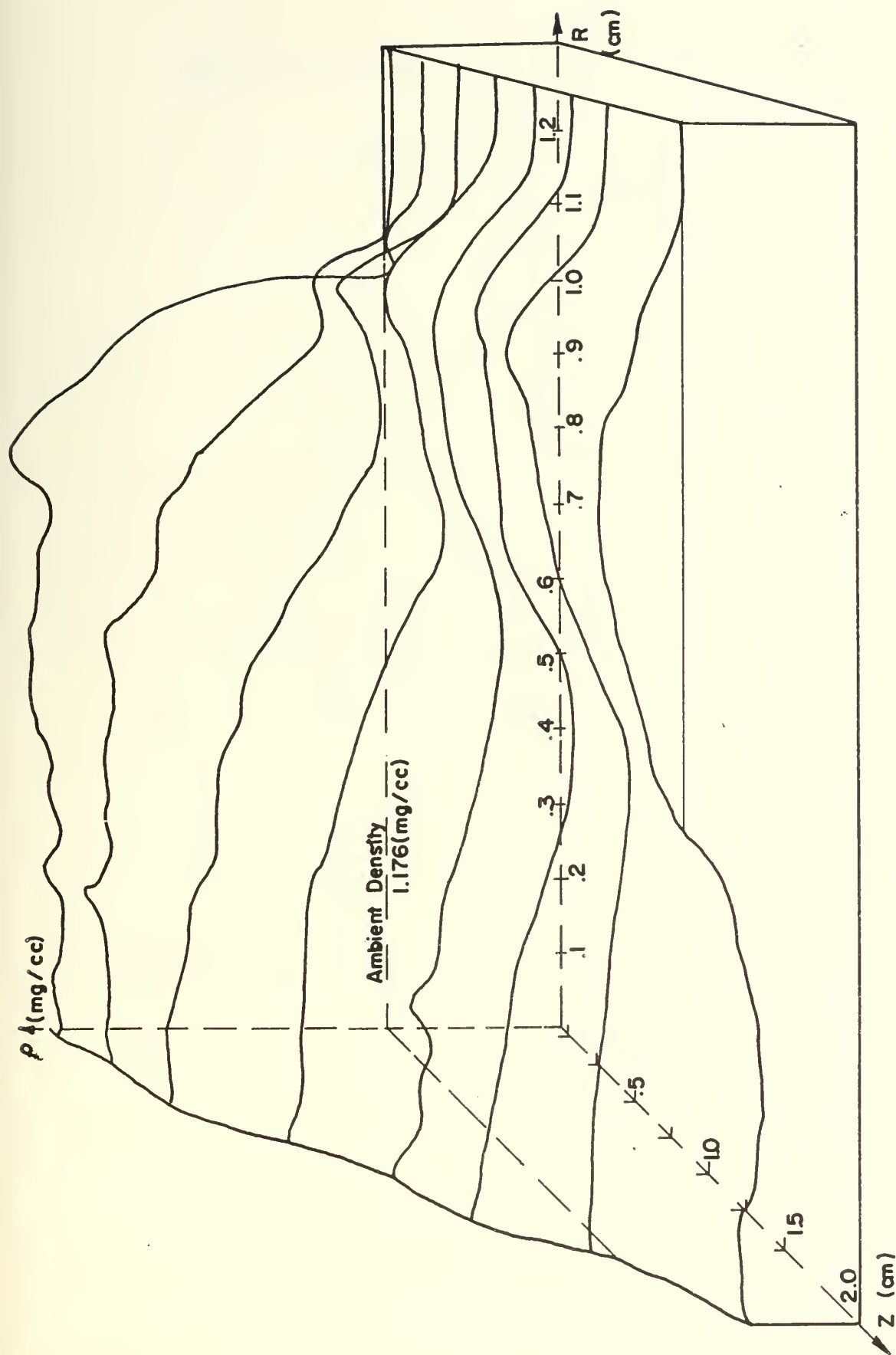


FIGURE 32 TOPOGRAPHICAL PLOT OF THE AXISYMMETRIC DENSITY SOLUTION OF A FREE JET AT 60 PSIG.

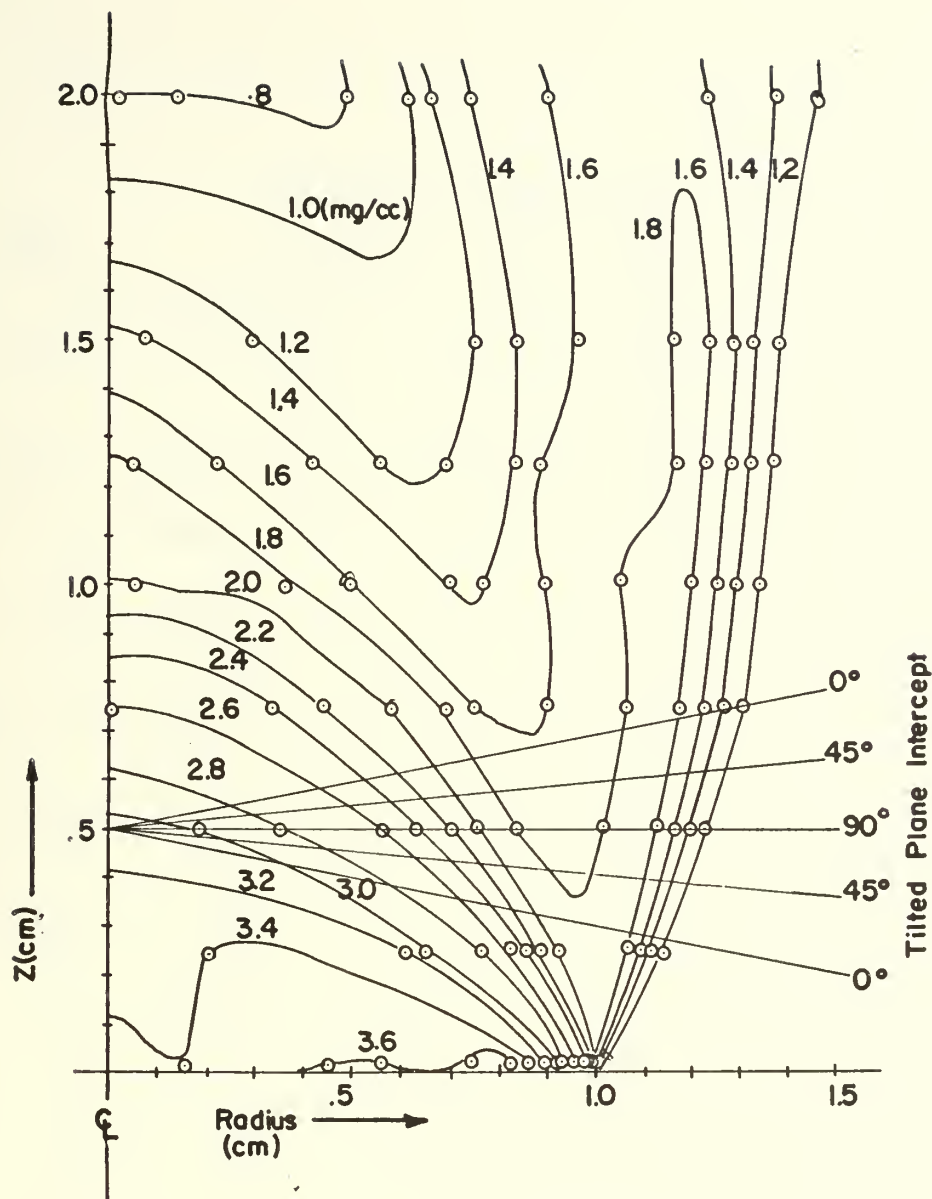


FIGURE 33. ISODENSITY LINE PLOT OF THE AXISYMMETRIC SOLUTION, 60 PSIG

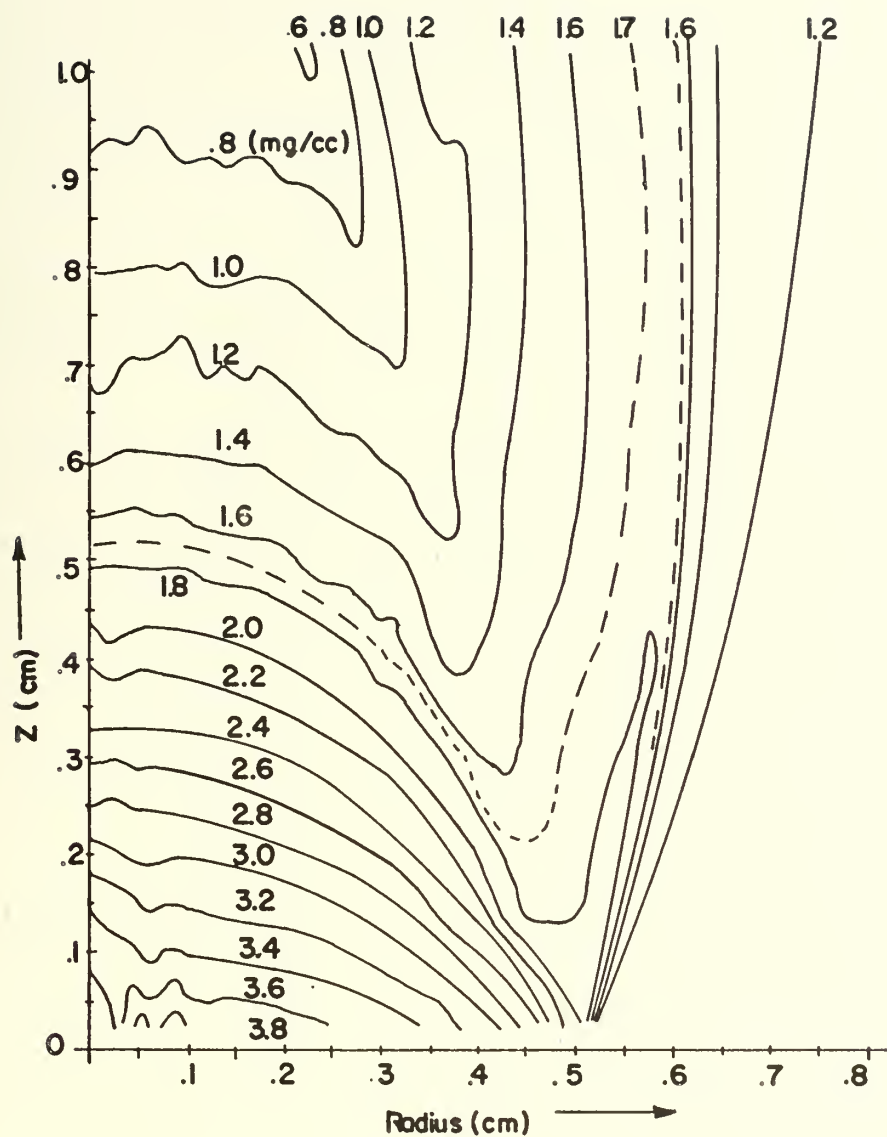


FIGURE 34 SKETCH OF THE AXISYMMETRIC DENSITY SOLUTION OF A 1.0 CM DIAMETER FREE JET AT 60 PSIG, FROM WINCKLER.

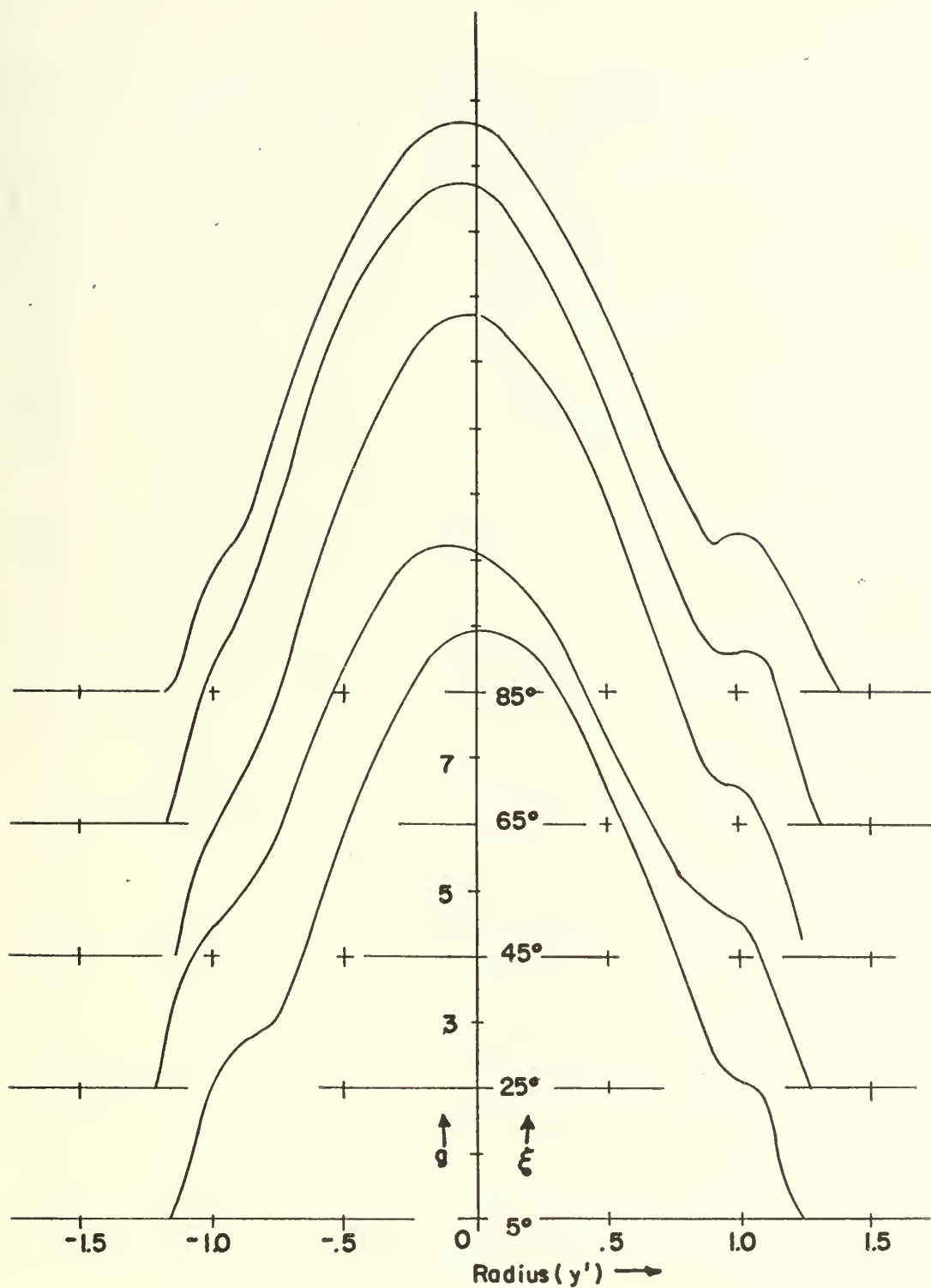


FIGURE 35. FRINGE NUMBER G CURVES OBTAINED FOR THE 11° TILT FREE JET AT 60 PSIG.

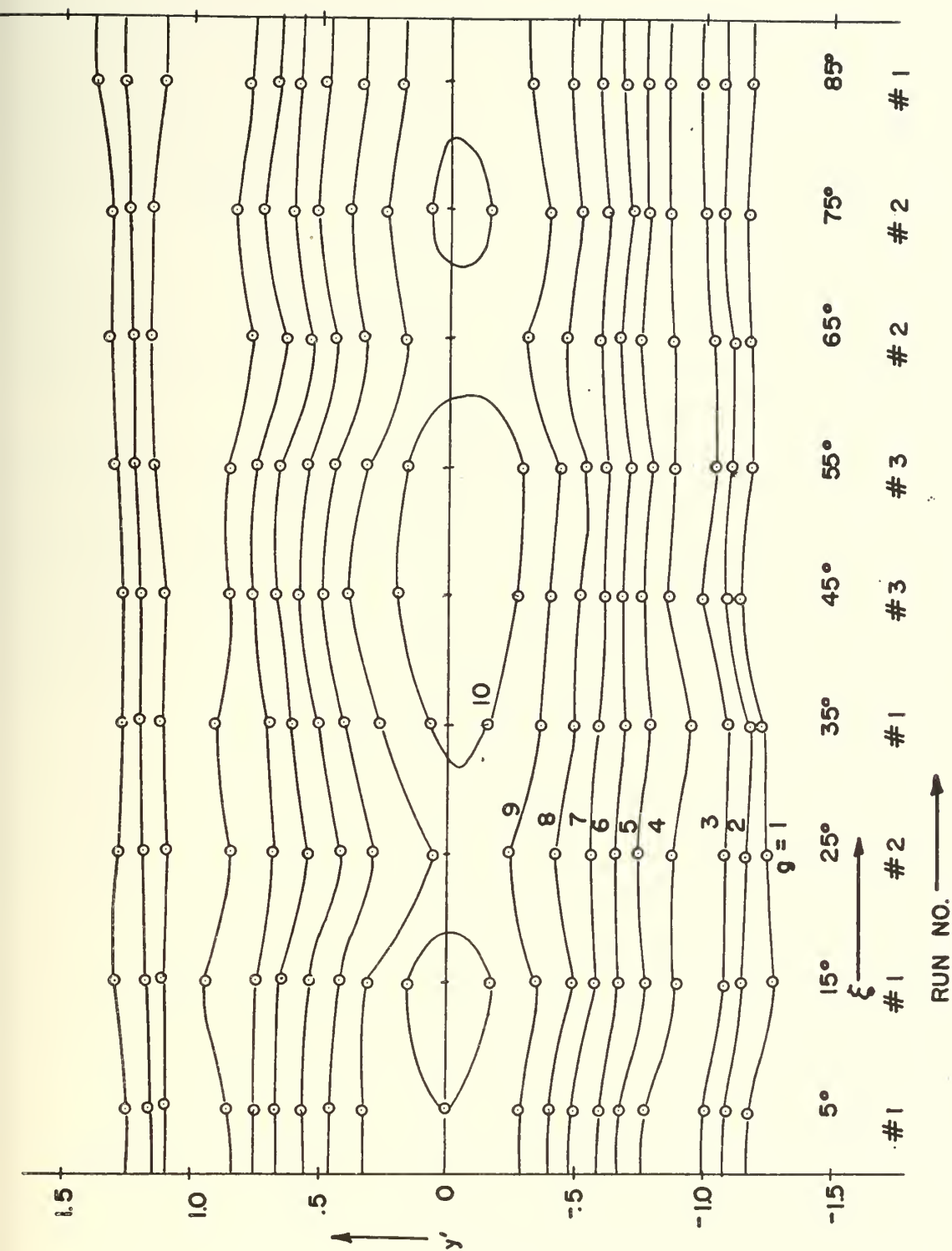


FIGURE 36. CONTOUR MAP OF THE FUNCTION G , 60 PSIG , 11° TILT

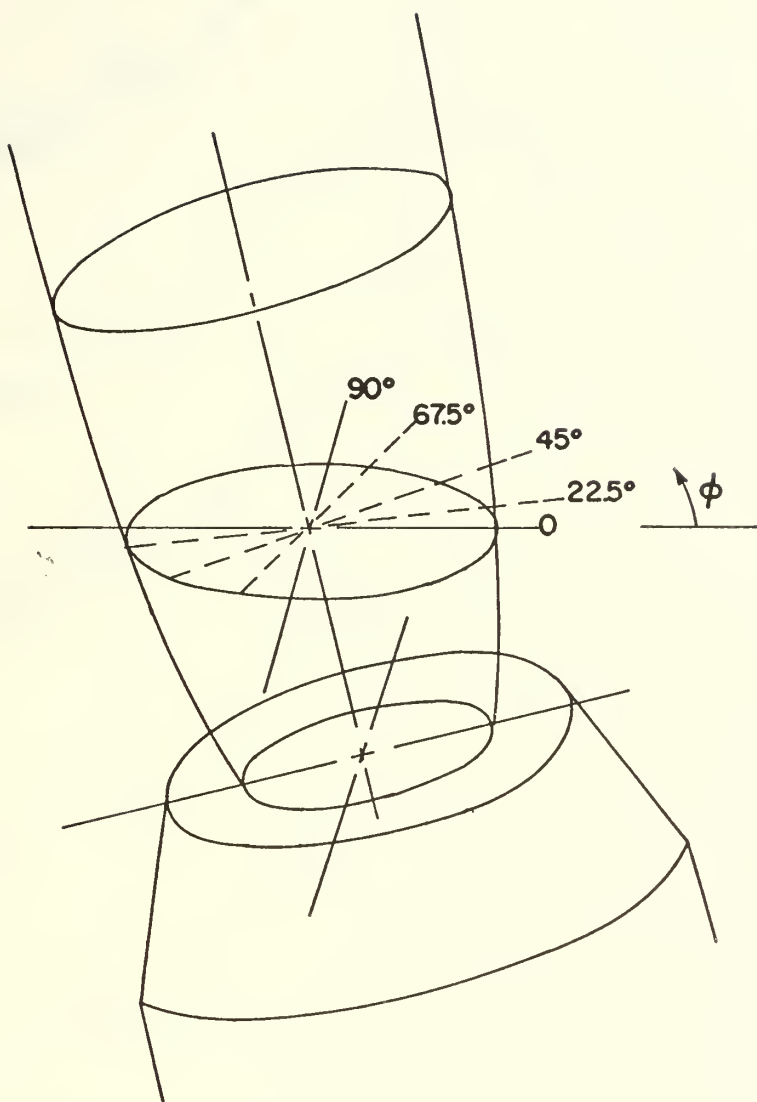


FIGURE 37 SKETCH OF TILTED PLANE SHOWING SOLUTION LINES.

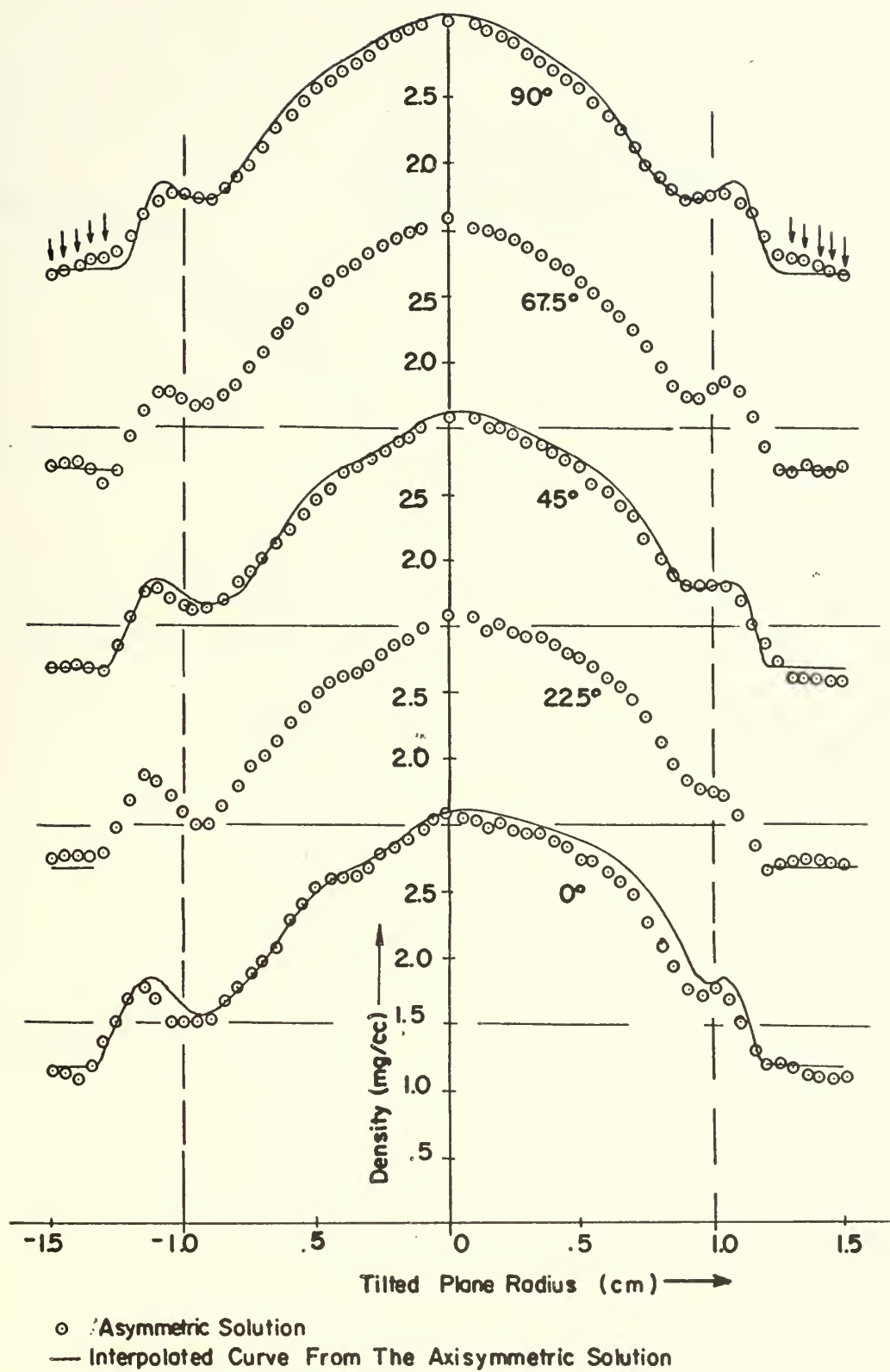


FIGURE 38 SOLUTION OF THE TILTED PLANE DENSITY ON FIVE DIAMETER LINES, 60 PSIG

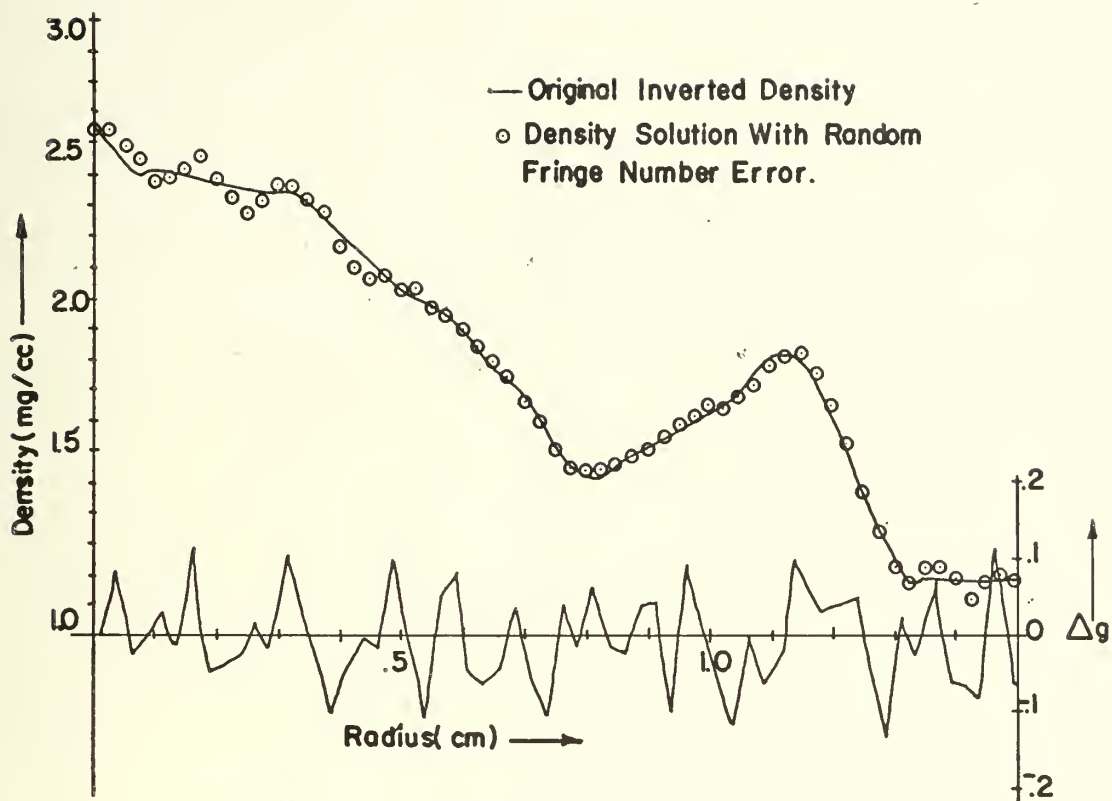


FIGURE 39 THE EFFECT OF RANDOM ERROR Δg ON THE AXISYMMETRIC SOLUTION AT $Z = .75$ CM

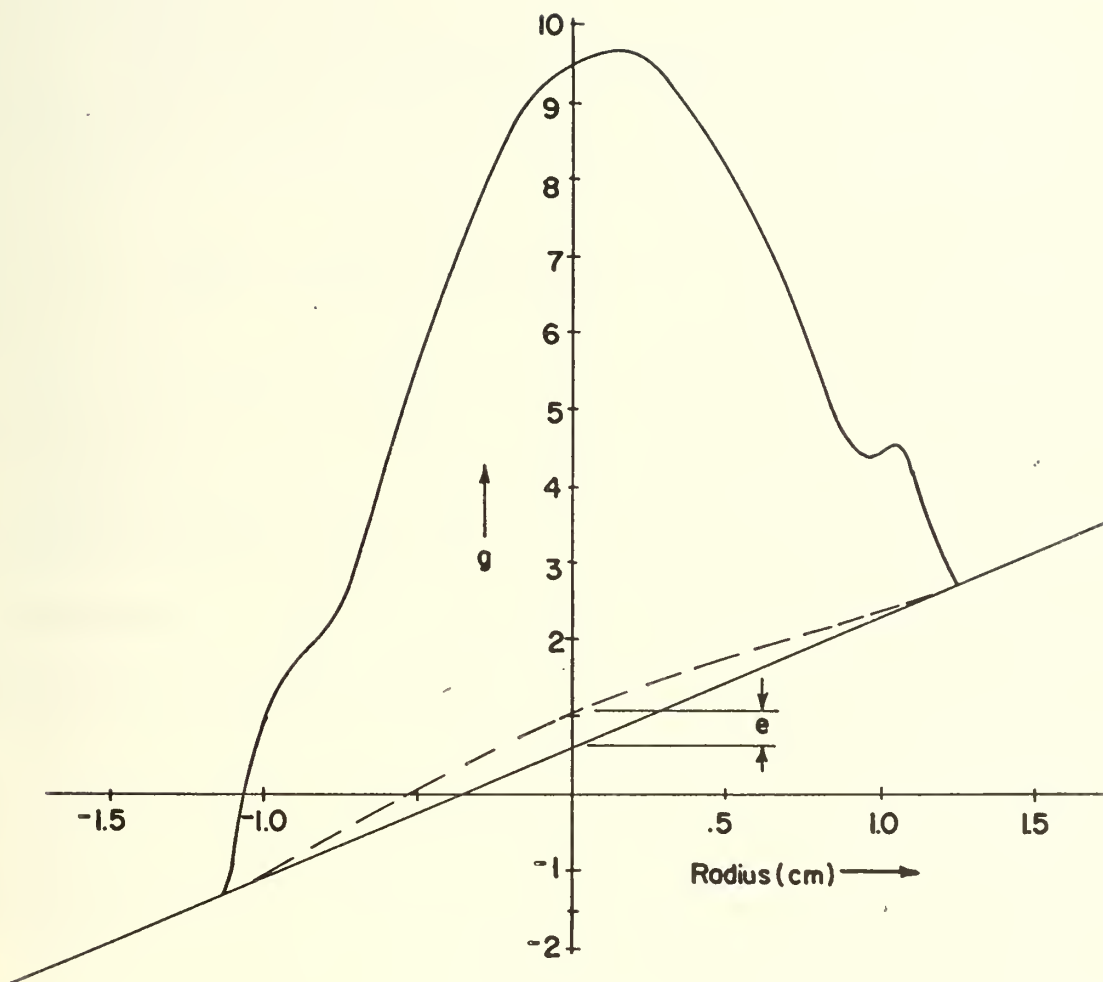


FIGURE 40 ILLUSTRATING POSSIBLE ERROR DUE TO NON-LINEAR BACKGROUND FRINGE.

APPENDIX A

OTHER INVERSION METHODS

1. The Abel Inversion

For the case of axisymmetry, the function f becomes invariant to a rotation of the coordinate system, and equation eleven reduces to:

$$g(y) = 2Q \int_y^{s/2} \frac{r f(r) dr}{(r^2 - y^2)^{1/2}} \quad (A1)$$

where $r = (x^2 + y^2)^{1/2}$, which is a form of Abel's integral equation with a well known solution. The Abel inversion has long been the standard method for reducing the data from axisymmetric interferograms. [Ladenberg, ed. 1954]. It has been well studied and optimized. Unmodified, the Abel solution overshoots the correct values when crossing shock wave discontinuities. Iterative methods have been developed which reduce this problem [Sangster and Shaw 1968]. In addition, there is the "reduced function" method previously mentioned.

2. The Generalized Abel Inversion

Recently a generalization of the Abel inversion by A. Pal has been reported [Cavanaugh, et.al. 1969] which applies to the two-dimensional function of equation eleven. It is in the process of being applied and evaluated at another laboratory. The method appears to have very similar application as the method utilized in this investigation.

3. Discrete Cubes

By representing the two-dimensional domain as a region of $N \times N$, discrete cubes of constant values (see figure five), one can represent equation eleven as a set of N^2 linear equations in N^2 unknown cube densities. The complexity of the resulting matrix inversion problem increases with the increasing size of the N^4 matrix of coefficients, however, and the method is not presently competitive.

4. Rowley's Method

An analytical method involving a two-dimensional fourier transform has been reported recently [Rowley, 1969], but no application of the method is known to have been attempted.

APPENDIX B MATHEMATICAL FOUNDATIONS

The selection of a set of functions which are orthogonal and defined over the domain has been made on the assumption that there exists a polynomial transform relationship which corresponds to the relationship between the functions f and g . Consider the operator notation of equation (11):

$$g = T f \quad (B1)$$

which has an inverse operation:

$$f = T^{-1} g \quad (B2)$$

One seeks a pair of orthogonal polynomial sets which, with an appropriate weighting function w , will satisfy the same transform operations.

Herlitz [1963], following a procedure from the diffraction theory of aberrations [Born and Wolf, 1959], for the cylindrically symmetric form of equation (11), and for the domain $r \leq 1$, used the Chebyshev functions [Madelung, 1953]:

$$V_k(\gamma) = \sin^{-1}(k \cos^{-1} \gamma) \quad (B3)$$

which satisfy the orthogonality relation

$$\int_{-1}^{+1} V_k(\gamma) V_l(\gamma) (1-\gamma^2) d\gamma = \int_{-\pi}^{\pi} \sin(k\theta) \sin(l\theta) d\theta = \frac{\pi}{2} \delta_{kl} \quad (B4)$$

and the Zernike polynomials, which have the form of the Legendre polynomials of argument $t = 2r^2 - 1$, and are orthogonal over the unit circle:

$$2(2k+1) \int_0^1 P_k(t) P_l(t) r dr = \delta_{kl} \quad (B5)$$

Using the Mehler integral [Whittaker and Watson, 1927]:

$$P_k(\cos \phi) = \frac{2^{\frac{1}{2}}}{\pi} \int_0^\phi \frac{\cos(k + \frac{1}{2}) \psi d\psi}{(\cos \psi - \cos \phi)} \quad (B6)$$

where $\cos \frac{\phi}{2} = r$ and $\cos \frac{\psi}{2} = \gamma$, Herlitz reports the transform pair:

$$T P_k(t) = \frac{2}{2k+1} V_{2k+1}(\gamma) \quad (B7)$$

and

$$P_k(t) = \frac{2}{2k+1} T^{-1} V_{2k+1}(\gamma) \quad (B8)$$

Thus, by expanding $f(r)$ in the Zernike polynomials with unknown coefficients

$$f(r) = \sum_{k=0}^{\infty} A_k P_k(t) \quad (B9)$$

and applying the transform relation (B1), one gets:

$$g(\gamma) = \sum_{k=0}^{\infty} \frac{2 A_k}{2k+1} V_{2k+1}(\gamma) \quad (B10)$$

The orthogonality relationship (B4) allows the determination of the unknown coefficients

$$A_k = \frac{2k+1}{\pi} \int_{-1}^1 g(\gamma) V_{2k+1}(\gamma) (1-\gamma^2)^{\frac{1}{2}} d\gamma \quad (B11)$$

Application of the evaluated coefficients A_k to the expansion of equation (B9) yields the desired solution for the density.

Maldonado [1965], in a similar analysis for the axisymmetric case over the entire domain $r \leq \infty$, using a generating procedure attributed to Bhatia and Wolf [1954], obtained the orthogonal polynomials:

$$U_{2k}(\alpha x, \alpha y) = (-1)^k \frac{\alpha}{\pi^{1/2}} L_k(\alpha^2 x^2 + \alpha^2 y^2) \quad (B12)$$

in which L_k are the Laguerre polynomials, defined over the interval $r \leq \infty$,

which have a transform relationship with gaussian weighting function:

$$\int_{-\infty}^{\infty} U_{2k}(\alpha x, \alpha y) e^{-\alpha^2 x^2} dx = \frac{1}{k! 2^{2k}} H_{2k}(\alpha y) \quad (B13)$$

where $H_{2k}(\alpha y)$ are the Hermite polynomials.

Hermite polynomials have the following orthogonality relationship:

$$\int_{-\infty}^{\infty} H_{2k}(\alpha y) H_{2l}(\alpha y) e^{-\alpha^2 y^2} dy = \frac{\delta_{kl}}{\alpha} \left[\pi 2^{2k} 2^{2l} (2k)! (2l)! \right]^{\frac{1}{2}} \quad (B14)$$

Expanding the function f in terms of the polynomials U :

$$f(x, y) = \sum_{k=0}^{\infty} C_{2k}(\alpha) U_{2k}(\alpha x, \alpha y) e^{-(\alpha^2 x^2 + \alpha^2 y^2)} \quad (B15)$$

and applying the transform $g = T f$, one obtains:

$$g(y) = \sum_{k=0}^{\infty} \frac{1}{k! 2^{2k}} C_{2k}(\alpha) H_{2k}(\alpha y) e^{-\alpha^2 y^2} \quad (B16)$$

Again, the application of the orthogonality relationship (B14) provides for the evaluation of the unknown expansion coefficients:

$$C_{2k}(\alpha) = \frac{\alpha k!}{(2k)! \pi^{\frac{1}{2}}} \int_{-\infty}^{\infty} g(y) H_{2k}(\alpha y) dy \quad (B17)$$

As one can see, the logical structure of the development is the same as the Herlitz expansion, with the exception that the domain is here defined over the entire x, y plane. The evaluation of the unknown density function is made by evaluating equation (B15) with the coefficients obtained from (B17).

The same procedure is used for the asymmetric case. The polynomials chosen are [Maldonado, 1966]:

$$U_{m+2k}^{\pm m}(\alpha x, \alpha y) = (-1)^k \frac{\alpha}{\pi^{\frac{1}{2}}} \left[\frac{k!}{(m+k)!} \right]^{\frac{1}{2}} (\alpha^2 x^2 + \alpha^2 y^2)^{\frac{m}{2}} e^{\pm i m \phi} L_k^m(\alpha^2 x^2 + \alpha^2 y^2) \quad (B18)$$

which have been chosen to have the property of "invariance in form" to a rotation of the coordinate system [Maldonado, 1965].

The "invariance in form" is demonstrated: suppose one makes a rotation of the axis by angle ξ . The polynomial $U_{m+2k}^{\pm m}$ becomes:

$$U_{m+2k}^{\pm m}(\alpha x', \alpha y') = (-1)^k \frac{\alpha}{\pi^{1/2}} \left[\frac{k!}{(m+k)!} \right]^{1/2} (\alpha x'^2 + \alpha y'^2)^{\frac{m}{2}} e^{\pm i m (\phi - \xi)} L_k^m(\alpha x'^2 + \alpha y'^2) \quad (B19)$$

or:

$$U_{m+2k}^{\pm m}(\alpha x', \alpha y') = e^{\mp i m \xi} U_{m+2k}^{\pm m}(\alpha x, \alpha y) \quad (B20)$$

Clearly, the form of the polynomial has remained unchanged.

The polynomials, $U_{m+2k}^{\pm m}(\alpha x, \alpha y)$ have a gaussian transform of:

$$\begin{aligned} I_{m+2k}^{\pm m}(\xi, dy') &= \int_{-\infty}^{\infty} U_{m+2k}^{\pm m}(\alpha x, \alpha y) e^{-\alpha^2 x'^2} dx' \\ &= \int_{-\infty}^{\infty} U_{m+2k}^{\pm m}(\alpha x', \alpha y') e^{\mp i m \xi} e^{-\alpha^2 x'^2} dx' \\ &= \frac{e^{\pm i m \xi} H_{m+2k}(\alpha y')}{\left[k! (m+k)! \right]^{1/2} 2^{m+2k}} \end{aligned} \quad (B21)$$

where the orthogonality relationship becomes:

$$\begin{aligned} \int_{-\pi}^{\pi} e^{\pm i m \xi} e^{\mp i n \xi} d\xi \int_{-\infty}^{\infty} H_{m+2k}(\alpha y') H_{n+2l}(\alpha y') e^{-\alpha^2 y'^2} dy' &= \\ \frac{2\pi}{\alpha} \left[\frac{3/2}{(m+2k)! (n+2l)! 2^{m+2k} 2^{n+2l}} \right] \delta_{mn} \delta_{(m+2k)(n+2l)} \end{aligned} \quad (B22)$$

The property of "invariance in form" preserves the form of the relationships for both the transform operation (B21) and the orthogonality condition (B22) during arbitrary rotations of the axes, ξ .

A similar expansion of the function f in terms of the polynomial

$U_{m+2k}^{\pm m}$ is:

$$f(x, y) = \sum_{m=0}^{\infty} \sum_{k=0}^{\infty} \epsilon_m C_{m+2k}^{\pm m}(\alpha) U_{m+2k}^{\pm m}(\alpha x, \alpha y) e^{-(\alpha^2 x^2 + \alpha^2 y^2)} \quad (B23)$$

followed by a similar application of the transform operator $g = Tf$ yields:

$$g(y', \xi) = \sum_{m=0}^{\infty} \sum_{k=0}^{\infty} \epsilon_m \left[k! (m+k)! 2^{2(m+2k)} \right]^{-\frac{1}{2}} C_{m+2k}^{\pm m}(\alpha) e^{\pm i m \xi} H_{m+2k}(\alpha y') e^{-\alpha^2 y'^2} \quad (B24)$$

from which an application of the orthogonality relationship yields an

evaluation of the unknown coefficients $C_{m+2k}^{\pm m}$:

$$C_{m+2k}^{\pm m} = \frac{\alpha}{2\pi^{3/2}} \left[\frac{[k! (m+k)!]^{1/2}}{(m+2k)!} \right] \int_{-\pi}^{\pi} \int_{-\infty}^{\infty} g(y', \xi) H_{m+2k}(\alpha y') e^{\mp i m \xi} dy' d\xi \quad (B25)$$

which allow the evaluation of the expanded function f of equation (B23).

The progressive application of the same logical sequence, which has been given, demonstrates the development of this method of inversion by orthogonal polynomial expansion.

APPENDIX C

HOLOFER,

A FORTRAN IV COMPUTER PROGRAM FOR INVERTING THE
LINE INTEGRAL DATA OF HOLOGRAPHIC INTERFEROMETRY
FOR ASYMMETRIC FIELDS

1. The Description of Input Parameters
2. A Sample Terminal Dialogue
3. The Terminal Executive Files
4. The Program
5. The Input Data Files Used in the Experiment

1. The Description of Input Parameters:

CMS	selects CP/CMS (terminal) or OS/MVT (batch) computer operation of the program. The selection is made by choice of the proper CMS definition card in the calling routine HOLOVERT.
IMAX	is the number of intervals of the input data in the radial direction, from $y' = -S/2$ to $+S/2$. 1 IMAX 201.
JMAX/2	is the number of intervals of the input data in the azimuthal direction, from $\xi = 0^\circ$ to the edge of the orthogonal subinterval. $0 \leq JMAX/2 \leq 36$, if JMAX/2 is set to zero, the value of JMAX will default to 1. This applies to the axisymmetric case where only one line of data is needed.
NOTE:	The dimension statements for G and GA in HOLOVERT set a limiting value of IMAX*JMAX at 5151. This would be exceeded if both values were individually set to their maximum. Only the dimension statements in HOLOVERT need be changed to change program dimensions.
KLIMIT	sets the number of B and D coefficients which will be computed corresponding to each k index of the double series. $1 \leq KLIMIT \leq 1000$ for asymmetric (SYM = 0) $1 \leq KLIMIT \leq 2000$ for symmetric (SYM = 0)
MLIMIT	sets the number of KLIMIT sets of B and D coefficients which will be computed corresponding to each m index of the double series. $1 \leq MLIMIT$. MLIMIT may be any size, limited only by the disk space available for storage. Values greater than 50 are not desirable, however.
KEXTRA	is the number of extra terms that will be included in the evaluation of the k series after the term size has failed the epsilon criterion. $0 \leq KEXTRA \leq KLIMIT$. This value insures that the term size has stabilized at a small value prior to truncating the evaluation. When the evaluation fails to converge prior to reaching KLIMIT terms, the last KEXTRA terms are averaged.

- MEXTRA the number of extra M series that will be evaluated after the K series evaluations have become small. MEXTRA has the same effect upon the m term evaluation as does KEXTRA on the K series.
 $0 \leq \text{MEXTRA} \leq \text{MLIMIT}$.
- ALPHA the scale factor for the Hermite and Laguerre polynomials. $1.0 \leq \text{ALPHA} \leq 5.0$
 Maldonado, et.al. have shown that the factor Alpha has a significant effect upon the convergence criteria of the series. The guide line given is to match the edge slopes of the G function to a gaussian curve: $G = e^{-\alpha^2 y^2}$
 Then one uses the value α which matches. For the G functions used in this investigation, the variable SIZE has been adjusted to keep the function edges near .8 on the unit circle. ALPHA = 2.0 has been satisfactory for the experimental inversions.
- SIZE defines the diameter of the region from which data is taken, i.e. the diameter of the inversion circle. SIZE has been 2.5 or 3.0 for all experimental inversions, 2.0 for all mode 1 test runs.
- EPS is the convergence criterion. When the Nth term of the series becomes less than EPS times the partial sum to date, the KEXTRA or MEXTRA terms begin counting extra terms. If the (N+KEXTRA) term remains less than EPS*SUM, the series is truncated. EPS=.0001 was used in most inversions.
- RHO-INF is the atmospheric density, in mg/cc., entered as an input for the density conversion of the output data. 1.176 mg/cc. was used for the experimental inversions.
- LAMBDA is the wavelength of the hologram source light in angstroms, $\lambda = 6941.0 \text{ \AA}$ for ruby laser holograms. $\lambda = 6328.0 \text{ \AA}$ for helium-neon holograms.
- BETA is the first term binomial expansion coefficient of the relation between index of refraction and density. BETA=.000291 for red light (6900A) BETA=.000293 for yellow-green light (5500A).

MODE selects the manner in which the G-array will be obtained. The three modes are described in the text and in the subroutine comment cards of the program. In addition to modes 1, 2, and 3, the parameter may be modified. Mode = -1, -2, or -3 will utilize subroutine FIELD2 which generates the B and D coefficients individually as needed. It requires much more time, but does not use offline disk space. MODE = 11, 12, or 13 will assume the B and D coefficients are already stored on the disk, will bypass subroutine BDGEN and use the previously computed coefficients. This provides a restart capability to the program. Once the coefficients have been generated, one can vary the output parameters for repeat inversions.

SYM selects the symmetry parameters of the field to be inverted. SYM is called JSYM in the program.
 SYM = 0 - completely asymmetric field
 SYM = 1, 2, 3, 4, ... - 1, 2, 3, 4, ... regularly spaced planes of symmetry exist in the field, aligned with plane number one on the X-Z plane.
 SYM > JMAX - an axisymmetric field.

POINTS is the number of points to be inverted on each sampling line. POINTS ≥ 1

LINES is the number of lines of points through the field to be inverted LINES ≥ 1

DIAGNOS provides a series of levels of diagnostic printout. It is helpful if errors show up in the program to printout the parameters as they are computed. No explanation will be made here, as the use of this parameter involves detailed study of the program anyway. DIAGNOS = 0. for normal operation.

STD.DEV. provides the ability to add a random error of given standard deviation to the add-on function G-array. The resulting inversion will reflect the effect of random errors to the data. This parameter allows some degree of error estimate to the experimental data.
 STD.DEV. = 0.0 for normal operation
 STD.DEV. = .0625 for $\pm 1/8$ fringe number error in the data.

PHIZERO is the angle in degrees, which the first line to be inverted will make with the X axis. PHIZERO = 0.0 for most uses.

DELPHI is the angular incrementation, in degrees, that successive inversion lines will make with the X-axis. The second line will be at $\text{PHI} = \text{PHIZERO} + \text{DELPHI}$, etc.

YPZERO is the y' position of the first line to be inverted, in the primed coordinate system rotated by angle PHI

YPRANGE is the range over which y' will uniformly vary for the number of lines to be inverted. If one sets $\text{DELPHI} = 0$. and $\text{YPRANGE} \neq 0$. A cartesian array of points will be selected, if $\text{DELPHI} \neq 0$. and $\text{YPRANGE} = 0$. A cylindrical array of points will be selected.

XPZERO is the position of the beginning of each line to be inverted (in the primed coordinate system).

XPRANGE is the range over which the number of points selected will range, beginning at XPZERO.

TST.FUN is the number of the function to be inverted. In mode 1 this number corresponds to the function number in subroutine FUNCT. In modes 2 and 3 it serves as a run identifying number on the output.

ADD.FUN is the number of the function in FUNCT to be used as an add-on function. $\text{ADD.FUN} = 0$. will default the use of an add-on function.

GARRAY is the output parameter for printout of the G-array used.
GARRAY =

- 0. -- no printout.
- 1. -- prints the G-array.
- 2. -- prints the G-array with a pause for paper spacing on the terminal prior to printing.
- 3. -- prints both G-array and the add-on G-array.
- 4. -- prints both G-arrays with terminal pauses for spacing.
- 1. -- punches the G-array on a deck of cards and prints the G-array
- 3. -- punches the modified G-array sum of both on a deck of cards, then prints both G-arrays separately.

GRAPH prints a graph of each line of the G-array. GRAPH =

0. -- no graph.
1. -- a graph of G-array for each J.
2. -- same as 1. , with terminal pause.
3. -- both G-array and add-on G-array are on each graph.
4. -- same as 3. , with terminal pause.

LIN.PRT prints the inversion results LIN.PRT =

0. -- G-array is set up, inversion results are not printed.
Inversion is not performed unless MAP.BND=0.
1. -- prints the inversion results a line at a time.
2. -- prints the inversion results with a terminal pause
prior to each line of points , for paper spacing.
It also sets a terminal pause prior to MAP output ,
if MAP is used.

MAP.BND prints a map of the inversion array on the printer. Uses
library subroutine MTMPII. MAP.BND=

0. -- map is not printed.
- ≠0. -- the number used defines the interval between con-
tours of the function f on the map , e. g. 0.2.

A,B,C,D,E,P are variable function parameters for the functions in
subroutine FUNCT , as used in mode 1 inversion.

S,T,U,V,W,Q are variable function parameters for the functions of sub-
routine FUNCT , as used for the add-on function.

PHISYM is an input angle entered in the data cards for mode 2 or 3
operation that defines a rotation between the inversion
coordinate system and the laboratory , or output coordinate
system , e.g. if the plane of symmetry of the function was
at 5° in the laboratory system , one would enter 5.0 in the
data cards. Output would then be in the laboratory coordinate
system. Raw data for mode 2 is entered in the laboratory
coordinate system; G-array data for mode 3 is entered in the
data plane coordinate system.

XO,YO are the laboratory coordinates of the estimated center of the
function , entered in the data cards used in mode 2 , to provide
a well-centered inversion. Output is in laboratory coordinates.

INPUT DATA for batch operation, input data cards are read in order:

- 1) 7 cards of input data, format 89 of calling program HOLOVERT; data corresponds exactly to parameters in the sample dialogue.
- 2) IF USED: data cards for numerical function, formats 88, 89 of subroutine FREAD.
- 3) IF USED: data cards for numerical add-on function, formats 88, 89 of subroutine FREAD.
- 4) input data for mode 2 or mode 3
 - mode 2: formats 59, 58 of subroutine SHEET;
if NCODE.GE.1: format 29 of subroutine SIM.
 - mode 3: formats 39, 38 of subroutine READ.
- 5) a blank card if another data set follows, otherwise a FINISH card; format 60, HOLOVERT.

For terminal operation, input data 2), 3), and 4) are entered in the above formats in separate files and given optional filenames/filetypes. The organization of files for execution is handled by exec file HOLOFER.

A sample terminal dialogue follows.

2. A Sample Terminal Dialogue on the Cambridge Monitor System.

```
holofer
ERASE FILE FT03F001 *
ERASE FILE FT04F001 *
SPLIT INPUT DATA FILE FT04F001 1 EOF
EOF REACHED
FILE MODIFIED
```

ANSWER YES OR NO...

DO YOU WISH INFO TYPEOUT?
no

DO YOU WISH INPUT DATA TYPED OUT OR CHANGED?
yes

THE INPUT VALUES FOLLOW:

```
--1) IF CHANGES ARE DESIRED TYPE NEW VALUE(S) UNDER OLD
--2) IF NO CHANGES, HIT SPACE BAR AND RETURN
--3) TO CHANGE A NON-ZERO NUMBER TO ZERO, TYPE "999."
```

\$ SETUP
EXECUTION BEGINS...

```
*****
*   IMAX   * JMAX/2 * KLIMIT * MLIMIT * KEXTRA * MEXTRA *
*   60.    * 18.    * 250.    * 30.    * 5.      * 2.      *
*   41.    * 999.   *          * 1.      *          *          *
*   ALPHA  * SIZE   * EPS.   * RHO-INF * LAMBDA * BETA   *
*   2.000  * 3.000  * 0.000500 * 1.1760 * 6941.0 * 0.000291
*          * 2.      * .001      *          *          *
*****
```



```

)  *  MODE  *  SYM.  *  POINTS  *  LINES  *  DIAGNOS  *  STD.DEV  *
    3.      1.      31.      9.      0.0      0.0
    1.      100.     21.      1.
*  PHIZERO  *  DELPHI  *  YPZERO  *  YPRANGE  *  XPZERO  *  XPRANGE  *
    0.0      22.500    0.0      0.0      0.0      1.500
                                1.
*  TST FUN  *  ADD FUN  *  GARRAY  *  GRAPH  *  LIN PRT  *  MAP BND  *
    60.      0.0      1.      0.0      1.      0.0
    5.      999.
*  A  *  B  *  C  *  D  *  E  *  P  *
    1.000    0.700    0.900    0.071    0.071    0.0
    1.      1.
*  S  *  T  *  U  *  V  *  W  *  Q  *
    0.0      1.000    1.000    0.0      0.0      1.000

```

```

*****
IHC0021 STOP 0
ERASE INPUT DATA *
SPLIT FILE FT04F001 INPUT DATA 1 EOF
EOF REACHED
FILE MODIFIED
*****

```

```

DO YOU WISH THE TEST DATA READ IN?
no

```

```

WILL ADD-ON FUNCTION DATA BE READ IN? (EQ'N. NO. 8)
no

```

```

EXECUTE THE PROGRAM?
no
R; T=0.97/2.82 15.32.16

```


[illegible]


```

NPIS=AR(15)
NNLINS=AR(16)
SL=AR(19)
DELP=AR(19)
YYPZ=AR(20)
YPRNG=AR(21)
XPRNG=AR(22)
XPRNG=AR(23)
XPRNG=AR(24)
NGP=AR(25)
NNAT=AR(27)
IPT=AR(27)
LPT=AR(28)
LBN=AR(30)
A=AR(32)
B=AR(32)
C=AR(34)
DEP=AR(34)
STE=AR(36)
TUE=AR(36)
V=AR(41)
W=AR(41)
Q=AR(42)
IF (DGN.EE.4) WRITE (6,89) (AR(I),I=1,42)
NNN=2
IF (MODE.LT.0) NNN=1
IF (MODE.GT.5) NNN=3
IF (MODE.GT.5) MODE=MODE-10
NGP=0
IF (KLIMIT.LT.KEXTRA) KEXTRA=KLIMIT
IF (MLIMIT.LT.MEXTRA) MEXTRA=MLIMIT
IF (IPT.LT.0) NGP=IPT
IF (IPT.LT.0) IPT=-IPT
ISYM=2.1-(FLOAT(JSYM)/2.-FLOAT(JSYM/2))*2
IF (JSYM.GT.JMAX) ISYM=1
IF (JSYM.GT.JMAX) ISYM=2
IF (ISYM.EQ.1) JMAX=((JMAX+1)/2)*2
RJMX=JMAX
RJSYM=JSYM
IF ((MSYM.EQ.0).OR.(MSYM.GT.JMAX)) MSYM=1
IFCU=ISYM*JSYM*JMAX
ISYM=ISYM.GT.JMAX
ISYM=FCU/RJMX
ISYM=(1/MZX+ISYM-1)/ISYM

```


CALCCG970
 CALCCG920
 CALCCG990
 CALCCG1000
 CALCCG1010
 CALCCG1020
 CALCCG1030
 CALCCG1040
 CALCCG1050
 CALCCG1060
 CALCCG1070
 CALCCG1080
 CALCCG1090
 CALCCG1100
 CALCCG1110
 CALCCG1120
 CALCCG1130
 CALCCG1140
 CALCCG1150
 CALCCG1160
 CALCCG1170
 CALCCG1180
 CALCCG1190
 CALCCG1200
 CALCCG1210
 CALCCG1220
 CALCCG1230
 CALCCG1240
 CALCCG1250
 CALCCG1260
 CALCCG1270
 CALCCG1280
 CALCCG1290
 CALCCG1300
 CALCCG1310
 CALCCG1320
 CALCCG1330
 CALCCG1340
 CALCCG1350
 CALCCG1360
 CALCCG1370
 CALCCG1380
 CALCCG1390
 CALCCG1400
 CALCCG1410
 CALCCG1420
 CALCCG1430

```

JMS=JMAX.EQ.1) JMS=(JMAX/2+1)/2
IF (JSYM.EQ.0) JMS=JMAX/2
MODE=ABS(AR(13))
XC=0.
YC=0.
ZD=0.
PHIS=0.
FHS=ISIZ/2.
RHCS=1.286
BUTX=RHCS
RPTS=ENRPTIS
XPR=0.
IF (NPTS.GT.1) XPR=XPRNG/(PPTS-1.)/2.
XPM=-XPR
PIE=3.141592653589793
MONE=1.
WRITE (6,58) IMAX,JMAX,IMS,JMS,ISYM,JSYM,MSYM,QSYM,FCU,FCU',/
FORMAT (3X,'IMAX,JMAX,IMS,JMS,ISYM,JSYM,MSYM,QSYM,FCU',/
715,2F7.3/)
1 NTWC=2
IX=IMAX+JMAX
NE=IN1
IF ((MODE.EQ.1.).AND.(NOF.EQ.8).AND.(DGN.GE.1.)) WRITE (6,69)
IF ((MODE.EQ.1.).AND.(NOF.EQ.8)) CALL FREAD (NO,RO,NF,ZD)
Z=ZD
IF (DGN.GE.1.) WRITE (6,68)
CALL GARRAY (G,GA,NOF,DGN,MONE,XC,YO,PHISYM)
LM=1
IF ((LPT.EQ.0.).AND.(BND.EQ.0.)) LM=0
IF (LMX=IMAX+1
IJMX=JMAX+1
IJMX=IMAX+JMAX
NBD=1
IF (JSYM.EQ.0) NBD=2
IF (D=KLIMIT*NBD
DO 15 IJ=1,IJMX
GA(IJ)=0.
IF (NAF.EQ.0) GO TO 16
NE=IN2
IF ((NAF.EQ.8).AND.(DGN.GE.1.)) WRITE (6,69)
IF (NAF.EQ.8) CALL FREAD (NA,RA,NF,ZD)
MODE=MODE
WRITE (6,68)
IF (DGN.GE.1.) WRITE (6,68)
IF (NAF.NE.0) CALL GARRAY (GA,G,NAF,DGN,NTWC,XO,YO,PHISYM)
MODE=MODE
DO 15 IJ=1,IJMX
  
```





```

      1 C      H(II,3)=-H(II,1),3)
      1 C      H(II,2)=2.*H(II,3)*H(II,1)-1.) /3.
      1 C      H(II,1)=H(II,3)
      1 C      H(IIM,1)=H(II,1)
      1 C      H(IIM,2)=H(II,2)
      1 C      H(IIM,3)=H(II,3)
      1 C      H(IIM,4)=H(II,4)
      1 C      H(IIM,5)=H(II,5)
      1 C      H(IIM,6)=H(II,6)
      1 C      SIGN=1.
      1 C      IF IIM.EQ.1 THEN SIN/CCS ARRAY:
      1 C      DO J=1,JJMX
      1 C      RJM=J-1
      1 C      SCF(J,1)=0.
      1 C      SCF(J,2)=1.
      1 C      SCF(J,3)=SIN(RJM*DXI-PIE/2.)
      1 C      SCF(J,4)=CCS(RJM*DXI-PIE/2.)
      1 C      SCF(J,5)=C.
      1 C      SCF(J,6)=C.
      1 C      NS=0
      1 C      IF IIM.EQ.1 THEN THE M LOOP:
      1 C      DO MP=1,MLIMIT
      1 C      NM=MP-1
      1 C      RM=M
      1 C      SIGN=-SIGN
      1 C      IF IIM.EQ.-4) WRITE (6,88) SCF(1,1),SCF(2,1),SCF(1,2),SCF(2,2)
      1 C      TEST FOR SYMMETRY SKIPS:
      1 C      IF ((MS.EQ.MSYM) .AND. MS=C)
      1 C      THEN GO TO 6
      1 C      IF MS=MS+1
      1 C      THEN GO TO 6
      1 C      IF MS=MS+1
      1 C      THEN THE K LOOP:
      1 C      DO KP=1,KLIMIT
      1 C      XK=KP-1
      1 C      YK=KP
      1 C      INDEX=X+1
      1 C      IF X.EQ.INDX+1 COEFFICIENTS AND WRITE THEM ON DISK:
      1 C      CALL FDC (M,K,G,H,SCF,3,D,JJMX6)
      1 C      IF ((DGN.LEE.-2) .AND. N,K,B,D)
      1 C      THEN WRITE (6,89) N,K,B,D
      1 C      IF ((DGN.LEE.-4) .AND. H(1,1),H(1,2),H(1,4),H(1,5))
      1 C      THEN WRITE (6,89) H(1,1),H(1,2),H(1,4),H(1,5)
      1 C      KK=KK+NBD+1
      1 C      K2=KK+NBD
      1 C      BC1(K2)=B
      1 C      BC2(K2)=B
      1 C      PERATE(M+2*XK+1)
      1 C      PERATE(M+2*XK+1)
      1 C      GENERATE SORT(PK*(PK+RM))/ORDER

```


SUBROUTINE FIELD2 (RS,SIG,SCLN,G,H,SCF,DGN)
 FIELD2 COMPUTES THE SAME INVERSION AS SURROUTINE FIELD, EXCEPT THAT
 THE COEFFICIENTS R AND D ARE COMPUTED INDIVIDUALLY AS USED BY
 CALLING ROUTINE. DISK STORAGE IS NOT REQUIRED, BUT COMPUTING TIME IS
 MUCH GREATER. FIELD2 IS UTILIZED BY SPECIFYING A NEGATIVE MODE ON
 THE INPUT PARAMETER. THE VALUE OF THE FIELD FUNCTION AT A PARTICULAR
 POINT DESIGNATED IN CYLINDRICAL COORDINATES, BY USING THE INVERSION
 EQUATION OF MALDONADO, ET AL. FIELD CALLS SUBROUTINES RC & GAPRAY.
 COMMON IMAX,JMAX,IMX,JMX,IJMX,ALPHA,SIZE,EPS,MODE,POX,SD,IX,7
 COMMON /TAB/ INDEX,KEXTRA,MEXTRA,KLIMIT,MLIMIT,OSYM
 COMMON /SYM/ ISYM,JSYM,MSYM,FCL,IMS,JMS,OSYM
 DIMENSION G(IJMX),H(IJMX,5),SCF(IJMX,6)
 INITIALIZE THE VALUES:
 IN INDEX=C
 MTIME=C
 KOUT=0
 MOUT=0
 MMAX=0
 KUTAL=C
 JIMX=JIMX*5
 JIMX2=(IIMX+1)/2
 AR=ALPHA*2
 ARG=ARG*2
 ARGON=EXP(-ARG)
 FIEP=2.141592653589793
 APP=ALPHA/PIE/PIE
 M=C
 RM=M
 RIMAX=IMAX
 RJMAX=JMAX

SUBROUTINE FIELD2 (RS,SIG,SCLN,G,H,SCF,DGN)
 FIELD2 COMPUTES THE SAME INVERSION AS SURROUTINE FIELD, EXCEPT THAT
 THE COEFFICIENTS R AND D ARE COMPUTED INDIVIDUALLY AS USED BY
 CALLING ROUTINE. DISK STORAGE IS NOT REQUIRED, BUT COMPUTING TIME IS
 MUCH GREATER. FIELD2 IS UTILIZED BY SPECIFYING A NEGATIVE MODE ON
 THE INPUT PARAMETER. THE VALUE OF THE FIELD FUNCTION AT A PARTICULAR
 POINT DESIGNATED IN CYLINDRICAL COORDINATES, BY USING THE INVERSION
 EQUATION OF MALDONADO, ET AL. FIELD CALLS SUBROUTINES RC & GAPRAY.
 COMMON IMAX,JMAX,IMX,JMX,IJMX,ALPHA,SIZE,EPS,MODE,POX,SD,IX,7
 COMMON /TAB/ INDEX,KEXTRA,MEXTRA,KLIMIT,MLIMIT,OSYM
 COMMON /SYM/ ISYM,JSYM,MSYM,FCL,IMS,JMS,OSYM
 DIMENSION G(IJMX),H(IJMX,5),SCF(IJMX,6)
 INITIALIZE THE VALUES:
 IN INDEX=C
 MTIME=C
 KOUT=0
 MOUT=0
 MMAX=0
 KUTAL=C
 JIMX=JIMX*5
 JIMX2=(IIMX+1)/2
 AR=ALPHA*2
 ARG=ARG*2
 ARGON=EXP(-ARG)
 FIEP=2.141592653589793
 APP=ALPHA/PIE/PIE
 M=C
 RM=M
 RIMAX=IMAX
 RJMAX=JMAX

[illegible]


```

SUBROUTINE GARRY (G,GA,NOF,DGN,NUMR,XC,YO,PHISYM)
  GARRY FILLS THE DATA ARRAY OVER AN ORTHOGONAL AREA WITH
  THE REGULAR DATA OBTAINED BY THE METHOD CORRESPONDING TO THE
  PARTICULAR MODE:
      MODE 1 - DATA OBTAINED BY SAMPLING A KNOWN FUNCTION SUPPLIED
                IN SUBROUTINE FUNCT AND SAMPLED IN SUBROUTINE GOLF.
      MODE 2 - DATA OBTAINED BY GENERATING A REGULAR ARRAY FROM
                IPRERULAR EXPERIMENTAL INPUT DATA READ IN. CALLS
                SUBROUTINE SHEET. (EXPERIMENTAL DATA MAY
                BE SIMULATED, SEE 'SHEET')
      MODE 3 - UTILIZES RAW DATA TAKEN AT THE PROPER INTERVAL, THE
                OR PREVIOUSLY GENERATED, AND READ DIRECTLY INTO THE
                GARRY. CALLS SUBROUTINE READ.

```



```

COMMON IMAX,JMAX,IIMX,IJMX,ISYM,JSYM,MSYM,FCU,IMS,JMS,QSYM
COMMON /SYM/ ISYM,JSYM,MSYM,FCU,IMS,JMS,QSYM
COMMON /IO/ CMS,IN1,IN2,IN4
COMMON ION,G(IMAX,JMAX),G4(IMAX,JMAX)
PIE=3.141592653589793
P3=SIZE/2*GT.3) MODE=1
IF (MODE.GT.3) MODE=1
RIMX=IMAX
RJMXX=JMAX
LRLR=SIZE/RIMX
DELXI=2.*PIE/FCU
IF (MODE.GT.1) GO TO 2
DO 1 J=1,JMS
RJ=J
XI=(RJ-.5)*DELXI-PIE
J2=J+2*(JMS-J)
J3=J+JMAX/2
DO 1 I=1,IMS
PI=I
II=IMAX+I-1
R=(PI-.5)*DELX-HS
CALL GCLF (R,XI,GIJ,NCF,DGN,NUMB)
G(I,J)=GIJ
IF (ISYM.EQ.2) G(II,J)=GIJ
IF (ISYM.EQ.2) GO TO 1
G(II,J3)=GIJ
IF (JSYM.EQ.0) GO TO 1
G(II,J2)=GIJ
G(II,J4)=GIJ
CONTINUE
IF (MODE.GT.2) GO TO 3
CALL VSHEET (G,GA,XO,YO,PHISYM,NCF)
GO TO 4
CALL READ (Z,XO,YO,PHISYM,NCF,IMAX,JMAX,G)
CALL DGN.GE.2) WRITE (6,35)
RETURN
DEMAT ( ' GAPRAY RETURNS')
END
CCCCCCC

```


SUBROUTINE GOLF (R,XI,GIJ,NCF,DGN,NUMB)
 GOLF COMPUTES THE FUNCTION G(R,XI) FOR A PARTICULAR LINE OF SIGHT
 FROM A KNOWN FUNCTION CONTAINED IN SUBROUTINE FUNCT.
 COMMON IMAX,JMAX,IIMX,JJMX,IJMX,ALPHA,SIZE,EPS,MODE,BOX,SD,IX,Z
 ZERO=0.
 LMAX=IMAX*3
 RLMAX=LMAX
 DELXP=SIZE/RLMAX
 SXI=SIZE/RLMAX
 CXI=SIZE/RLMAX
 DELXS=DELXP*SXI
 DELYS=DELXP*SXI
 XS=DELXP*SXI
 XS=XI-DELXP*SXI
 YS=XI+DELXP*SXI
 GIJ=0.
 L=1,LMAX
 DO 1 I=1,LMAX
 CALL FUNCT(XS,YS,F,NCF,DGN,NUMB)
 GIJ=GIJ+F
 XS=XS+DELXS
 YS=YS+DELYS
 IF (ABS(GIJ-0.)) GIJ=GIJ*DELXP*BOX
 IF (NUMB.EQ.0.) OR (NUMB.EQ.1.) GC TO 2
 IF (DGN.GE.3) WRITE(3,28) IX
 CALL GAUSS(IX,SD,ZERO,RV)
 GIJ=GIJ+RV
 IF (DGN.GE.3) WRITE(6,29) R,XI,GIJ
 RETURN
 FORMAT (1, R=1,F8.3,1, XI=1,F8.3,1, GIJ=1,F8.3)
 FORMAT (1, GAUSS, IX=1,I8)
 END
 CCCCCC

SUBROUTINE GOLF (R,XI,GIJ,NCF,DGN,NUMB)
 GOLF COMPUTES THE FUNCTION G(R,XI) FOR A PARTICULAR LINE OF SIGHT
 FROM A KNOWN FUNCTION CONTAINED IN SUBROUTINE FUNCT.
 COMMON IMAX,JMAX,IIMX,JJMX,IJMX,ALPHA,SIZE,EPS,MODE,BOX,SD,IX,Z
 ZERO=0.
 LMAX=IMAX*3
 RLMAX=LMAX
 DELXP=SIZE/RLMAX
 SXI=SIZE/RLMAX
 CXI=SIZE/RLMAX
 DELXS=DELXP*SXI
 DELYS=DELXP*SXI
 XS=DELXP*SXI
 XS=XI-DELXP*SXI
 YS=XI+DELXP*SXI
 GIJ=0.
 L=1,LMAX
 DO 1 I=1,LMAX
 CALL FUNCT(XS,YS,F,NCF,DGN,NUMB)
 GIJ=GIJ+F
 XS=XS+DELXS
 YS=YS+DELYS
 IF (ABS(GIJ-0.)) GIJ=GIJ*DELXP*BOX
 IF (NUMB.EQ.0.) OR (NUMB.EQ.1.) GC TO 2
 IF (DGN.GE.3) WRITE(3,28) IX
 CALL GAUSS(IX,SD,ZERO,RV)
 GIJ=GIJ+RV
 IF (DGN.GE.3) WRITE(6,29) R,XI,GIJ
 RETURN
 FORMAT (1, R=1,F8.3,1, XI=1,F8.3,1, GIJ=1,F8.3)
 FORMAT (1, GAUSS, IX=1,I8)
 END
 CCCCCC

SUBROUTINE FUNCT (XS,YS,F,NCF,DGN,NUMB)
 FUNCT EVALUATES AN INPUT FUNCTION AT POSITION (X,Y) IN THE TEST
 SECTION COORDINATE SYSTEM. NCF IDENTIFIES THE EQUATION USED.
 COMMON IMAX,JMAX,IIMX,JJMX,IJMX,ALPHA,SIZE,EPS,MODE,BOX,SD,IX,Z
 /EQPARA/ A,B,C,D,E,P,Q,S,T,U,V,W,X,Y,Z
 DIMENSION RO(101),RA(101)
 A=1



[illegible]

```

CC01  BB=BB
CC02  CC=CC
CC03  DD=DD
CC04  EE=EE
CC05  IF (NUMP.LE.1) GO TO 5C
CC06  IF (AA=ST)
CC07  CC=U
CC08  DD=V
CC09  EE=W
CC10  PI=3.141592653589793
CC11  FS=SIZE/2.
CC12  R=SQRT(XS**2+YS**2)/HS
CC13  F=0.
CC14  IF (R.GT.1.) GO TO 11
CC15  IF (NOF.LE.C) GO TO 11
CC16  1.  AXISYMMETRIC GAUSSIAN:
CC17  IF (NOF.GT.1) GO TO 2
CC18  F=AA*EXP(-1.*(R*HS/RP)**2)
CC19  GO TO 11
CC20  2.  ADJUSTABLE RECTANGULAR STEP FUNCTION:
CC21  IF (NOF.GT.2) GO TO 3
CC22  F=PP
CC23  IF ((ABS(XS-DD).LE.BR).AND.(ABS(YS-EE).LE.CC)) F=AA
CC24  GO TO 11
CC25  3.  DISPLACABLE ELLIPTICAL GAUSSIAN:
CC26  IF (NOF.GT.3) GO TO 4
CC27  F=AA*EXP(-1.*(((XS-DD)/BR)**2+((YS-EE)/CC)**2))
CC28  GO TO 11
CC29  4.  CONSTANT:
CC30  IF (NOF.GT.4) GO TO 5
CC31  F=AA
CC32  GO TO 11
CC33  5.  ADJUSTABLE AND DISPLACABLE ELLIPTIC RAMP FUNCTION:
CC34  IF (NOF.GT.5) GO TO 6
CC35  RBC=SQRT(((XS-DD)/RB)**2+((YS-EE)/CC)**2)
CC36  F=0.
CC37  IF (RBC.LT.1.) F=AA*((1.-RBC)*PP)
CC38  GO TO 11
CC39  6.  DISPLACABLE ELLIPTIC STEP FUNCTION:

```



```

S      IF (NCF.GT.6) GO TO 7
      RRC=SQRT(((XS-DD)/(RB)**2+((YS-EE)/(CC)**2)
      F=0
      IF (RBC.LT.1.) F=4A
      GO TO 11
C      7. CIRCULAR COSINE-SQUARED FUNCTION OF BB MAXIMA:
      IF (NCF.GT.7) GO TO 8
      F=4A+CCS((2.*RB-1.)*PIE*R/2.))**2
      GO TO 11
C      8. NUMERICAL FUNCTION: REQUIRES AN INPUT ARRAY READ IN BY
      SUBROUTINE FREAD: N FOLLOWED BY N POINT VALUES. (101 MAX)
      A CONSTANT VALUE 4A IS ADDED TO THE FUNCTION.
      IF (NCF.GT.8) GO TO 9
      IF (NUMB.LE.1) N=NC
      IF (NUMB.GT.1) N=NA
      NM=N-1
      NM=N-2
      QN=NM
      QN=NM*(QN-1.))+1.
      RI=INT(RI)
      IR=FLCAT(IR)
      QI=RI-IR
      IF (NUMB.LE.1) F=RQ(IR)
      IF (NUMB.GT.1) F=RA(IR)
      IF ((IR.NE.N).AND.(NUMB.LE.1)) F=F+DI*(RQ(IR+1)-RQ(IR))
      IF ((IR.NE.N).AND.(NUMB.GT.1)) F=F+DI*(RA(IR+1)-RA(IR))
      F=F+4A+BB
      GO TO 11
C      9. SPECIAL FUNCTION: MAY BE WRITTEN FOR THE OCCASION AND
      INSERTED IN SUBROUTINE SPFUN
      IF (NCF.GT.9) GO TO 10
      CALL SPFUN (XS,YS,E)
      GO TO 11
C      EQUATIONS NO. 10 AND BEYOND ARE SET TO ZERO.
      F=C.
C      10
C      11
C      IF (DGN.GE.4) WRITE (6,99) XS,YS,F
      FORMAT (' XS=',F8.3,' YS=',F8.3,' F=',F8.3)
      RETURN
      END
CCCCC

```


00000 70

[illegible]


```

C      FUNCTION ATANM(Y,X)
C      COMPUTES THE ARCTAN C
C      P I=2.1415926535897
P I=PI/2.
P I=SIGN(P I2,Y)
A T A N M=A
R E T U R N=P
A T A N M=-
R E T U R N
C
C000011

```

[illegible]

SUBOE3330
SUBOE3340
SUBOE3350
SUBOE3360
SUBOE3370
SUBOE3380
SUBOE3390
SUBOE3400

```

YD=YN
IF (YH.NE.Y1) XD=X1-(Y1-YN)*(XH-X1)/(YH-Y1)
RETURN
FORMAT (1CF7.3)
END

```

CCCCC12
C

SUBOC0030
SUBOC0040
SUBOC0050
SUBOC0060
SUBOC0070
SUBOC0080
SUBOC0090
SUBOC0100
SUBOC0110
SUBOC0120
SUBOC0130
SUBOC0140
SUBOC0150
SUBOC0160
SUBOC0170

```

SUBROUTINE FREAD (NC,RC,NF,ZZ)
  READ READS THE NUMERIC ARRAY WHICH IS USED FOR EQUATION 8 OF
  SUBROUTINE FUNCT. FIRST CARD IS NUMBER OF POINTS (N.GE.1),
  FOLLOWED BY ONE POINT PER CARD.

```

```

  DIMENSION RO(101)
  READ (NF,99) NO,ZZ
  READ (NF,98) (RC(I),I=1,NO)
  FORMAT (1E,99.3)
  RETURN
END

```

CCCCC13
C

SUBOC180
SUBOC190
SUBOC200
SUBOC210
SUBOC220
SUBOC230
SUBOC240
SUBOC250
SUBOC260
SUBOC270
SUBOC280
SUBOC290
SUBOC300
SUBOC310
SUBOC320
SUBOC330
SUBOC340
SUBOC350
SUBOC360
SUBOC370

```

SUBROUTINE GPRINT (G,NUMB)
  GPRINT PRINTS THE DATA ARRAY 'G' WHICH WAS INPUT TO
  THE PROGRAM IN SUBROUTINE GARRY.

```

```

  COMMON IMAX,JMAX,IMX,JMX,IJMX,ALPHA,SIZE,EPS,MODE,BOX,SD,IX,Z
  DIMENSION X(15)
  DATA FYP,VERT,1H-,1H/,
  IF (NUMB.EQ.1) WRITE (6,99) MODE,Z
  IF (NUMB.EQ.2) WRITE (6,92) Z
  JMAX=JMAX/2
  JIMAX=JMAX
  RJMAX=JMAX
  EX=SIZE/RJMAX
  IXI=360/EX
  INTRVL=SEAL
  CN INTRVL=1
  IF INTRVL=1
  IF IR+INTRVL-1

```

```

  INTRVL=SEAL
  CN INTRVL=1
  IF INTRVL=1
  IF IR+INTRVL-1

```

CCCC
C

[illegible][illegible]


```

12 YINT=Y(K)
13 RETURN
14 K=K-1
15 GO TO 6
16 I=1, XINT
17 PRINT(8PC,XINT = E18.9,32H, PUT OF RANGE FOR INTERPOLATION)
101 FORMAT(X(K+1)-XINT)*(C(1,K)*(X(K+1)-XINT)**2+C(3,K))
11 YINT=YINT+(XINT-X(K))*(C(2,K)*(XINT-X(K))**2+C(4,K))
12 RETURN
END

```

```

SUBROUTINE SPLICC(X,Y,M,C)
DIMENSION X(M),Y(M),C(4,300),D(300),P(300),E(300),A(300,3),B(300),
17(300)
MM=M-1
DO 2 K=1,MM
D(K)=X(K+1)-X(K)
D(K)=D(K)/6.
P(K)=(Y(K+1)-Y(K))/D(K)
3 DO 3 K=2,MM
B(K)=E(K)-E(K-1)
A(1,2)=-1.-D(1)/D(2)
A(1,3)=D(1)/D(2)
A(2,2)=D(2)-P(1)*A(1,3)
A(2,3)=2.*P(1)+P(2)-P(1)*A(1,2)
4 DO 4 K=3,MM
B(K)=B(K)/A(2,2)
A(K,2)=2.*P(K-1)+P(K)-P(K-1)*A(K-1,3)
E(K)=B(K)-P(K-1)*B(K-1)
A(K,3)=B(K)/A(K,2)
5 DO 5 M=2,MM-1
G=D(M-2)/D(M-1)
A(M,1)=1.+G+A(M-2,3)
A(M,2)=-G-A(M,1)*A(M-1,3)
A(M,3)=B(M)/A(M,2)
Z(M)=B(M)-A(M,1)*A(M,2)
DO 6 I=1,MN
K=M-I
Z(K)=A(K,3)*Z(K+1)
Z(1)=-A(1,2)*Z(2)-A(1,3)*Z(3)
C(1,K)=Z(K)
C(2,K)=Z(K+1)*Q
C(3,K)=Y(K)-Z(K)*P(K)

```



```

7 C(4,K)=Y(K+1)/D(K)-Z(K+1)*P(K)
  RETURN
  END

```

```

SPLO11100
SPLO11110
SPLO11120

```

```

CCCCC2C

```

```

*****
SUBROUTINE MTMPII
PURPOSE
    MTMPII WILL PRODUCE, ON THE PRINTER, A CONTOUR MAP
    OF ANY SINGLE PRECISION TWO DIMENSIONAL ARRAY.

USAGE
    CALL MTMPII(Y,N,M,T,RND,AZ,BZ,AMIN,IJT,ICCN)

DESCRIPTION OF PARAMETERS
    Y - THE ARRAY TO BE CONTOURED. DIMENSIONED Y(N,M)
    N - NUMBER OF ROWS IN Y.
    M - NUMBER OF COLUMNS IN Y.
    T - ARRAY FOR PLOT TITLE. REAL*4 T(24).
    RND - A BANDWIDTH WILL BE CALCULATED AS FOLLOWS
        BND=(MAX(Y)-MIN(Y))/15. MAYBE PERFORMED ON
        A LINEAR TRANSFORMATION FOLLOWING FORM AZ*Y+BZ.
        IF AZ=0 THEN AZ WILL BE COMPUTED SUCH THAT
        MAX(1 MAX(Y), 1, 1 MIN(Y)) WILL BE LESS THAN 1,
        AND BZ WILL BE LEFT AS INPUT.
    AZ - SEE UNDER AZ
    BZ - SEE UNDER AZ
    AMIN - THE LEVEL AT WHICH COUTOURING WILL BEGIN. IF
        AMIN > MIN(Y) THEN AMIN WILL BE CALCULATED.
        TCNTR=MIN(Y) REFERENCE AT ZERO, THE NEXT LOWER
        CONTOUR LEVEL
    AND IJT=0 AMIN WILL BE CALCULATED AS DESCRIBED
    IF IJT=0 AMIN WILL BE CALCULATED AS DESCRIBED
    IF IJT=0 AMIN WILL BE CALCULATED AS DESCRIBED
    ICN - IF ICN=0 NO CONTOURING WILL BE DONE BUT THE
        ARRAY Y WILL BE PRINTED IN THE PLOT FORMAT.

REMARKS
    MTMPII REQUIRES A PRINTER WITH 132 PRINT POSITIONS.
    IF NECESSARY THE MAP WILL BE SEGMENTED COLUMNWISE.
    THE NECESSARY AND COLUMNS ARE NUMBERED ALONG THE EDGES.
    THAT A SEGMENTED MAP MAY BE EASILY JOINED TOGETHER.

```

```

NETOCC010
NETOCC020
NETOCC030
NETOCC040
NETOCC050
NETOCC060
NETOCC070
NETOCC080
NETOCC090
NETOCC100
NETOCC110
NETOCC120
NETOCC130
NETOCC140
NETOCC150
NETOCC160
NETOCC170
NETOCC180
NETOCC190
NETOCC200
NETOCC210
NETOCC220
NETOCC230
NETOCC240
NETOCC250
NETOCC260
NETOCC270
NETOCC280
NETOCC290
NETOCC300
NETOCC310
NETOCC320
NETOCC330
NETOCC340
NETOCC350
NETOCC360
NETOCC370
NETOCC380
NETOCC390
NETOCC400
NETOCC410
NETOCC420

```


ONLY THREE SIGNIFICANT FIGURES WILL BE PRINTED AT
EACH POINT. THE POSITION OF THE FIRST SIGNIFICANT
DIGIT WILL BE DETERMINED BY MAX(Y), I, IMIN(Y), I).
THE PLOT WILL BE PRODUCED ON A 1 INCH INCH GRID. IT
WILL BE ASSUMED THAT THE SPACING BETWEEN POINTS IN
BOTH DIRECTIONS IS THE SAME AND EQUAL FOR ALL POINTS

SUBROUTINES REQUIRED
NONE

METHOD

THE CONTOUR LEVELS ARE DETERMINED BY SIMPLE LINEAR
INTERPOLATION FROM THE FOUR SURROUNDING POINTS.

MTMPII SUBROUTINE FOR ONE-INCH GRID SPACING
CLIKES CODE 5105 15 JAN 69

SUBROUTINE MTMPII(Y,A,M,T,BND,AZ,RZ,AMIN,IJT,ICON)

REAL*4 IP,KG,ITJZ R(140),C(140),D(140),IH(20),Y(N,M),TP(10),TPX(10)
Z,DIMENSION A(140),RTM(10),RTX(10),RT(10),KG(10),T(24)
Z,DIMENSION E(140),F(140),G(140),H(140)

DATA DUE/4F /,EPL/4H+ /,EMI/4H- /,IH/1H0,1H ,IH1,1H ,IH2,
11F,1F2,1F ,IH4,1H ,IH5,1H ,IH7,1H ,IH8,1H /,KG/
21F,1F1,1F2,1H3,1H4,1H5,1H7,1H8,1H9/,BLK/4H /

YMIN=Y(1,1)
YMAX=Y(1,1)
DO 20 I=1,N
DO 20 J=1,N
YMIN=AMIN(YMIN,Y(J,I))
YMAX=AMAX(YMAX,Y(J,I))

100 CONTINUE
100 CUELY=YMAX-X-YMIN
100 IF(BND) Y=25,25,30
100 IF(BND) Y=15,15,30
100 IF(BND) Y=31,31,32
100 IF(BND) Y=32,32,33
100 IF(BND) Y=33,33,34
100 IF(BND) Y=34,34,35
100 IF(BND) Y=35,35,36
100 IF(BND) Y=36,36,37
100 IF(BND) Y=37,37,38
100 IF(BND) Y=38,38,39
100 IF(BND) Y=39,39,40
100 IF(BND) Y=40,40,41
100 IF(BND) Y=41,41,42
100 IF(BND) Y=42,42,43
100 IF(BND) Y=43,43,44
100 IF(BND) Y=44,44,45
100 IF(BND) Y=45,45,46
100 IF(BND) Y=46,46,47
100 IF(BND) Y=47,47,48
100 IF(BND) Y=48,48,49
100 IF(BND) Y=49,49,50
100 IF(BND) Y=50,50,51
100 IF(BND) Y=51,51,52
100 IF(BND) Y=52,52,53
100 IF(BND) Y=53,53,54
100 IF(BND) Y=54,54,55
100 IF(BND) Y=55,55,56
100 IF(BND) Y=56,56,57
100 IF(BND) Y=57,57,58
100 IF(BND) Y=58,58,59
100 IF(BND) Y=59,59,60
100 IF(BND) Y=60,60,61
100 IF(BND) Y=61,61,62
100 IF(BND) Y=62,62,63
100 IF(BND) Y=63,63,64
100 IF(BND) Y=64,64,65
100 IF(BND) Y=65,65,66
100 IF(BND) Y=66,66,67
100 IF(BND) Y=67,67,68
100 IF(BND) Y=68,68,69
100 IF(BND) Y=69,69,70
100 IF(BND) Y=70,70,71
100 IF(BND) Y=71,71,72
100 IF(BND) Y=72,72,73
100 IF(BND) Y=73,73,74
100 IF(BND) Y=74,74,75
100 IF(BND) Y=75,75,76
100 IF(BND) Y=76,76,77
100 IF(BND) Y=77,77,78
100 IF(BND) Y=78,78,79
100 IF(BND) Y=79,79,80
100 IF(BND) Y=80,80,81
100 IF(BND) Y=81,81,82
100 IF(BND) Y=82,82,83
100 IF(BND) Y=83,83,84
100 IF(BND) Y=84,84,85
100 IF(BND) Y=85,85,86
100 IF(BND) Y=86,86,87
100 IF(BND) Y=87,87,88
100 IF(BND) Y=88,88,89
100 IF(BND) Y=89,89,90
100 IF(BND) Y=90,90,91
100 IF(BND) Y=91,91,92
100 IF(BND) Y=92,92,93
100 IF(BND) Y=93,93,94
100 IF(BND) Y=94,94,95
100 IF(BND) Y=95,95,96
100 IF(BND) Y=96,96,97
100 IF(BND) Y=97,97,98
100 IF(BND) Y=98,98,99
100 IF(BND) Y=99,99,100
100 IF(BND) Y=100,100,101
100 IF(BND) Y=101,101,102
100 IF(BND) Y=102,102,103
100 IF(BND) Y=103,103,104
100 IF(BND) Y=104,104,105
100 IF(BND) Y=105,105,106
100 IF(BND) Y=106,106,107
100 IF(BND) Y=107,107,108
100 IF(BND) Y=108,108,109
100 IF(BND) Y=109,109,110
100 IF(BND) Y=110,110,111
100 IF(BND) Y=111,111,112
100 IF(BND) Y=112,112,113
100 IF(BND) Y=113,113,114
100 IF(BND) Y=114,114,115
100 IF(BND) Y=115,115,116
100 IF(BND) Y=116,116,117
100 IF(BND) Y=117,117,118
100 IF(BND) Y=118,118,119
100 IF(BND) Y=119,119,120
100 IF(BND) Y=120,120,121
100 IF(BND) Y=121,121,122
100 IF(BND) Y=122,122,123
100 IF(BND) Y=123,123,124
100 IF(BND) Y=124,124,125
100 IF(BND) Y=125,125,126
100 IF(BND) Y=126,126,127
100 IF(BND) Y=127,127,128
100 IF(BND) Y=128,128,129
100 IF(BND) Y=129,129,130
100 IF(BND) Y=130,130,131
100 IF(BND) Y=131,131,132
100 IF(BND) Y=132,132,133
100 IF(BND) Y=133,133,134
100 IF(BND) Y=134,134,135
100 IF(BND) Y=135,135,136
100 IF(BND) Y=136,136,137
100 IF(BND) Y=137,137,138
100 IF(BND) Y=138,138,139
100 IF(BND) Y=139,139,140
100 IF(BND) Y=140,140,141
100 IF(BND) Y=141,141,142
100 IF(BND) Y=142,142,143
100 IF(BND) Y=143,143,144
100 IF(BND) Y=144,144,145
100 IF(BND) Y=145,145,146
100 IF(BND) Y=146,146,147
100 IF(BND) Y=147,147,148
100 IF(BND) Y=148,148,149
100 IF(BND) Y=149,149,150
100 IF(BND) Y=150,150,151
100 IF(BND) Y=151,151,152
100 IF(BND) Y=152,152,153
100 IF(BND) Y=153,153,154
100 IF(BND) Y=154,154,155
100 IF(BND) Y=155,155,156
100 IF(BND) Y=156,156,157
100 IF(BND) Y=157,157,158
100 IF(BND) Y=158,158,159
100 IF(BND) Y=159,159,160
100 IF(BND) Y=160,160,161
100 IF(BND) Y=161,161,162
100 IF(BND) Y=162,162,163
100 IF(BND) Y=163,163,164
100 IF(BND) Y=164,164,165
100 IF(BND) Y=165,165,166
100 IF(BND) Y=166,166,167
100 IF(BND) Y=167,167,168
100 IF(BND) Y=168,168,169
100 IF(BND) Y=169,169,170
100 IF(BND) Y=170,170,171
100 IF(BND) Y=171,171,172
100 IF(BND) Y=172,172,173
100 IF(BND) Y=173,173,174
100 IF(BND) Y=174,174,175
100 IF(BND) Y=175,175,176
100 IF(BND) Y=176,176,177
100 IF(BND) Y=177,177,178
100 IF(BND) Y=178,178,179
100 IF(BND) Y=179,179,180
100 IF(BND) Y=180,180,181
100 IF(BND) Y=181,181,182
100 IF(BND) Y=182,182,183
100 IF(BND) Y=183,183,184
100 IF(BND) Y=184,184,185
100 IF(BND) Y=185,185,186
100 IF(BND) Y=186,186,187
100 IF(BND) Y=187,187,188
100 IF(BND) Y=188,188,189
100 IF(BND) Y=189,189,190
100 IF(BND) Y=190,190,191
100 IF(BND) Y=191,191,192
100 IF(BND) Y=192,192,193
100 IF(BND) Y=193,193,194
100 IF(BND) Y=194,194,195
100 IF(BND) Y=195,195,196
100 IF(BND) Y=196,196,197
100 IF(BND) Y=197,197,198
100 IF(BND) Y=198,198,199
100 IF(BND) Y=199,199,200
100 IF(BND) Y=200,200,201
100 IF(BND) Y=201,201,202
100 IF(BND) Y=202,202,203
100 IF(BND) Y=203,203,204
100 IF(BND) Y=204,204,205
100 IF(BND) Y=205,205,206
100 IF(BND) Y=206,206,207
100 IF(BND) Y=207,207,208
100 IF(BND) Y=208,208,209
100 IF(BND) Y=209,209,210
100 IF(BND) Y=210,210,211
100 IF(BND) Y=211,211,212
100 IF(BND) Y=212,212,213
100 IF(BND) Y=213,213,214
100 IF(BND) Y=214,214,215
100 IF(BND) Y=215,215,216
100 IF(BND) Y=216,216,217
100 IF(BND) Y=217,217,218
100 IF(BND) Y=218,218,219
100 IF(BND) Y=219,219,220
100 IF(BND) Y=220,220,221
100 IF(BND) Y=221,221,222
100 IF(BND) Y=222,222,223
100 IF(BND) Y=223,223,224
100 IF(BND) Y=224,224,225
100 IF(BND) Y=225,225,226
100 IF(BND) Y=226,226,227
100 IF(BND) Y=227,227,228
100 IF(BND) Y=228,228,229
100 IF(BND) Y=229,229,230
100 IF(BND) Y=230,230,231
100 IF(BND) Y=231,231,232
100 IF(BND) Y=232,232,233
100 IF(BND) Y=233,233,234
100 IF(BND) Y=234,234,235
100 IF(BND) Y=235,235,236
100 IF(BND) Y=236,236,237
100 IF(BND) Y=237,237,238
100 IF(BND) Y=238,238,239
100 IF(BND) Y=239,239,240
100 IF(BND) Y=240,240,241
100 IF(BND) Y=241,241,242
100 IF(BND) Y=242,242,243
100 IF(BND) Y=243,243,244
100 IF(BND) Y=244,244,245
100 IF(BND) Y=245,245,246
100 IF(BND) Y=246,246,247
100 IF(BND) Y=247,247,248
100 IF(BND) Y=248,248,249
100 IF(BND) Y=249,249,250
100 IF(BND) Y=250,250,251
100 IF(BND) Y=251,251,252
100 IF(BND) Y=252,252,253
100 IF(BND) Y=253,253,254
100 IF(BND) Y=254,254,255
100 IF(BND) Y=255,255,256
100 IF(BND) Y=256,256,257
100 IF(BND) Y=257,257,258
100 IF(BND) Y=258,258,259
100 IF(BND) Y=259,259,260
100 IF(BND) Y=260,260,261
100 IF(BND) Y=261,261,262
100 IF(BND) Y=262,262,263
100 IF(BND) Y=263,263,264
100 IF(BND) Y=264,264,265
100 IF(BND) Y=265,265,266
100 IF(BND) Y=266,266,267
100 IF(BND) Y=267,267,268
100 IF(BND) Y=268,268,269
100 IF(BND) Y=269,269,270
100 IF(BND) Y=270,270,271
100 IF(BND) Y=271,271,272
100 IF(BND) Y=272,272,273
100 IF(BND) Y=273,273,274
100 IF(BND) Y=274,274,275
100 IF(BND) Y=275,275,276
100 IF(BND) Y=276,276,277
100 IF(BND) Y=277,277,278
100 IF(BND) Y=278,278,279
100 IF(BND) Y=279,279,280
100 IF(BND) Y=280,280,281
100 IF(BND) Y=281,281,282
100 IF(BND) Y=282,282,283
100 IF(BND) Y=283,283,284
100 IF(BND) Y=284,284,285
100 IF(BND) Y=285,285,286
100 IF(BND) Y=286,286,287
100 IF(BND) Y=287,287,288
100 IF(BND) Y=288,288,289
100 IF(BND) Y=289,289,290
100 IF(BND) Y=290,290,291
100 IF(BND) Y=291,291,292
100 IF(BND) Y=292,292,293
100 IF(BND) Y=293,293,294
100 IF(BND) Y=294,294,295
100 IF(BND) Y=295,295,296
100 IF(BND) Y=296,296,297
100 IF(BND) Y=297,297,298
100 IF(BND) Y=298,298,299
100 IF(BND) Y=299,299,300
100 IF(BND) Y=300,300,301
100 IF(BND) Y=301,301,302
100 IF(BND) Y=302,302,303
100 IF(BND) Y=303,303,304
100 IF(BND) Y=304,304,305
100 IF(BND) Y=305,305,306
100 IF(BND) Y=306,306,307
100 IF(BND) Y=307,307,308
100 IF(BND) Y=308,308,309
100 IF(BND) Y=309,309,310
100 IF(BND) Y=310,310,311
100 IF(BND) Y=311,311,312
100 IF(BND) Y=312,312,313
100 IF(BND) Y=313,313,314
100 IF(BND) Y=314,314,315
100 IF(BND) Y=315,315,316
100 IF(BND) Y=316,316,317
100 IF(BND) Y=317,317,318
100 IF(BND) Y=318,318,319
100 IF(BND) Y=319,319,320
100 IF(BND) Y=320,320,321
100 IF(BND) Y=321,321,322
100 IF(BND) Y=322,322,323
100 IF(BND) Y=323,323,324
100 IF(BND) Y=324,324,325
100 IF(BND) Y=325,325,326
100 IF(BND) Y=326,326,327
100 IF(BND) Y=327,327,328
100 IF(BND) Y=328,328,329
100 IF(BND) Y=329,329,330
100 IF(BND) Y=330,330,331
100 IF(BND) Y=331,331,332
100 IF(BND) Y=332,332,333
100 IF(BND) Y=333,333,334
100 IF(BND) Y=334,334,335
100 IF(BND) Y=335,335,336
100 IF(BND) Y=336,336,337
100 IF(BND) Y=337,337,338
100 IF(BND) Y=338,338,339
100 IF(BND) Y=339,339,340
100 IF(BND) Y=340,340,341
100 IF(BND) Y=341,341,342
100 IF(BND) Y=342,342,343
100 IF(BND) Y=343,343,344
100 IF(BND) Y=344,344,345
100 IF(BND) Y=345,345,346
100 IF(BND) Y=346,346,347
100 IF(BND) Y=347,347,348
100 IF(BND) Y=348,348,349
100 IF(BND) Y=349,349,350
100 IF(BND) Y=350,350,351
100 IF(BND) Y=351,351,352
100 IF(BND) Y=352,352,353
100 IF(BND) Y=353,353,354
100 IF(BND) Y=354,354,355
100 IF(BND) Y=355,355,356
100 IF(BND) Y=356,356,357
100 IF(BND) Y=357,357,358
100 IF(BND) Y=358,358,359
100 IF(BND) Y=359,359,360
100 IF(BND) Y=360,360,361
100 IF(BND) Y=361,361,362
100 IF(BND) Y=362,362,363
100 IF(BND) Y=363,363,364
100 IF(BND) Y=364,364,365
100 IF(BND) Y=365,365,366
100 IF(BND) Y=366,366,367
100 IF(BND) Y=367,367,368
100 IF(BND) Y=368,368,369
100 IF(BND) Y=369,369,370
100 IF(BND) Y=370,370,371
100 IF(BND) Y=371,371,372
100 IF(BND) Y=372,372,373
100 IF(BND) Y=373,373,374
100 IF(BND) Y=374,374,375
100 IF(BND) Y=375,375,376
100 IF(BND) Y=376,376,377
100 IF(BND) Y=377,377,378
100 IF(BND) Y=378,378,379
100 IF(BND) Y=379,379,380
100 IF(BND) Y=380,380,381
100 IF(BND) Y=381,381,382
100 IF(BND) Y=382,382,383
100 IF(BND) Y=383,383,384
100 IF(BND) Y=384,384,385
100 IF(BND) Y=385,385,386
100 IF(BND) Y=386,386,387
100 IF(BND) Y=387,387,388
100 IF(BND) Y=388,388,389
100 IF(BND) Y=389,389,390
100 IF(BND) Y=390,390,391
100 IF(BND) Y=391,391,392
100 IF(BND) Y=392,392,393
100 IF(BND) Y=393,393,394
100 IF(BND) Y=394,394,395
100 IF(BND) Y=395,395,396
100 IF(BND) Y=396,396,397
100 IF(BND) Y=397,397,398
100 IF(BND) Y=398,398,399
100 IF(BND) Y=399,399,400
100 IF(BND) Y=400,400,401
100 IF(BND) Y=401,401,402
100 IF(BND) Y=402,402,403
100 IF(BND) Y=403,403,404
100 IF(BND) Y=404,404,405
100 IF(BND) Y=405,405,406
100 IF(BND) Y=406,406,407
100 IF(BND) Y=407,407,408
100 IF(BND) Y=408,408,409
100 IF(BND) Y=409,409,410
100 IF(BND) Y=410,410,411
100 IF(BND) Y=411,411,412
100 IF(BND) Y=412,412,413
100 IF(BND) Y=413,413,414
100 IF(BND) Y=414,414,415
100 IF(BND) Y=415,415,416
100 IF(BND) Y=416,416,417
100 IF(BND) Y=417,417,418
100 IF(BND) Y=418,418,419
100 IF(BND) Y=419,419,420
100 IF(BND) Y=420,420,421
100 IF(BND) Y=421,421,422
100 IF(BND) Y=422,422,423
100 IF(BND) Y=423,423,424
100 IF(BND) Y=424,424,425
100 IF(BND) Y=425,425,426
100 IF(BND) Y=426,426,427
100 IF(BND) Y=427,427,428
100 IF(BND) Y=428,428,429
100 IF(BND) Y=429,429,430
100 IF(BND) Y=430,430,431
100 IF(BND) Y=431,431,432
100 IF(BND) Y=432,432,433
100 IF(BND) Y=433,433,434
100 IF(BND) Y=434,434,435
100 IF(BND) Y=435,435,436
100 IF(BND) Y=436,436,437
100 IF(BND) Y=437,437,438
100 IF(BND) Y=438,438,439
100 IF(BND) Y=439,439,440
100 IF(BND) Y=440,440,441
100 IF(BND) Y=441,441,442
100 IF(BND) Y=442,442,443
100 IF(BND) Y=443,443,444
100 IF(BND) Y=444,444,445
100 IF(BND) Y=445,445,446
100 IF(BND) Y=446,446,447
100 IF(BND) Y=447,447,448
100 IF(BND) Y=448,448,449
100 IF(BND) Y=449,449,450
100 IF(BND) Y=450,450,451
100 IF(BND) Y=451,451,452
100 IF(BND) Y=452,452,453
100 IF(BND) Y=453,453,454
100 IF(BND) Y=454,454,455
100 IF(BND) Y=455,455,456
100 IF(BND) Y=456,456,457
100 IF(BND) Y=457,457,458
100 IF(BND) Y=458,458,459
100 IF(BND) Y=459,459,460
100 IF(BND) Y=460,460,461
100 IF(BND) Y=461,461,462
100 IF(BND) Y=462,462,463
100 IF(BND) Y=463,463,464
100 IF(BND) Y=464,464,465
100 IF(BND) Y=465,465,466
100 IF(BND) Y=466,466,467
100 IF(BND) Y=467,467,468
100 IF(BND) Y=468,468,469
100 IF(BND) Y=469,469,470
100 IF(BND) Y=470,470,471
100 IF(BND) Y=471,471,472
100 IF(BND) Y=472,472,473
100 IF(BND) Y=473,473,474
100 IF(BND) Y=474,474,475
100 IF(BND) Y=475,475,476
100 IF(BND) Y=476,476,477
100 IF(BND) Y=477,477,478
100 IF(BND) Y=478,478,479
100 IF(BND) Y=479,479,480
100 IF(BND) Y=480,480,481
100 IF(BND) Y=481,481,482
100 IF(BND) Y=482,482,483
100 IF(BND) Y=483,483,484
100 IF(BND) Y=484,484,485
100 IF(BND) Y=485,485,486
100 IF(BND) Y=486,486,487
100 IF(BND) Y=487,487,488
100 IF(BND) Y=488,488,489
100 IF(BND) Y=489,489,490
100 IF(BND) Y=490,490,491
100 IF(BND) Y=491,491,492
100 IF(BND) Y=492,492,493
100 IF(BND) Y=493,493,494
100 IF(BND) Y=494,494,495
100 IF(BND) Y=495,495,496
100 IF(BND) Y=496,496,497
100 IF(BND) Y=497,497,498
100 IF(BND) Y=498,498,499
100 IF(BND) Y=499,499,500
100 IF(BND) Y=500,500,501
100 IF(BND) Y=501,501,502
100 IF(BND) Y=502,502,503
100 IF(BND) Y=503,503,504
100 IF(BND) Y=504,504,505
100 IF(BND) Y=505,505,506
100 IF(BND) Y=506,506,507
100 IF(BND) Y=507,507,508
100 IF(BND) Y=508,508,509
100 IF(BND) Y=509,509,510
100 IF(BND) Y=510,510,511
100 IF(BND) Y=511,511,512
100 IF(BND) Y=512,512,513
100 IF(BND) Y=513,513,514
100 IF(BND) Y=514,514,515
100 IF(BND) Y=515,515,516
100 IF(BND) Y=516,516,517
100 IF(BND) Y=517,517,518
100 IF(BND) Y=518,518,519
100 IF(BND) Y=519,519,520
100 IF(BND) Y=520,520,521
100 IF(BND) Y=521,521,522
100 IF(BND) Y=522,522,523
100 IF(BND) Y=523,523,524
100 IF(BND) Y=524,524,525
100 IF(BND) Y=525,525,526
100 IF(BND) Y=526,526,527
100 IF(BND) Y=527,527,528
100 IF(BND) Y=528,528,529
100 IF(BND) Y=529,529,530
100 IF(BND) Y=530,530,531
100 IF(BND) Y=531,531,532
100 IF(BND) Y=532,532,533
100 IF(BND) Y=533,533,534
100 IF(BND) Y=534,534,535
100 IF(BND) Y=535,535,536
100 IF(BND) Y=536,536,537
100 IF(BND) Y=537,537,538
100 IF(BND) Y=538,538,539
100 IF(BND) Y=539,539,540
100 IF(BND) Y=540,540,541
100 IF(BND) Y=541,541,542
100 IF(BND) Y=542,542,543
100 IF(BND) Y=543,543,544
100 IF(BND) Y=544,544,545
100 IF(BND) Y=545,545,546
100 IF(BND) Y=546,546,547
100 IF(BND) Y=547,547,548
100 IF(BND) Y=548,548,549
100 IF(BND) Y=549,549,550
100 IF(BND) Y=550,550,551
100 IF(BND) Y=551,551,552
100 IF(BND) Y=552,552,553
100 IF(BND) Y=553,553,554
100 IF(BND) Y=554,554,555
100 IF(BND) Y=555,555,556
100 IF(BND) Y=556,556,557
100 IF(BND) Y=557,557,558
100 IF(B


```

NCP=NCP+1
NCP=NCP+13
IF(NCP-M)PC,8C,75
CONTINUE
J=-2
NLINE=NLINE+1
LLINE=N-NLINE+1
UPPEACCP-1) 95,95,9C
J=1
CO=100
I=1,135
A(I)=BLK
B(I)=BLK
F(I)=NLINE
CO=16C
L=NCP,NCP
J=J+5
KI=L
LI=100
I3C,I3C,I2C,I2C
IF(KI-10C) I3C,I2C,I2C
LL=KI/10C
A(J)=KC(LL+1)
KI=KI-10C+LL
GO TO I35
A(J)=KG(I)
J=J+1
I=KI-10C
I5C,I5C,I4C,I4C
LL=KI/10C
A(J)=KC(LL+1)
KI=KI-10C+LL
GO TO I55
A(J)=KG(I)
J=J+1
A(J)=KC(KI+1)
CONTINUE
PCCH OF ARRAY
GO FIRST 2C
NLINE=N-NLINE+1
IF(NLINE-N) I3C,I3C,I3C
A(I)=BLK
B(I)=BLK
C(I)=BLK
D(I)=BLK
E(I)=BLK
F(I)=BLK

```


[illegible]


```

I3=MODC((IFIX((TPM(I)-AMIN)/BND)),20)+I
I4=MODC((IFIX((XMT(I)-AMIN)/BND)),20)+I
I5=MODC((IFIX((BTM(I)-AMIN)/BND)),20)+I
I6=MODC((IFIX((BTX(I)-AMIN)/BND)),20)+I
I7=MODC((IFIX((BT(I)-AMIN)/BND)),20)+I
A(J)=IFH(I,I2)
B(J)=IFH(I,I3)
C(J)=IFH(I,I4)
D(J)=IFH(I,I5)
E(J)=IFH(I,I6)
GCONT=INLC
GO TO 3CP-1
250 NCY=NCOP-1
260 J=-2
265 IF(NCY) 265,265,270
265 J=-1
270 GO TO 330
270 NCY=NCY+1
280 IF(NCY-NCOP) 280,280,310
280 J=J+7
285 THLD=ALD+Y(NLINE,NCY)+BZ
285 IF(THLD) 285,290,290
290 GO TO 295
295 F(J)=FPL
295 FNUM=INT(ABS(THLD-INT(THLD))*.000.0+0.5)
295 NDS=100 KK=1,3
300 J=J+1
300 KI=NUM/NDS
300 F(J)=KG(KI+1)
300 NUM=NUM-KI*NDS
300 NDS=NUM/10
300 GO TO 370
310 IF(NCOP-M) 360,320,320
320 IF(J-127) 330,330,360
330 J=J+3
330 IF=NLIN
330 IF(KI-100) 340,335,335
330 FJ=KI/100
330 F(J)=KG(LL+1)
330 KI=KI-100
330 GO TO 330
340 F(J)=KG(I)
340 J=J+1

```



```

345 IF(KI-IC) 35C,345,345
    LL=KI/IC
    F(J)=KG(LL+1)
    KI=KI-IC*LL
35C GO TO 35E
35E F(J)=KG(I)
    J=J+1
    F(J)=KG(KI+1)
    J=J-1
    IF(NCY-1) 27C,27C,35C
36C IF(NLINT-1)362,362,368
362 PRINT, (A(I),I=1,132), (B(IP1),IP1=1,132), (H(IP2),IP2=1,132),
    GO TO 37C
368 PRINT, (A(I),I=1,132), (B(IP1),IP1=1,132), (C(IP2),IP2=1,132),
    GO TO 37C
37C PRINT, (B(IP3),IP3=1,132), (E(IP4),IP4=1,132), (F(IP5),IP5=1,132),
    GO TO 37C
37C PRINT, (IP6=1,132), (H(IP7),IP7=1,132)
    GO TO 37C
38C GO TO 39C IF=1,135
39C 4(I)=BLK
    F(I)=BLK
    C(I)=BLK
    C(I)=BLK
    CONTINUE
39C J=-2
    IF(NCCP-1) 395,395,40C
39C J=-1
39C L=NCCP,NCP
40C J=J+3
    J=L
    IF(KI-IC) 410,405,405
40C LL=KI/IC
    C(J)=KG(LL+1)
    KI=KI-IC*LL
41C GO TO 412
412 C(J)=KG(I)
    J=J+1
    IF(KI-IC) 420,415,415
41C LL=KI/IC
    C(J)=KG(LL+1)
    KI=KI-IC*LL
42C GO TO 422
422 C(J)=KG(I)
    J=J+1
    IF(KI-IC) 430,425,425
43C CONTINUE, (B(IP1),IP1=1,132), (C(IP2),IP2=1,132)
    PRINT, (M)2C,30C,50C
    IF(NC

```



```

SEEDS SHOULD BE CHOSEN IN ACCORDANCE WITH THE DISCUSSION THAT
GIVEN IN THE POINT RANDOM NUMBERS ARE DESIRED, AS ARE THE
IF AVAILABLE POINT RANDOM NUMBERS ARE CHANGED AND A TRAILING LOW
EVENING ZERO BIT IN THEIR PROBABILITY PART.
ORDER ZERO BIT IN THEIR PROBABILITY PART.

SUBROUTINES AND FUNCTION SUBPROGRAMS REQUIRED
NONE

METHOD
POWER RESIDUE METHOD DISCUSSED IN IBM MANUAL C20-8011,
RANDOM NUMBER GENERATION AND TESTING
.....

```

```

SUBROUTINE RANDU(IY, IY, YFL)
  IY=IX*65539
  IF(IY) 5,6,7
  IY=IY+2147483647+1
  YFL=YFL*IY*465661359
  RETURN
END

```


array hi45,0a Axisymmetric, 60 psia, $z = .05$ cm.

[illegible]

R; T=0.03/0.10 17.28.59

n_garry@ay hi45,2.5 Axisymmetric, 60 psia, $z = .25$ cm.

452	100	1	2	100	50	1
0.00	0.00	0.00	0.00	0.00	0.62	1.26
2.10	2.32	2.62	2.91	3.40	4.43	5.03
6.51	6.98	7.35	7.70	8.02	8.90	9.32
10.18	10.40	10.60	10.84	11.04	11.35	11.50
12.00	12.09	12.15	12.21	12.25	12.32	12.36
						1.64
						5.50
						9.03
						11.65
						12.38
						1.90
						6.00
						9.31
						11.70
						12.39

R; T=0.03/0.10 17.30.09

0 garray hi45,5a Axisymmetric, 60 psia, $z = .5$ cm.

[illegible]

R; T=0.03/0.10 17.31.06

p garray hi45,7.5 Axisymmetric, 60 psia, z= .75 cm

455	120	1	2	100	60	1			
0.00	0.00	0.00	0.00	0.00	0.00	0.00	0.00	0.00	0.18
0.68	0.98	1.45	1.75	2.28	2.55	2.73	2.84	2.95	3.02
3.08	3.10	3.11	3.12	3.13	3.11	3.09	3.06	3.06	3.12
3.25	3.40	3.59	3.75	3.93	4.10	4.30	4.50	4.66	4.83
5.00	5.13	5.35	5.50	5.65	5.85	6.03	6.17	6.28	6.38
6.50	6.58	6.64	6.72	6.78	6.84	6.88	6.90	6.94	6.96

R; T=0.03/0.10 17.32.03

p garray hi45,10. Axisymmetric, 60 psia, z= 1.0 cm.

4510	120	1	2	100	60	1			
1.0	0.00	0.00	0.00	0.00	0.00	0.00	0.15	0.38	0.65
0.00	1.30	1.60	2.10	2.37	2.62	2.78	2.91	3.03	3.15
1.04	3.30	3.34	3.36	3.34	3.28	3.20	3.12	3.05	2.98
3.22	2.90	2.90	2.90	2.92	2.97	3.00	3.06	3.12	3.18
2.92	3.35	3.42	3.52	3.63	3.74	3.81	3.90	3.99	4.05
3.28	4.27	4.22	4.27	4.32	4.37	4.40	4.42	4.48	4.50

R; T=0.03/0.10 17.33.11

p garray hi45,12. Axisymmetric, 60 psia, z= 1.25 cm.

4512	120	1	2	100	60	1			
1.25	0.00	0.00	0.00	0.00	0.04	0.20	0.44	0.70	1.10
0.00	1.88	2.18	2.36	2.52	2.62	2.77	2.87	2.94	3.02
1.55	3.16	3.20	3.24	3.20	3.16	3.11	3.01	2.88	2.70
3.03	2.47	2.38	2.28	2.21	2.14	2.10	2.05	2.05	2.06
2.56	2.16	2.20	2.25	2.31	2.37	2.43	2.50	2.55	2.60
2.10	2.71	2.78	2.85	2.90	2.95	2.99	3.02	3.05	3.07

R; T=0.03/0.10 17.34.27

p garray hi45,15. Axisymmetric, 60 psia, z=1.5 cm.

4515	120	1	2	100	60	1			
01.5									
0.01	0.02	0.03	0.05	0.08	0.12	0.31	0.59	0.89	1.20
1.68	2.09	2.31	2.50	2.61	2.72	2.90	2.86	2.90	2.95
2.98	3.00	2.99	2.98	2.94	2.86	2.79	2.68	2.58	2.44
2.28	2.15	2.00	1.85	1.76	1.70	1.63	1.59	1.55	1.52
1.51	1.49	1.48	1.47	1.45	1.46	1.47	1.48	1.49	1.50
1.51	1.52	1.53	1.55	1.57	1.58	1.59	1.60	1.61	1.61

R; T=0.03/0.10 17.35.38

p garray hi45,20. Axisymmetric, 60 psia, z=2.0 cm.

4520	120	1	2	100	60	1			
2.0									
0.00	0.03	0.10	0.20	0.35	0.58	0.79	0.90	1.07	1.30
1.55	1.75	2.00	2.28	2.45	2.60	2.72	2.85	2.95	3.02
3.09	3.11	3.15	3.17	3.18	3.17	3.16	3.10	3.04	2.97
2.89	2.79	2.68	2.54	2.38	2.14	1.87	1.69	1.50	1.35
1.18	1.03	0.92	0.79	0.65	0.58	0.48	0.39	0.34	0.30
0.25	0.21	0.20	0.20	0.19	0.19	0.18	0.18	0.18	0.17

R; T=0.03/0.10 17.36.38

9.72	9.70	9.65	9.50	9.22	8.90	8.52	8.15	7.73	7.32
6.88	6.32	5.80	5.13	4.50	3.77	3.30	2.89	2.50	2.10
1.65	1.12	0.28	0.00	0.00	0.00	0.00	0.00	0.00	0.00
0.00	0.00	0.00	0.00	0.15	0.90	1.77	2.16	2.57	2.71
2.72	2.70	2.88	3.14	3.61	4.14	4.70	5.24	4.77	6.28
6.75	7.20	7.60	8.00	8.33	8.63	8.90	9.13	9.34	9.51
9.64	9.62	9.57	9.45	9.30	9.09	8.81	8.48	8.07	7.55
7.11	6.52	5.98	5.32	4.70	4.16	3.60	3.05	2.76	2.55
2.21	1.47	0.67	0.05	0.00	0.00	0.00	0.00	0.00	0.00
0.00	0.00	0.00	0.00	0.32	1.00	1.83	2.31	2.59	2.58
2.55	2.59	2.73	3.05	3.45	3.97	4.52	5.05	5.56	6.11
6.62	7.10	7.55	7.95	8.32	8.62	9.00	9.28	9.50	9.62
9.69	9.69	9.65	9.53	9.34	9.00	8.00	6.70	5.33	3.00
7.53	7.17	6.59	5.89	5.17	4.54	3.90	3.37	2.84	2.53
2.12	1.50	0.84	0.10	0.00	0.00	0.00	0.00	0.00	0.00
0.00	0.00	0.00	0.00	0.50	1.20	1.84	2.28	2.40	2.30
2.30	2.42	2.67	2.97	3.38	3.82	4.32	4.78	5.30	5.82
6.29	6.78	7.00	7.33	7.70	8.02	8.35	8.62	8.90	9.09
9.21	9.19	9.10	9.00	8.86	8.65	8.42	8.10	7.75	7.38
6.92	6.45	5.96	5.42	4.78	4.17	3.40	2.87	2.53	2.18
1.69	1.06	0.38	0.00	0.00	0.00	0.00	0.00	0.00	0.00
0.00	0.00	0.03	0.36	0.80	1.25	1.61	1.92	2.22	2.38
2.38	2.30	2.38	2.70	3.02	3.50	3.93	4.42	5.01	5.56
5.95	6.35	6.72	7.03	7.45	7.77	8.08	8.32	8.50	8.62
8.70	8.68	8.60	8.50	8.35	8.20	7.98	7.70	7.38	7.00
6.64	6.20	5.70	5.12	4.52	3.89	3.25	2.62	2.25	2.00
1.70	1.17	0.47	0.09	0.00	0.00	0.00	0.00	0.00	0.00

R: T=0.09/0.60 17.44.25

BIBLIOGRAPHY

- Bennet, F. D. , Carter, W. C. , and Bergdolt, V. E. , "Interferometric Analysis of Airflow About Projectiles in Free Flight," Journal of Applied Physics, Vol. 23, No. 4, pp. 453-469, April 1952.
- Born, M. , and Wolf, E. , Principles of Optics, Pergamon Press, Ltd. , London, 1959.
- Bhatia, A. B. , and Wolf, E. , Proceedings of the Cambridge Philosophical Society, 50, 40, 1954.
- Brandt, G. B. , "Techniques and Applications of Holography," Electro-Technology , pp. 53-72, April 1968.
- Brooks, R. E. , Heflinger, L. O. , Wuerker, R. F. , and Briones, R. A. , "Holographic Photography of High Speed Phenomena with Conventional and Q-Switched Ruby Lasers," Applied Physics Letters, Vol. 7, No. 4, pp. 92-94, 15 August 1965.
- Brooks, R. E. , "New Dimension for Interferometry," Electronics, pp. 88-93, 15 May 1967.
- Brooks, R. E. , Heflinger, L. O. , and Wuerker, R. F. , "9A9-Pulsed Laser Holograms," IEEE Journal of Quantum Electronics, Vol. QE-2, No. 8, pp. 275-299, August 1966.
- Cavanaugh, L. , Cain, D. , and Hauer, A. , Third Quarterly Technical Report on Optical Methods for the Visualization and Measurement of Flow in Turbomachinery, Pratt and Whitney Aircraft Report PWA-3870, January 1970. (Third of a series of three quarterly reports).
- Chambers, R. P. , and Courtney-Pratt, J. S. , "Bibliography on Holograms, I, II, and III," Journal of the SMPTE: Vol. 75, pp. 373-435, April 1966; Vol. 75, pp. 759-809, August 1966; Vol. 76, pp. 392-395, April 1967.
- Erdelyi, A. , Magnus, F. , Oberhettinger, F. , and Tricomi, F. G. , Tables of Integral Transforms, Vols. I, II, McGraw Hill, New York, 1963; Higher Transcendental Functions, Vols. I, II, III, McGraw Hill, New York, 1963.

- Gabor, D. , "A New Microscopic Principle," Nature, Vol. 161, pp. 777-778, May, 1948.
- Gabor, D. , "Microscopy by Reconstructed Wavefronts," Proceedings of the Royal Society, Vol. A197, pp. 454-487, 1949.
- Gabor, D. , "Microscopy by Reconstructed Wavefronts: II," Proceedings of the Physical Society, Vol. 64, pt. 6, pp. 449-470, 1 June 1951.
- Heflinger, L. O. , Wuerker, R. F. , and Brooks, R. E. , "Holographic Interferometry," Journal of Applied Physics, Vol. 37, No. 2. , pp. 642-649, February 1966.
- Herlitz, S. I. , "A Method for Computing the Emission Distribution in Cylindrical Light Sources," Arkiv för Fysik, Band 23, No. 49, pp. 571-574, 1 March 1963.
- Hildebrand, F. B. , Introduction to Numerical Analysis, McGraw-Hill, New York, 1956.
- Holds, J. H. , Aeronautical Applications of Holographic Interferometry, Masters Thesis, Naval Postgraduate School, 1967.
- Holds, J. H. , and Fuhs, A. E. , "A Refined Analysis of a Holographic Interferogram," Journal of Applied Physics, Vol. 38, No. 13, pp. 5408-5409, December 1967.
- Ladenberg, R. , Van Voorhis, C. C. , and Winckler, J. , "Interferometric Studies of Faster than Sound Phenomena. , Part II. Analysis of Supersonic Air Jets," Physical Review, Vol. 76, No. 5, pp. 662-677, 1 September, 1949.
- Ladenberg, R. W. , et. al. , ed. , Physical Measurements in Gas Dynamics and Combustion, Princeton University Press, 1954.
- Latta, J. N. , "A Classified Bibliography on Holography and Related Fields," Journal of the SMPTE , Vol. , 77, pp. 422-458, April 1968.
- Liepmann, H. W. , and Roshko, A. , Elements of Gas Dynamics, p. 165, John Wiley and Sons, Inc. , 1957.
- Madelung, E. , "Die Mathematischen Hilfsmittel des Physikers," 5th. ed. , Springer-Verlag, Berlin, 1953.



- Maldonado, C. D. , Caron, A. P. , and Olsen, H. N. , "New Method for Obtaining Emission Coefficients from Emitted Spectral Intensities. Part I-Circularly Symmetric Light Sources," Journal of the Optical Society of America, Vol. 55, No. 10, pp. 1247-1254, October 1965.
- Maldonado, C. D. , "Note on Orthogonal Polynomials which are 'Invariant in Form' to Rotations of Axes," Journal of Mathematical Physics, Vol. 6, No. 12, pp. 1935-1938, December 1965.
- Maldonado, C. D. , and Olsen, H. N. , "New Method for Obtaining Emission Coefficients from Emitted Spectral Intensities. Part II-Asymmetrical Sources," Journal of the Optical Society of America, Vol. 56, No. 10, pp. 1305-1313, October 1966.
- Mathews, B. J. , and Wuerker, R. F. , The Investigation of Liquid Rocket Combustion Using Pulsed Laser Holography, Paper prepared for the AIAA 5th Propulsion Joint Specialist Conference, U.S. Air Force Academy, Colorado Springs, Colorado, 9-13 June 1969.
- Matulka, R. D. , Holds, J. H. , Sullivan, J. G. , and Fuhs, A. E. , Aeronautical Application of Holographic Interferometry, Naval Postgraduate School Report NPS-57FU8101A, 1968.
- Olsen, H. N. , Maldonado, C. D. , Duckworth, G. D. , and Caron, A. P. , Investigation of the Interaction of an External Magnetic Field with an Electric Arc, Aerospace Research Laboratories Report ARL66-0016, January 1966.
- Olsen, H. N. , Maldonado, C. D. , and Duckworth, G. D. , "A Numerical Method for Obtaining Internal Emission Coefficients from Externally Measured Spectral Intensities of Asymmetrical Plasmas," J. Quant. Spectrosc. Radiat. Transfer, Vol. 8, pp. 1419-1430, 1968.
- Rowley, P. D. , "Quantitative Interpretation of Three-Dimensional Weakly Refractive Phase Objects Using Holographic Interferometry," Journal of the Optical Society of America, Vol. 59, pp. 1496-1498, November 1969.
- Sangster, D. K. , and Shaw, G. A. , Analysis of Errors in the Reduction of Interferometric Data, A. C. Electronics-Defense Research Laboratory Report TR68-59, October 1968.

Sansone, G. , Orthogonal Functions, Chapt. IV, Interscience Publishers , Inc. , New York 1959.

Sullivan, J. G. , An Investigation of Three-Dimensionality in Holographic Interferometry, Masters Thesis, Naval Postgraduate School, 1968.

Whittaker, E. T. , and Watson, G. N. , A Course In Modern Analysis , 4th. ed. , Cambridge University Press, Cambridge, 1927.

Winckler, J. , "The Mach Interferometer Applied to Studying an Axially Symmetric Supersonic Airjet," The Review of Scientific Instruments, Vol. 19, No. 5, pp. 307-322, May 1948.

Witte, A. B. , and Wuerker, R. F. , Laser Holographic Interferometry Study of High Speed Flow Fields, project report, Advanced Research Projects Agency, DOD Contract No. DAHC 60-69-C-0006, 1968.

INITIAL DISTRIBUTION LIST

	No. Copies
1. Defense Documentation Center Cameron Station Alexandria, Virginia 22314	2
2. Library, Code 0212 Naval Postgraduate School Monterey, California 93940	2
3. Chairman, Department of Aeronautics Naval Postgraduate School Monterey, California 93940	1
4. Professor D. J. Collins, Code 57Co (thesis advisor) Department of Aeronautics Naval Postgraduate School Monterey, California 93940	46
5. LCDR Robert D. Matulka, USN Office of Naval Research Arlington, Virginia 22217	3
6. Professor T. H. Gawain Department of Aeronautics Naval Postgraduate School Monterey, California 93940	1
7. Professor R. L. Kelly Department of Physics Naval Postgraduate School Monterey, California 93940	1
8. Associate Professor L. V. Schmidt Department of Aeronautics Naval Postgraduate School Monterey, California 93940	1
9. Associate Professor G. D. Sackman Department of Electrical Engineering Naval Postgraduate School Monterey, California 93940	1

INITIAL DISTRIBUTION LIST (Cont'd)

	No. Copies
10. Professor Allen E. Fuhs Department of Aeronautics Monterey, California 93940	1
11. Arvel B. Witte, R4/2050 TRW Systems Group One Space Park Redondo Beach, California 90278	1



DOCUMENT CONTROL DATA - R & D

(Security classification of title, body of abstract and indexing annotation must be entered when the overall report is classified)

1. ORIGINATING ACTIVITY (Corporate author) Naval Postgraduate School Monterey, California 93940		2a. REPORT SECURITY CLASSIFICATION Unclassified	
		2b. GROUP	
3. REPORT TITLE The Application of Holographic Interferometry to the Determination of Asymmetric Three-Dimensional Density Fields in Free Jet Flow			
4. DESCRIPTIVE NOTES (Type of report and, inclusive dates) Ph. D. Thesis (June 1970)			
5. AUTHOR(S) (First name, middle initial, last name) Robert Dale Matulka			
6. REPORT DATE June 1970		7a. TOTAL NO. OF PAGES 156	7b. NO. OF REFS 37
8a. CONTRACT OR GRANT NO. NAVAIR A33-330-551-69		9a. ORIGINATOR'S REPORT NUMBER(S)	
b. PROJECT NO.			
c.		9b. OTHER REPORT NO(S) (Any other numbers that may be assigned this report)	
d.			
10. DISTRIBUTION STATEMENT This document has been approved for public release and sale; its distribution is unlimited.			
11. SUPPLEMENTARY NOTES		12. SPONSORING MILITARY ACTIVITY Naval Postgraduate School Monterey, California 93940	
13. ABSTRACT The successful application of holographic interferometry, and an associated mathematical reduction process, to the determination of an asymmetric three-dimensional density field of an aerodynamic phenomenon is reported. An integral inversion method from the field of plasma physics has been computerized, extensively evaluated and applied to the determination of functions, both axisymmetric and asymmetric, which simulate aerodynamic density fields. The application of holographic interferometry has been extended to provide multiple holograms about a test region, with sufficient coverage to provide interferometric data for the successful solution of the density field. The analytical and experimental methods developed were applied to an experimental axisymmetric test field, the supersonic flow from a free jet, and shown to be comparable to a previous solution obtained by the Abel inversion method. Further, the free jet was tilted to provide a test field which was asymmetric in the plane of solution. Comparison of the resulting asymmetric solution was shown to be self-consistent with the previously obtained axisymmetric solution.			

KEY WORDS	LINK A		LINK B		LINK C	
	ROLE	WT	ROLE	WT	ROLE	WT
1. Holography						
2. Interferometry						
3. Three-Dimensional						
4. Asymmetric						
5. Three-Dimensional Density Measurement						
6. Asymmetric Field Solution						

26 OCT 73
26 OCT 73

19435
19369
19369
2057

Thesis
M3835
c.1

Matulka

122517

The application of
holographic inter-
ferometry to the
determination of
asymmetric three-
dimensional density
fields in free jet
flow.

26 OCT 73

19435
19369

Thesis
M3835
c.1

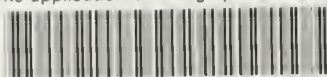
Matulka

122517

The application of
holographic inter-
ferometry to the
determination of
asymmetric three-
dimensional density
fields in free jet
flow.

thesM3835

The application of holographic interfero



3 2768 002 12535 3

DUDLEY KNOX LIBRARY